Cell Journal (Yakhteh)

Guide for Authors

Aims and Scope: The "Cell Journal (Yakhteh)" is a peer review and monthly English publication of Royan Institute of Iran. The aim of the journal is to disseminate information through publishing the most recent scientific research studies on exclusively Cellular, Molecular and other related topics. **Cell J**, has been certified by the Ministry of Culture and Islamic Guidance since 1999 and also accredited as a scientific and research journal by HBI (Health and Biomedical Information) Journal Accreditation Commission since 2000 which is an open access journal. **This journal holds the membership of the Committee on Publication Ethics (COPE).**

1. Types of articles

The articles in the field of Cellular and Molecular can be considered for publications in **Cell J.** These articles are as below:

A. Original articles

Original articles are scientific reports of the original research studies. The article consists of English Abstract (structured), Introduction, Materials and Methods, Results, Discussion, Conclusion, Acknowledgements, Author's Contributions, and References **(Up to 40).**

B. Review articles

Review articles are the articles written by well experienced authors and those who have excellence in the related fields. The corresponding author of the review article must be one of the authors of at least three published articles appearing in the references. The review article consists of English Abstract (unstructured), Introduction, Conclusion, Author's Contributions, and References **(Up to 70).**

C. Systematic Reviews

Systematic reviews are a type of literature review that collect and critically analyzes multiple research studies or papers. The Systematic reviews consist of English Abstract (unstructured), Introduction, Materials and Methods, Results, Discussion, Conclusion, Acknowledgements, Author's Contributions, and References **(Up to 70).**

D. Short communications

Short communications are articles containing new findings. Submissions should be brief reports of ongoing researches. The short communication consists of English Abstract (unstructured), the body of the manuscript (should not hold heading or subheading), Acknowledgements, Author's Contributions, and References **(Up to 30).**

E. Case reports

Case reports are short discussions of a case or case series with unique features not previously described which make an important teaching point or scientific observation. They may describe novel techniques or use equipment, or new information on diseases of importance. It consists of English Abstracts (Unstructured), Introduction, Case Report, Discussion, Acknowledgements, Author's Contributions, and References **(Up to 30).**

F. Editorial

Editorials are articles should be written in relevant and new data of journals' filed by either the editor in chief or the editorial board.

G. Imaging in biology

Images in biology should focus on a single case with an interesting illustration such as a photograph, histological specimen or investigation. Color images are welcomed. The text should be brief and informative.

H. Letter to the editors

Letter to the editors are in response to previously published **Cell J** articles, and may also include interesting cases that do not meet the requirement of being truly exceptional, as well as other brief technical or clinical notes of general interest.

I. Debate

Debates are articles which show a discussion of the positive and negative view of the author concerning all aspect of the issue relevant to scientific research.

2. Submission process

It is recommended to see the guidelines for reporting different kinds of manuscripts. This guide explains how to prepare the

manuscript for submission. Before submitting, we suggest authors to familiarize themselves with **Cell J** format and content by reading the journal via the website (www.celljournal.com). The corresponding author ensures that all authors are included in the author list and agree with its order, and they must be aware of the manuscript submission.

A. Author contributions statements

It is essential for authors to include a statement of responsibility in the manuscript that specifies the contribution of every one of them. This participation must include conception and design of the manuscript, data acquisition or data analysis and interpretation, drafting of the manuscript and/or revising it for critically important intellectual content, revision and final approval of the manuscript and statistical analysis, obtaining funding, administrative, technical, or material support, or supervision. Authors who do not meet the above criteria should be acknowledged in the **Acknowledgments section.**

B. Cover letter and copyright

Each manuscript should be accompanied by a cover letter, signed by all authors specifying the following statement: "The manuscript has been seen and approved by all authors and is not under active consideration for publication. It has neither been accepted for publication nor published in another journal fully or partially (except in abstract form). **Also, no manuscript would be accepted in case it has been pre-printed or submitted to other websites.** I hereby assign the copyright of the enclosed manuscript to **Cell J.**" Corresponding author must confirm the proof of the manuscript before online publishing. Also, it is needed to suggest three peer reviewers in the field of their manuscript.

C. Manuscript preparation

Authors whose first language is not English encouraged to consult a native English speaker in order to confirm his manuscripts to American or British (not a mixture) English usage and grammar. It is necessary to mention that we will check the plagiarism of your manuscript by iThenticate Software. The manuscript should be prepared in accordance with the "International Committee of Medical Journal Editors (ICMJE)". Please send your manuscript in two formats word and PDF (including: title, name of all the authors with their degree, abstract, full text, references, tables and figures) and also send tables and figures separately in the site. The abstract and text pages should have consecutive line numbers in the left margin beginning with the title page and continuing through the last page of the written text. Each abbreviation must be defined in the abstract and text when they are mentioned for the first time. Avoid using abbreviation in the title. Please use the international and standard abbreviations and symbols

It should be added that an essential step toward the integration and linking of scientific information reported in published literature is using standardized nomenclature in all fields of science and medicine. Species names must be italicized (*e.g., Homo sapiens*) and also the full genus and species written out in full, both in the title of the manuscript and at the first mention of an organism in a paper.

It is necessary to mention that genes, mutations, genotypes, and alleles must be indicated in italics. Please use the recommended name by consulting the appropriate genetic nomenclature database, e.g., HUGO for human genes. In another words; if it is a human gene, you must write all the letters in capital and italic (*e.g., OCT4, c-MYC*). If not, only write the first letter in capital and italic (*e.g., Oct4, c-Myc*). **In addition, protein designations are the same as the gene symbol but are not italicized.**

Of note, Cell J will only consider publishing genetic association study papers that are novel and statistically robust. Authors are advised to adhere to the recommendations outlined in the STREGA statement (http://www.strega-statement.org). The following criteria must be met for all submissions:

1. Hardy-Weinberg Equilibrium (HWE) calculations must be carried out and reported along with the P-values if applicable [see Namipashaki et al. 2015 (Cell J, Vol 17, N 2, Pages: 187-192) for a discussion].

2. Linkage disequilibrium (LD) structure between SNPs (if multiple SNPs are reported) must be presented.

3. Appropriate multiple testing correction (if multiple independent SNPs are reported) must be included.

Submissions that fail to meet the above criteria will be rejected before being sent out for review.

Each of the following manuscript components should begin in the following sequence:

Authors' names and order of them must be carefully considered (full name(s), highest awarded academic degree(s), email(s), and institutional affiliation(s) of all the authors in English. Also, you must send mobile number and full postal address of the corresponding author).

Changes to Authorship such as addition, deletion or rearrangement of author names must be made only before the manuscript has been accepted in the case of approving by the journal editor. In this case, the corresponding author must explain the reason of changing and confirm them (which has been signed by all authors of the manuscript). If the manuscript has already been published in an online issue, an erratum is needed.

Title is providing the full title of the research (do not use abbreviations in title).

Running title is providing a maximum of 7 words (no more than 50 characters).

Abstract must include Objective, Materials and Methods, Results, and Conclusion (no more than 300 words).

Keywords, three to five, must be supplied by the authors at the foot of the abstract chosen from the Medical Subject Heading (MeSH). Therefore; they must be specific and relevant to the paper.

The following components should be identified after the abstract:

Introduction: The Introduction should provide a brief background to the subject of the paper, explain the importance of the study, and state a precise study question or purpose.

Materials and Methods: It includes the exact methods or observations of experiments. If an apparatus is used, its manufacturer's name and address should be stipulated in parenthesis. If the method is established, give reference but if the method is new, give enough information so that another author can perform it. If a drug is used, its generic name, dose, and route of administration must be given. Standard units of measurements and chemical symbols of elements do not need to be defined.

Statistical analysis: Type of study and statistical methods should be mentioned and specified by any general computer program used.

Ethical considerations*:* Please state that informed consent was obtained from all human adult participants and from the parents or legal guardians of minors and include the name of the appropriate institutional review board that approved the project. It is necessary to indicate in the text that the maintenance and care of experimental animals complies with National Institutes of Health guidelines for the humane use of laboratory animals, or those of your Institute or agency.

Clinical trial registration: All of the Clinical Trials performing in Iran must be registered in Iranian Registry of Clinical Trials (www.irct.ir). The clinical trials performed abroad, could be considered for publication if they register in a registration site approved by WHO or www.clinicaltrials.gov. If you are reporting phase II or phase III randomized controlled trials, you must refer to the CONSORT Statement for recommendations to facilitate the complete and transparent reporting of trial findings. Reports that do not conform to the CONSORT guidelines may need to be revised before peer-reviewing.

Results: They must be presented in the form of text, tables, and figures. Take care that the text does not repeat data that are presented in tables and/or figures. Only emphasize and summarize the essential features of the main results. Tables and figures must be numbered consecutively as appeared in the text and should be organized in separate pages at the end of the manuscript while their location should be mentioned in the main text.

Tables and figures: If the result of your manuscript is too short, it is better to use the text instead of tables & figures. Tables should have a short descriptive heading above them and also any footnotes. Figure's caption should contain a brief title for the whole figure and continue with a short explanation of each part and also the symbols used (no more than 100 words). All figures must be prepared based on cell journal's guideline in color (no more than 6 Figures and Tables) and also in GIF or JPEG format.

Of Note: Please put the tables & figures of the result in the results section not any other section of the manuscript.

Supplementary materials would be published on the online version of the journal. This material is important to the understanding and interpretation of the report and should not repeat material within the print article. The amount of supplementary material should be limited. Supplementary material should be original and not previously published and will undergo editorial and peer review with the main manuscript. Also, they must be cited in the manuscript text in parentheses, in a similar way as when citing a figure or a table. Provide a caption for each supplementary material submitted.

Discussion: It should emphasize the present findings and the variations or similarities with other researches done by other researchers. The detailed results should not be repeated in the discussion again. It must emphasize the new and important aspects of the study.

Conclusion: It emphasizes the new and important aspects of the study. All conclusions are justified by the results of the study.

Acknowledgements: This part includes a statement thanking those who contributed substantially with work relevant to the study but does not have authorship criteria. It includes those who provided technical help, writing assistance and name of departments that provided only general support. You must mention financial support in the study. Otherwise; write this sentence "There is no financial support in this study".

Conflict of interest: Any conflict of interest (financial or otherwise) and sources of financial support must be listed in the Acknowledgements. It includes providers of supplies and services from a commercial organization. Any commercial affiliation must be disclosed, regardless of providing the funding or not.

Of Note: If you have already any patent related to the subject of your manuscript, or you are going to apply for such a patent, it must be mentioned in this part.

References: The references must be written based on the Vancouver style. Thus the references are cited numerically in the text and listed in the bibliography by the order of their appearance. The titles of journals must be abbreviated according to the style used in the list of Journals Indexed in PubMed. Write surname and initials of all authors when there are six or less. In the case of seven or more authors, the names of the first six authors followed by "et al." must be listed. You can download Endnote file for Journal references style: endnote file

The reference of information must be based on the following order:

Article:

Surname(s) and first letter of name &middle name(s) of author(s) .Manuscript title. Journal title (abbr).publication date (year); Volume & Issue: Page number.

Example: Manicardi GC, Bianchi PG, Pantano S, Azzoni P, Bizzaro D, Bianchi U, et al. Presence of endogenous nicks in DNA of ejaculated human spermatozoa and its relationship to chromomycin A3 accessibility. Biol Reprod. 1995; 52(4): 864-867.

Book:

Surname(s) and first letter of name & middle name(s) of author(s).Book title. Edition. Publication place: publisher name; publication date (year); Page number.

Example: Edelman CL, Mandle CL. Health promotion throughout the lifespan. 2nd ed. ST Louis: Mosby; 1998; 145-163.

Chapter of book:

Surname(s) and first letter of name & middle name(s) of author(s).Chapter title. In: Surname(s) and first letter of name & middle name(s) of editor(s), editors. Book title. Edition. Publication place: publisher name; publication date (year); Page number.

Example: Phillips SJ, Whisnant JP. Hypertension and stroke. In: Laragh JH, Brenner BM, editors. Hypertension: pathophysiology, diagnosis, and management. 2nd ed. New York: Raven Press; 1995; 465-478.

Abstract book:

Example: Amini rad O.The antioxidant effect of pomegranate juice on sperm parameters and fertility potential in mice. Cell J. 2008;10 Suppl 1:38.

Thesis:

Name of author. Thesis title. Degree. City name. University. Publication date (year).

Example: Eftekhari Yazdi P. Comparison of fragment removal and co-culture with Vero cell monolayers on development of human fragmented embryos. Presented for the Ph.D., Tehran. Tarbiyat Modarres University. 2004.

Internet references

Article:

Example: Jahanshahi A, Mirnajafi-Zadeh J, Javan M, Mohammad-Zadeh M, Rohani M. Effect of low-frequency stimulation on adenosineA1 and A2A receptors gene expression in dentate gyrus of perforant path kindled rats. Cell J. 2008; 10 (2): 87-92. Available from: http://www.celljournal.org. (20 Oct 2008).

Book:

Example: Anderson SC, Poulsen KB. Anderson's electronic atlas of hematology.[CD-ROM]. Philadelphia: Lippincott Williams & Wilkins; 2002.

D. Proofs are sent by email as PDF files and should be checked and returned within 72 hours of receipt. It is the authors' responsibility to check that all the text and data as contained in the page proofs are correct and suitable for publication. **We are requested to pay particular attention to author's names and affiliations as it is essential that these details be accurate when the article is published.**

E. Pay for publication: Publishing an article in **Cell J** requires Article Processing Charges (APC) that will be billed to the submitting author following the acceptance of an article for publication. For more information please see www.celljournal.org.

F. Ethics of scientific publication: Manuscripts that have been published elsewhere with the same intellectual material will refer to duplicate publication. If authors have used their own previously published work or work that is currently under review, as the basis for a submitted manuscript, they are required to cite the previous work and indicate how their submitted manuscript offers novel contributions beyond those of the previous work. Research and publication misconduct is considered a serious breach of ethics.

The Journal systematically employs iThenticate, plagiarism detection and prevention software designed to ensure the originality of written work before publication. Plagiarism of text from a previously published manuscript by the same or another author is a serious publication offence. Some parts of text may be used, only where the source of the quoted material is clearly acknowledged.

3. General information

A. You can send your manuscript via online submission system which is available on our website. If the manuscript is not prepared according to the format of **Cell J**, it will be returned to authors.

B. The order of article appearance in the Journal is not demonstrating the scientific characters of the authors.

C. Cell J has authority to accept or reject the manuscript.

D. The received manuscript will be evaluated by associate editor. **Cell J** uses a single-blind peer review system and if the manuscript suits the journal criteria, we select the reviewers. If three reviewers pass their judgments on the manuscript, it will be presented to the editorial board of **Cell J.** If the editorial board has a positive judgment about the manuscript, reviewers' comments will be presented to the corresponding author (the identification of the reviewers will not be revealed). The executive member of journal will contact the corresponding author directly within 3-4 weeks by email. If authors do not receive any reply from journal office after the specified time, they can contact journal office. Finally, executive manager will respond promptly to authors' request.

The Final Checklist

The authors must ensure that before submitting the manuscript for publication, they have to consider the following parts:

1. The first page of manuscript should contain title, name of the author/coauthors, their academic qualifications, designation & institutions they are affiliated with, mailing address for future correspondence, email address, phone, and fax number.

2. Text of manuscript and References prepared as stated in the "guide for authors" section.

3. Tables should be on a separate page. Figures must be sent in color and also in JPEG (Jpg) format.

4. Cover Letter should be uploaded with the signature of all authors.

5. An ethical committee letter should be inserted at the end of the cover letter.

The Editor-in-Chief: Ahmad Hosseini, Ph.D.

Cell Journal *(Yakhteh)*

P.O. Box: 16635-148, Iran

Tel/Fax: + 98-21-22510895

Emails: Celljournal@royaninstitute.org

info@celljournal.org

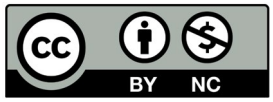

Dr. Saeed Kazemi Ashtiani

IN THE NAME OF GOD

Gone But not Forgotten

In the memory of the late Director of Royan Institute, Founder of Stem Cells Research in Iran and Chairman of ***Cell Journal*** *(Yakhteh)*. May he rest in peace.

PUBLISHED & SPONSORED BY:
Publication of Royan Institute (ACECR)

Indexed in:
1. Thomson Reuters (ISI)
2. PubMed
3. PubMed Central (PMC)
4. National Library Medicine (NLM)
5. Biosis Preview
6. Index Medicus for the Eastern Mediterranean Region (IMEMR)
7. Regional Information Center for Sciences and Technology (RICeST)
8. Index Copernicus International
9. Cambridge Scientific Abstract (CSA)
10. EMBASE
11. Scopus
12. Cinahl Database
13. Google Scholar
14. Chemical Abstract Service (CAS)
15. Proquest
16. Directory of Open Access Journals (DOAJ)
17. Open Academic Journals Index (OAJI)
18. Directory of Research Journals Indexing (DRJI)
19. Scientific Information Database (SID)
20. Iranmedex
21. Islamic World Science Citation Center (ISC)
22. Magiran
23. Science Library Index
24. Biological Abstracts
25. Essential Science Indicators
26. EuroPub

ACECR

Editorial Office Address (Dr. Ahmad Hosseini):
Royan Institute, P.O.Box: 16635-148,
Tehran, Iran
Tel & Fax: (+9821)22510895
Website: www.celljournal.org
Emails: info@celljournal.org
celljournal@royaninstitute.org

Printing Company:
Naghshe e Johar Co.
No. 103, Fajr alley, Tehranpars Street,
Tehran, Iran.

Cell Journal(Yakhteh), Vol 24, No 2, February 2022, Serial Number: 97, Pages: 55-104

CONTENTS

Original Articles

Commentary

Original Article

Differentiation of Human Wharton's Jelly Mesenchymal Stem Cells into SOX17 Expressing Cells Using a Wnt/ß-catenin Pathway Agonist on Polylactic Acid/Chitosan Nanocomposite Scaffold

Elham Hoveizi, Ph.D.[1, 2*], Shima Tavakol, Ph.D.[3]

1. Department of Biology, Faculty of Science, Shahid Chamran University of Ahvaz, Ahvaz, Iran
2. Stem Cells and Transgenic Technology Research Center (STTRC), Shahid Chamran University of Ahvaz, Ahvaz, Iran
3. Cellular and Molecular Research Center, Iran University of Medical Sciences, Tehran, Iran

**Corresponding Address: P.O.Box: 61375, Department of Biology, Faculty of Science, Shahid Chamran University of Ahvaz, Ahvaz, Iran*
Email: e.hoveizi@scu.ac.ir

Received: 15/May/2020, Accepted: 24/October/2020

Abstract

Objective: The β-catenin signaling pathway promises the potential for differentiation of stem cells into definitive endoderm (DE) cells as precursors of beta cells. Therefore, it can be considered as an inducer for cell replacement therapies in diabetes. The main goal of this research is to successfully culture and induce differentiation of human Wharton's jelly mesenchymal stem cells (hWJMSCs) into Sox17-expressing cells using a Wnt/β-catenin pathway agonist (SKL2001) plus nanoparticles on a polylactic acid/chitosan (PLA/Cs) nanocomposite scaffold.

Materials and Methods: In this experimental study, the nanocomposite was prepared through an electrospinning method and hWJMSCs were isolated through an explant technique. The morphology and the cell viability were evaluated by scanning electron microscopy (SEM) and 3-(4, 5- Dimethylthiazol-2)-2, 5-diphenyltetrazolium bromide (MTT) assay. Here, we present two differentiation protocols: the first one is induction with SKL2001; and the second one is with a combination of SKL2001 and zinc oxide nanoparticles (nZnO). Real-time quantitative reverse transcription (QRT-PCR) and immunocytochemistry analysis are carried out to examine the expression of specific markers in the differentiated cells.

Results: The nanocomposite had appropriate biocompatibility for cell adhesion and growth. While the hWJMSCs cultured on the PLA/Cs scaffolds differentiated into DE cells in the presence of SKL2001, introducing nZnO to their environment increased the differentiation process. Analyses of DE-specific markers including *SOX17, FOXA2*, and gooscoid (GSC) genes in mRNA level, indicated significantly high levels of expression in the SKL2001/nZnO group, followed by SKL2001 group compared to the control.

Conclusion: Our results show the beneficial effects of the Wnt/β-catenin pathway agonist in three-dimensional (3D) cultures in cell replacement therapy for diabetes.

Keywords: Differentiation, Nanoparticles, Tissue Engineering, Wharton's Jelly, Wnt/β-Catenin Pathway

Cell Journal(Yakhteh), Vol 24, No 2, February 2022, Pages: 55-61

Citation: Hoveizi E, Tavakol Sh. Differentiation of human wharton's jelly mesenchymal stem cells into SOX17 expressing cells using a Wnt/β-catenin pathway agonist on polylactic acid/chitosan nanocomposite scaffold. Cell J. 2022; 24(2): 55-61. doi: 10.22074/cellj.2022.7622.

Introduction

Treatment of chronic endoderm-derived organ failures, such as hepatic cirrhosis and diabetes, is rather challenging since no complete cure is known (1). Today, organ transplantation is the major treatment for these disorders. However, it is accompanied with many difficulties, including shortage of donors, transplant rejections, surgical complications, and high costs. Today, cell therapy has been considered as an alternative approach to remove some of these barriers (2).

Mesenchymal stem cells (MSCs) are multipotent and differentiate into various cells and tissues, as these cells have been found in most adult tissues (2, 3). Recently, the application of human wharton's jelly MSCs (hWJMSCs) in therapy has come to attention. Because of high potency, multipotent properties amongst adult stem cells, fast and relatively inexpensive extraction, and their non-tumorigenic state, hWJMSCs have been suggested as a promising candidate for cell therapy (4). Suitably for our studies, it has been shown that hWJMSCs may be induced to differentiate into a variety of cell types including definitive endoderm (DE), beta cells, and hepatocytes (5, 6).

The first and basic developmental step in formation of endodermal organs is the induction of DE (7). Notably, the pancreas, lungs, liver, and other organs of the gastrointestinal tract are derived from DE during embryogenesis (8, 9). Multiple signaling pathways such as Nodal, Activin A, and Wnt3a could cause differentiation of DE through signaling intermediates. In addition, the Wnt/β-catenin signaling has a critical role in cell morphology, proliferation, motility, axis determination, differentiation, and organ development. SKL2001, as an agonist for Wnt/β-catenin signaling, has been shown to inhibit the phosphorylation of β-catenin (by an alternative mechanism and independent of inhibition of GSK-3β activity), thus increasing the levels of intracellular β-catenin (10).

According to previous studies, zinc is considered as an abundant trace metal and a catalyzer for various enzymes

in the body (11, 12). Besides, zinc protects insulin from degradation and stimulates insulin biosynthesis, secretion, and its storage. Different zinc transporters, such as zinc transporter-8, exist in pancreatic β-cells and affect insulin secretion. Also, zinc improves insulin signaling by several mechanisms, such as increasing insulin receptor phosphorylation, inhibition of glycogen synthase kinase-3 (GK), and increasing PI3K activity (11). Indeed, based on recent reports, zinc oxide nanoparticles (nZnO) reduce blood glucose and significantly increase blood insulin in diabetic animal models, when compared to ZnO (12).

On the other hand, not only intracellular signaling pathways, but also cell interactions with the extracellular matrix (ECM) are taken as critical parameters in behavior, adhesion, morphology, migration, proliferation, and differentiation of the cells (13). In tissue engineering, a suitable scaffold can provide this platform. Also, the electrospinning technology can be applied to fabricate three-dimensional (3D) synthesized scaffolds. The electrospun scaffolds with diameters of tens to hundreds of nanometers are designed to mimic the ECM in cell and tissue culture (10, 14).

Thus in this study, we used SKL2001 as a Wnt/β-catenin pathway agonist alone or in combination with nZnO to induce differentiation of hWJMSCs into *SOX17*-expressing cells (as DE like-cells) on PLA/Cs three-dimensional scaffolds.

Material and Methods

All animal procedures and experimental tests were approved by the Animal Ethics Committee of Shahid Chamran University of Ahvaz (93042515).

Preparation of scaffold by electrospinning

In this experimental study, the electrospinning technique was employed to fabricate polylactic acid/chitosan (PLA/Cs) scaffolds (Electronic, FNM, Iran). To obtain 2.5 (w/v) solutions, PLA and chitosan (Cs) were added in hexafluoroisopropanol (HFIP) and acetic acid, respectively. These solutions were blended in the ratio of 7:3 (PLA:Cs) to make a scaffold. The solution was shaken for 12 hours and inserted into a 10-ml plastic syringe, and connected to a high voltage (14-18 kV) at 25°C Aluminum foil was used to collect spray drift (at a distance of 10 centimeters). The electrospun fibrous membranes were dried in a vacuum oven for two days and separated from aluminum foil at the time of use (15, 16).

Cell seeding on PLA/Cs nanocomposite scaffold

The scaffold was cut into discs with a diameter of 1.6 centimeters and placed in 24-well plates. After that, the scaffolds were sterilized by ultraviolet irradiation for 2 hours and floated in Dulbecco's modified eagle medium (DMEM, Gibco, USA) medium supplemented with 1 µg/ml amphotericin B and 3% pen/strep overnight at 37°C. Then, hWJMSCs were cultured at a density of 6×10^4 cell/scaffold and incubated at 37°C and 5% CO_2.

Scanning electron microscopy

The morphology of the prepared PLA/Cs scaffolds was studied with scanning electron microscopy (SEM). The average diameter of the mats was measured by analyzing SEM images using Image J software (National Institutes of Health, USA). The diameter distribution was measured by examining at least 100 samples. To observe hWJMSCs cultured on PLA/Cs nanocomposite scaffolds, the samples were fixed with 2.5% glutaraldehyde for 2 hours. Then they were washed in phosphate buffer saline (PBS, Sigma, USA) and dehydrated in ethanol series (30, 50, 70, 80, 90 and 100%) at 37ºC for 15 minutes per solution. Then the scaffolds were sputter-coated with gold and studied by a SEM (model Philips XL-30, Netherland), operated at 15 kV.

Isolation and identification of hWJMSCs

Human WJMSCs were obtained as described previously (17, 18). In summary, human umbilical cord was obtained after delivery from term natural births. The cord blood was removed immediately, then it was cut into 1-centimeter pieces and washed. The pieces were soaked in PBS supplemented with 3% (v/v) pen/strep for 24 hours. The stem cells were isolated by explant cultures as each piece was cut carefully with a scalpel, then the vessels were removed and wharton jelly was collected. Then the jelly was sliced into 2-millimeter pieces, cultured in tissue culture flasks and maintained for 14 days to allow for cell migration and expansion. DMEM low glucose medium supplemented with 10% fetal bovine serum (FBS, Gibco, USA) and 1% penicillin/streptomycin was used and the medium was changed every 3 days as the cells were passaged by 0.25% trypsin. Also, hWJMSCs were characterized by flow cytometry for cell surface markers. Briefly, hWJMSCs were incubated with specific antibodies including CD146 (endometrial stem cell markers, 1:200, Santa Cruz, USA), CD90 (1:200, Santa Cruz, USA), CD105 (1:100, Santa Cruz, USA), CD34 (hematopoietic marker, 1:100, Santa Cruz, USA), and CD31 (endothelial marker, 1:100, Santa Cruz, USA) for 60 minutes at room temperature and analyzed by flow cytometry (Becton Dickinson, USA) after washing. Also, for differentiation of hWJMSCs into adipocytes and osteocytes, the cells were seeded at a concentration of 5×10^4 cells/well in a 24-well plate. When the cells reached 80% confluency, the medium was replaced with adipogenic- or osteogenic-inducing media as described previously (17). The differentiated cells were stained with Oil Red or Alizarin Red to detect adipocytes or osteocytes, respectively.

Assessment of cell viability

The viability of the hWJMSCs seeded on the PLA/CS scaffolds was assessed by the MTT (3-(4, 5-Dimethylthiazol-2)-2, 5-diphenyltetrazolium bromide) reduction assay. 6×10^4 cells were cultured on each scaffold

and incubated for 24 hours at 37°C in an incubator with 5% Co_2. Afterward, 300 µl of 0.5 mg/ml MTT solution was added to each well, and the plates were incubated for 3-4 hours at 37°C then the medium was removed, and DMSO was added to dissolve the formazan crystals. The samples were shaken by a mechanical shaker, next the absorbance was read at the wavelength of 490 nanometers in a microplate reader (Fax 2100, USA).

Acridine orange staining

For acridine orange/ethidium bromide double staining (Sigma, USA), 1 mg/ml ethidium bromide dye and 1 mg/ml acridine orange dye were prepared and mixed at a 1:1 ratio. After that, the cells were seeded on scaffolds (after 48 hours), were stained for 3 minutes and then examined under a fluorescent microscope (Olympus, Japan).

Human WJMSCs culture and differentiation into definitive endoderm cells

The cultured cells on PLA/Cs scaffolds were induced to differentiate using two different protocols. The first: the hWJMSCs were cultured on PLA/Cs scaffold and treated with 20 µM SKL2001 (Sigma, USA) and 0.2% FBS for 6 days. The second: the cells were cultured on PLA/Cs scaffold and treated with 20 µM SKL2001 in combination with 50 µg/ml nZnO (Loletics Germany, ≥70 nm avg.) for 6 days. As a control, hWJMSCs were cultured on the PLA/Cs scaffolds in the absence of differentiation factors for 6 days. DMEM medium was used during the differentiation phase. This medium was supplemented with FBS at 0.2% and 10% concentrations in the experimental and control groups, respectively. The medium in cell culture plates was replaced with fresh medium every two days.

RNA extraction and reverse transcriptase-polymerase chain reaction

The mRNA expression was examined by quantitative reverse transcriptase-polymerase chain reaction (qRT-PCR). On day 6 days of the culture, the cells were lysed by QIAzol lysis reagent (Qiagen, Hilden, Germany) and the total RNA was extracted according to the manufacturer's instructions. The extracted RNA (3 µg) was reverse transcribed by the TaqMan Reverse Transcription Kit (Applied Biosystems, CA, USA). QRT-PCR reactions were performed in 6-well plates in a StepOne™ Real-Time PCR machine (Corbett, Australia) using primers that are shown in Table 1. QRT-PCR was performed by SYBR green Supermix (Ampliqon, Denmark) and the applied protocol was: initial denaturation (95°C for 30 seconds), amplification (95°C for 5 seconds and 60°C for 33 seconds), and melting (95°C for 15 seconds, 60°C for 60 seconds, and 95°C for 1 second). The target genes' threshold cycle (Ct) was obtained from the StepOne software, and the values were normalized by *GAPDH*.

Immunofluorescence staining

The samples were fixed with paraformaldehyde (4%, Sigma, USA) for 40 minutes and permeabilized with 0.1% Triton X-100 in PBS at room temperature. Then the samples were blocked for 1 hour with 5% bovine serum albumin (BSA, Sigma, USA) at room temperature and stained with primary antibodies against human *FOXA2* (1: 500, Polyclonal rabbit IgG, Millipore, Germany, AB4125) and human *SOX17* (1: 20, Polyclonal Goat IgG, R&D, USA, AF1924) overnight at 4°C. After that, the samples were stained with secondary antibodies [Alexa fluor 594 donkey anti-rabbit (1:200, Gibco, USA, A-21207) or Alexa fluor 488 donkey anti-goat (1:200, Gibco, USA, A-11058)] for 60 minutes at room temperature. The cell nuclei were stained with DAPI (1 µg/ml, Sigma, USA, D8417) for 5 minutes and the samples were imaged under a fluorescent microscope (Olympus, Japan).

Statistical analysis

The data are presented as means ± standard deviation (SD) of three replications. Statistical analyses were carried out by a one-way ANOVA method followed by unpaired Student's t test and $P \leq 0.05$ was designated as significant difference. We used SPSS software version 16.

Table 1: Sequences of the quantitative reverse transcriptase-polymerase chain reaction (qRT-PCR) primers

Gene	Primer sequence (5´-3´)	Accession number	Product length (bp)
Forkhead box A2 (*FOXA2*)	F: GAGACAAATCTCAGCCTCCCA R: CGTTCTCGAACATGTTGCCC	NM_153675.3	110
SRY (sex determining region Y)-box 17 *(S0X17)*	F: TCAGCAAGCAGCTGGGATAC R: AACTGCAATTCTTCGGCAG	NM_003140.3	162
Goosecoid homeobox (*GSC*)	F: AACGCGGAGAAGTGGAACAA R: AGCATCGTCTGTCTGTGCA	NM_173849.3	158
GAPDH	F: CCATGGGGAAGGTGAAGGT R: AGTGATGGCATGGACTGTG	NM_002046.7	548

Results

Characterization of hWJMS cells

Human WJMSCs readily adhered to the bottom of the flask and were extractable. After 2 weeks, the cells were fully attached to the bottom of the flasks and had grown to 80% confluency. At this point they were passaged one last time and reached to the third passage, after which they were used for treatment. As shown in Figure 1, under the inverted microscope, the cells appeared to be normal with elongated and spindle-like shapes (Fig.1A). To confirm multipotency of the isolated hWJMSCs, they were treated with osteogenic and adipogenic inductive media, and their differentiation was confirmed by Alizarin Red, and Oil Red O staining, respectively (Fig.1B, C). In addition, when evaluating their cell surface markers by flow cytometry, our results indicated that the cells were expressing CD105, CD90, and CD146 markers, but not CD31 and CD34 (Fig.1D).

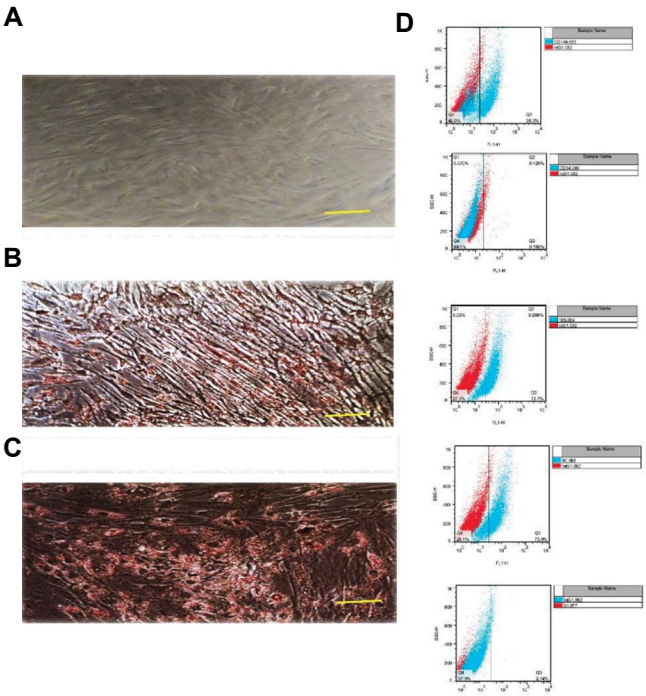

Fig.1: Characterization of human Wharton's jelly mesenchymal stem cells (hWJMSCs). **A.** Typical observation of hWJMSCs under phase-contrast microscopy. **B.** Differentiation of hWJMSCs into osteoblasts as shown by Alizarin Red staining. **C.** Differentiation of hWJMSCs into adipocytes as shown by Oil Red O staining. **D.** Flow cytometric analysis of the isolated hWJMSCs for MSC (CD146, CD105, and CD90), and hematopoietic (CD34) and endothelial (CD31) markers (scale bar: 100 µm).

Morphology of the electrospun PLA/Cs nanocomposite scaffold

We produced the PLA/Cs nanocomposite scaffolds by a solution blending method. As shown in Figure 1, the nanocomposite was a homogeneous scaffold with high porosity and average diameter of 70 micrometers. Also, the average thickness of this scaffold was about 460 micrometers. Indeed, the SEM images indicated random fibers without any beads with an improved porous network. Also, the study of culturing the adherent cells on the scaffold revealed that numerous hWJMSCs were attached and scattered on PLA/Cs scaffold after 72 hours following the seeding (Fig.2). These results proved that the PLA/Cs scaffold effectively supported cellular adhesion and growth of the hWJMSCs.

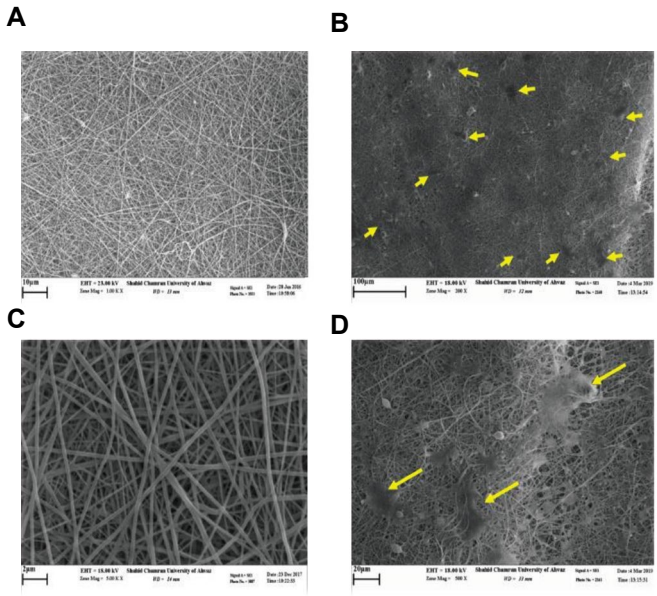

Fig.2: Scanning electron micrographs show the morphology of the plated human Wharton's jelly mesenchymal stem cells (hWJMSCs) on polylactic acid/chitosan (PLA/Cs) scaffold on day 3 after seeding. **A.** The fibers of PLA/Cs scaffold were randomly entangled to form a strong, flexible, and porous 3D matrix. **B.** The fibers of PLA/Cs scaffold with higher magnification, **C.** The plated hWJMSCs on PLA/Cs scaffold, **D.** The plated hWJMSCs on PLA/Cs scaffold with higher magnification. Yellow arrows show the plated hWJMSCs on the scaffold.

Measurement of cell viability

In this study, we evaluated cell viability of hWJMSCs on PLA/Cs scaffolds using the MTT assay for 6 days. Three days after plating the cells, no significant difference was observed between the viability of cells on PLA/Cs scaffold and the monolayer culture ($P<0.05$). However, on days 4 and 6 of the culture, the viability of the cells on PLA/Cs scaffolds significantly increased ($P<0.05$) compared to the monolayer culture. Therefore, it suggests that there is a time-dependent increase in stability and viability of the hWJMSCs on the nanocomposite scaffold compared to the monolayer culture (Fig.3A).

Acridine orange staining

Acridine orange is a double staining, such that live cells turn green, while apoptotic cells are orange, and if cells are in late stages of apoptosis, the nuclei get fragmented, compacted, and red. Our result suggested that the cultured cells on the PLA/Cs scaffold were normal, clear, green and without shrinkage, proving their viability (Fig.3).

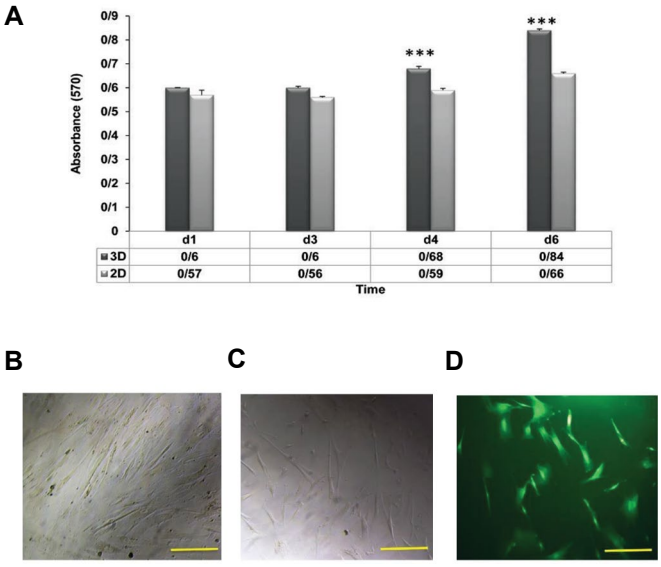

Fig.3: MTT assay and morphological study of hWJMSCs by an inverted microscope. **A.** Formosan absorbance has been expressed as a measure of cell viability from the hWJMSCs cultured on nanocomposite scaffold for 6 days. **B.** Passage 1 hWJMSCs after 3 days in culture, **C.** Passage 3 hWJMSCs after 7 days, **D.** The cell viability assay using acridine orange/ethidium bromide staining of hWJMSCs was performed on the cells cultured on PLA/Cs scaffold by fluorescent microscopy after 2 days (B, C, and D represent ×200, ×200, and ×100 magnification, respectively, scale bar: 100 µm). hWJMSCs; Human Wharton's jelly mesenchymal stem cells, PLA/Cs; Polylactic acid/chitosan, and ***; P<0.05 and values are mean (n=3).

Differentiation of hWJMSCs into definitive endoderm cells

To distiguish DE cells from hWJMSCs, two protocols (SKL2001 or SKL2001/ nZnO) were used and their efficiencies were compared. As shown in Figure 4, in response to SKL2001 induction, the expression of the hallmark genes of DE i.e. *FOXA2*, *SOX17*, and *GSC* were increased about 130, 159, and 90-fold, respectively. Also, the induction of hWJMSCs with SKL2001/nZnO resulted in a significant increase in the expression levels of *FOXA2*, *SOX17*, and *gsc* genes to 141, 204, and 92 folds, respectively. The expression levels of *FOXA2* and *SOX17* were also significantly higher (P<0.05) than their expressions in the cells induced by SKL2001 alone, but no obvious difference in *GSC* expression was found between these two groups (Fig.4). In this research, mRNAs expression of the DE marker genes in both experimental groups was significantly more than that in the control group. Based on these data, treatment with SKL2001 or especially with SKL2001/nZnO could obviously induce the differentiation of hWJMSCs into DE cells.

Immunocytochemical technique was performed for further evaluation of the more effective protocol i.e. SKL2001/nZnO. This analysis of the hWJMSCs-derived DE sample suggested that the main population of DE cells expressed SOX17 and FOXA2 proteins within the nuclei. Therefore, treatment with SKL2001/nZnO could successfully induce differentiation into DE cells (Fig.5).

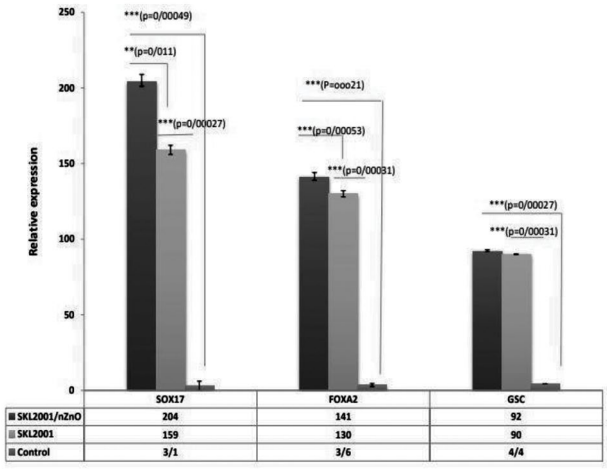

Fig.4: Quantitative expression analysis of DE cells derived from hWJMSCs cultured on PLA/Cs scaffold after 6 days. The results are collected from 3 independent experiments with 2 internal replicates per experiment. Differences observed were statistically significant when P≤0.05. Comparison of the gene expression levels of DE markers (*FOXA2*, *SOX17*, and *GSC*) in two experimental groups. hWJMSCs; Human Wharton's jelly mesenchymal stem cells, PLA/Cs; Polylactic acid/chitosan, DE; Definitive endoderm, ***; P<0.001, and **; P<0.01 untreated cells were considered as a control group.

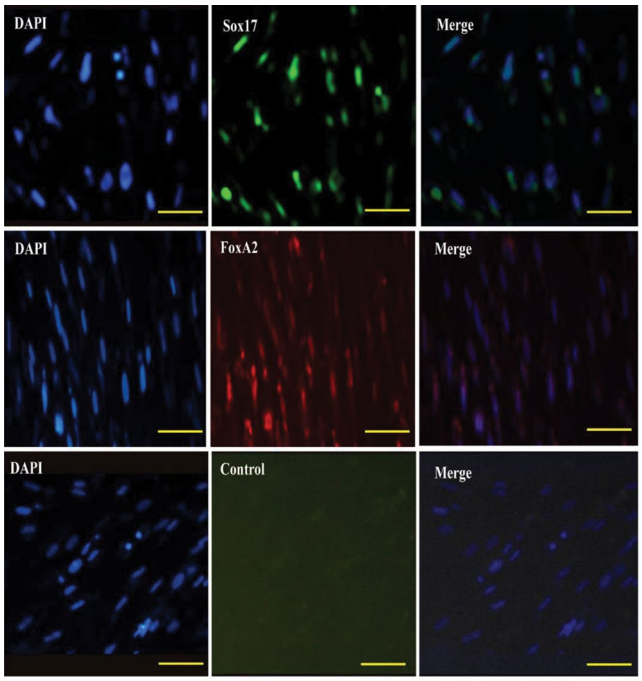

Fig.5: Immunocytochemistry performed for analyzing SOX17 and FOXA2 as endoderm-specific proteins by differentiated hWJMSCs on the scaffold after 6 days of culture. The staining of nuclei was performed by DAPI (×400 magnification, scale bar: 100 µm).

Discussion

In the present study, we have assessed the potentials of differentiation of hWJMSCs into DE cells using SKL2001 as a small molecule and nZnO as a nanoparticle on an electrospun nanocomposite scaffold. The analysis of qRT-PCR demonstrated that the expression of endodermal marker genes such as *FOXA2*, *SOX17*, and *GSC* in experimental groups were significantly more than the control group. Using immunocytochemistry, we also evaluated the expression levels of the protein products of these genes.

We can define tissue engineering as a multidisciplinary approach that provides a promising strategy for regenerative medicine (19). Various research projects have demonstrated the advantages of tissue engineering as a suitable therapeutic strategy for induction of cell differentiation (20, 21). Interestingly, these studies have proven that the use of tissue engineering improves cell proliferation, survival, and cell-cell interactions comparing to monolayer cultures (22-24). Today, the administration of synthetic polymers to prepare scaffolds has significantly increased, which is due to their suitable mechanical properties, cost-effectiveness, and convenient fabrication processes. Furthermore, polymer blending methods have been used to improve the hydrophilic properties of synthetic polymers and the adhesion of cells to scaffolds (25-28). In our study, PLA/Cs, as a blended scaffold, was a biocompatible and suitable scaffold in promoting cell viability and attachment. Also, the infiltration and extension of the cells into the PLA/Cs scaffold was confirmed by SEM studies. Furthermore, according to our results, the DE differentiation with high efficiency in the expression of *SOX17* was due to the treatment of hWJMSCs seeded on PLA/Cs with SKL2001 and nZnO.

It has been proved that the formation of DE can be considered as the first and most critical stage in the generation of stem cell-derived hepatocytes, beta cells, and other endoderm derived organs (29-31). D'Amour et al. (29) in 2006 presented a protocol for efficient induction of DE cells. Because of the high efficiency of this protocol, generally it has been used by many research groups (32, 33). Based on the recent studies, to induce DE cells from different stem cells, several factors including Nodal, Wnt3a, Activin A, and some of the small molecules have been used (31). For example, Borowiak et al. (34) showed that inducer of DE1 as a small molecule could increase DE differentiation, comparable to those induced by Activin A. In the present study, our results indicated that SKL2001/nZnO combination offers a practical method for DE differentiation from hWJMSCs in a 3D culture.

Previous studies have reported that zinc is effective in glucose metabolism, promoting hepatic glycogenesis by acting on insulin pathways and improving glucose utilization. Zinc plays an essential role in biosynthesis, secretion, and storage of insulin because it protects insulin structure. Moreover, beta cells contain several zinc transporters that stimulate insulin secretion (35). Also, nZnO has antidiabetic effects and it can decrease blood glucose, inhibit glucokinase (GK) activity, increase insulin level, and stimulate the expression of glucose transporter 2 in diabetic rats (12). Besides, in some studies, it has been reported that zinc ions act as signalling molecules (36, 37). Thus, we can divide the intracellular zinc functions into two categories: i. Protein binding zinc, contributing to enzyme's activity and structure protection, and ii. Labile zinc, with is non-binding to proteins and acts as a signal transferring molecule (38). Based on the existing evidence, nZnO may be conducive to the differentiation of DE through signaling pathways, especially by inhibiting GK activity. In this study we showed that the small molecule SKL2001 has synergistic effects with nZnO in induction of DE cell formation. We conclude that in this induction pathway, nZnO has synergies with SKL2001 via activation of β-catenin signaling, since nZnO can activate Wnt/β-catenin indirectly by inhibiting GK.

The Wnt/β-catenin has important functions in differentiation processes of various cells such as MSCs. Gwak et al. (39) in 2012 introduced SKL2001 as a novel agonist of the Wnt/β-catenin pathway after screening 270 000 synthetic chemical compounds. They identified the molecular mechanism of SKL2001, which leads to release of β-catenin, by opening up the Axin/β-catenin bond.

Maschio et al. declared that Wnt/β-catenin agonist plays a crucial function in cell differentiation and proliferation during embryogenesis. They specifically demonstrated that there is a relationship between the Wnt/β-catenin pathway and type 2 diabetes. Also, they found that the unregulated Wnt/β-catenin pathway leads to the disruption of beta cells in the early phase of diabetes (40).

Conclusion

Our findings indicated that the PLA/Cs nanocomposite scaffolds provide a protective and suitable environment for hWJMSCs' growth and viability. Here we showed for the first time that the small molecule SKL2001 as a Wnt/β-catenin pathway agonist could induce differentiation of hWJMSCs into DE cells. Also, our results showed that the treatment of hWJMSCs with SKL2001 combined with nZnO had a synergistic effect on DE cell induction. It has been suggested that we can provide an efficient method with the functional differentiation of DE cells via combining a suitable scaffold with essential supplements and a reliable cellular source. These results be used for further differentiation into pancreatic and hepatocytes cells.

Acknowledgments

The authors are sincerely grateful to Shahid Chamran University of Ahvaz (grant number 98). This study was financially supported by the Iran National Science Foundation (INSF) vice presidency for science and technology. The authors declare that there are no conflicts of interest.

Authors' Contributions

E.H.; Contributed to conception, design, all experimental work, and were responsible for overall supervision. S.T.; Contributed to data and statistical analysis, interpretation of data, and drafted the manuscript. All authors read and approved the final manuscript.

References

1. Li XY, Wu SY, Leung PS. Human fetal bone marrow-derived mesenchymal stem cells promote the proliferation and differentiation of pancreatic progenitor cells and the engraftment function of islet-like cell clusters. Int J Mol Sci. 2019; 20(17): 4083.
2. Cabezas J, Rojas D, Navarrete F, Ortiz R, Rivera G, Saravia F, et al. Equine mesenchymal stem cells derived from endometrial or adipose tissue share significant biological properties, but have distinctive pattern of surface markers and migration. Theriogenology. 2018; 106: 93-102.
3. Kamolz LP, Keck M, Kasper C. Wharton's jelly mesenchymal stem cells promote wound healing and tissue regeneration. Stem Cell Res Ther. 2014; 5(3): 62.
4. Jurewicz E, Wyroba E, Filipek A. Tubulin-dependent secretion of S100A6 and cellular signaling pathways activated by S100A6-integrin β1 interaction. Cell Signal. 2018; 42: 21-29.
5. Ghorbani-Dalini S, Azarpira N, Sangtarash MH, Soleimanpour-Lichaei HR, Yaghobi R, Lorzadeh S, et al. Optimization of activin-A: a breakthrough in differentiation of human induced pluripotent stem cell into definitive endoderm. 3 Biotech. 2020; 10(5): 215.
6. Mobarra N, Soleimani M, Ghayour-Mobarhan M, Safarpour S, Ferns GA, Pakzad R, et al. Hybrid poly-l-lactic acid/poly(ε-caprolactone) nanofibrous scaffold can improve biochemical and molecular markers of human induced pluripotent stem cell-derived hepatocyte-like cells. J Cell Physiol. 2019; 234(7): 11247-11255.
7. Hoveizi E, Tavakol S, Shirian S, Sanamiri K. Electrospun nanofibers for diabetes: tissue engineering and cell-based therapies. Curr Stem Cell Res Ther. 2019; 14(2): 152-168.
8. D'Amour KA, Agulnick AD, Eliazer S, Kelly OG, Kroon E, Baetge EE. Efficient differentiation of human embryonic stem cells to definitive endoderm. Nat Biotechnol. 2005; 23(12): 1534-1541.
9. He C, Sun J, Liu C, Jiang Y, Hao Y. Elevated H3K27me3 levels sensitize osteosarcoma to cisplatin. Clin Epigenetics. 2019; 11(1): 8.
10. Ghasemi-Mobarakeh L, Morshed M, Karbalaie K, Fesharaki MA, Nematallahi M, Nasr-Esfahani MH, et al. The thickness of electrospun poly (epsilon-caprolactone) nanofibrous scaffolds influences cell proliferation. Int J Artif Organs. 2009; 32(3): 150-158.
11. Jalali MT, Dayer D, Haghighizadeh MH, Karandish M. Very high prevalence of zinc deficiency in elderly hospitalized patients in Ahvaz, Iran. Saudi Med J. 2001; 32, 314-315.
12. Umrani RD, Paknikar KM. Zinc oxide nanoparticles show antidiabetic activity in streptozotocin-induced Type 1 and 2 diabetic rats. Nanomedicine (Lond). 2014; 9(1): 89-104.
13. Masia F, Glen A, Stephens P, Langbein W, Borri P. Label-free quantitative chemical imaging and classification analysis of adipogenesis using mouse embryonic stem cells. J Biophotonics. 2018; 11(7): e201700219.
14. Silva M, Ferreira FN, Alves NM, Paiva MC. Biodegradable polymer nanocomposites for ligament/tendon tissue engineering. J Nanobiotechnology. 2020; 18(1): 23.
15. Ebrahimi-Barough S, Hoveizi E, Yazdankhah M, Ai J, Khakbiz M, Faghihi F, et al. Inhibitor of PI3K/Akt signaling pathway small molecule promotes motor neuron differentiation of human endometrial stem cells cultured on electrospun biocomposite polycaprolactone/collagen scaffolds. Mol Neurobiol. 2017; 54(4): 2547-2554.
16. Hoveizi E, Mohammadi T. Differentiation of endometrial stem cells into insulin-producing cells using signaling molecules and zinc oxide nanoparticles, and three-dimensional culture on nanofibrous scaffolds. J Mater Sci Mater Med. 2019; 30(9): 101.
17. Hashemitabar M, Allahbakhshi E, Tabande MR, Orazizadeh M, Nejad Dehbashi F, Azandeh S, et al. Isolation and characterization of human umbilical cord mesenchymal stem cells and their differentiation into Pdx-1+ cells. J Biomed Eng. 2015; 8: 780-788.
18. Hoveizi E, Tavakol S. Therapeutic potential of human mesenchymal stem cells derived beta cell precursors on a nanofibrous scaffold: an approach to treat diabetes mellitus. J Cell Physiol. 2019; 234(7): 10196-10204.
19. Hoveizi E, Ebrahimi-Barough S, Tavakol S, Nabiuni M. In vitro comparative survey of cell adhesion and proliferation of human induced pluripotent stem cells on surfaces of polymeric electrospun nanofibrous and solution-cast film scaffolds. J Biomed Mater Res A. 2015; 103(9): 2952-2958.
20. Chayosumrit M, Tuch B, Sidhu K. Alginate microcapsule for propagation and directed differentiation of hESCs to definitive endoderm. Biomaterials. 2010; 31(3): 505-514.
21. Wang YJ, Qiao J, Baker R, Zhang J. Alkaline polymer electrolyte membranes for fuel cell applications. Chem Soc Rev. 2013; 42(13): 5768-5787.
22. Lai JY. Corneal stromal cell growth on gelatin/chondroitin sulfate scaffolds modified at different NHS/EDC molar ratios. Int J Mol Sci. 2013; 14(1): 2036-2055.
23. Serra T, Planell JA, Navarro M. High-resolution PLA-based composite scaffolds via 3-D printing technology. Acta Biomater. 2013; 9(3): 5521-5530.
24. Yim EK, Leong KW. Proliferation and differentiation of human embryonic germ cell derivatives in bioactive polymeric fibrous scaffold. J Biomater Sci Polym Ed. 2005; 16(10): 1193-1217.
25. Kim HW, Yu HS, Lee HH. Nanofibrous matrices of poly(lactic acid) and gelatin polymeric blends for the improvement of cellular responses. J Biomed Mater Res A. 2008; 87(1): 25-32.
26. Meng ZX, Wang YS, Ma C, Zheng W, Li L, Zheng YF. Electrospinning of PLGA/gelatin randomly-oriented and aligned nanofibers as potential scaffold in tissue engineering. Mater Sci Eng. 2010; 30(8): 1204-1210.
27. Hoveizi E, Nabiuni M, Parivar K, Rajabi-Zeleti S, Tavakol S. Functionalisation and surface modification of electrospun polylactic acid scaffold for tissue engineering. Cell Biol Int. 2014; 38(1): 41-49.
28. Zhang Y, Ouyang H, Lim CT, Ramakrishna S, Huang ZM. Electrospinning of gelatin fibers and gelatin/PCL composite fibrous scaffolds. J Biomed Mater Res B Appl Biomater. 2005; 72(1): 156-165.
29. D'Amour KA, Bang AG, Eliazer S, Kelly OG, Agulnick AD, Smart NG, et al. Production of pancreatic hormone-expressing endocrine cells from human embryonic stem cells. Nat Biotechnol. 2006; 24(11): 1392-1401.
30. Jiang W, Shi Y, Zhao D, Chen S, Yong J, Zhang J, et al. In vitro derivation of functional insulin-producing cells from human embryonic stem cells. Cell Res. 2007; 17(4): 333-344.
31. Kopper O, Benvenisty N. Stepwise differentiation of human embryonic stem cells into early endoderm derivatives and their molecular characterization. Stem Cell Res. 2012; 8(3): 335-345.
32. Hoveizi E, Massumi M, Ebrahimi-barough S, Tavakol S, Ai J. Differential effect of Activin A and WNT3a on definitive endoderm differentiation on electrospun nanofibrous PCL scaffold. Cell Biol Int. 2015; 39(5): 591-599.
33. Wartchow KM, Rodrigues L, Suardi LZ, Federhen BC, Selistre NG, Goncalves CA, et al. Short-term protocols to obtain insulin-producing cells from rat adipose tissue: signaling pathways and in vivo effect. Int J Mol Sci. 2019; 20(10): 2458.
34. Borowiak M, Maehr R, Chen S, Chen AE, Tang W, Fox JL, et al. Small molecules efficiently direct endodermal differentiation of mouse and human embryonic stem cells. Cell Stem Cell. 2009; 4(4): 348-358.
35. Wijesekara N, Chimienti F, Wheeler MB. Zinc, a regulator of islet function and glucose homeostasis. Diabetes Obes Metab. 2009; 4: 202-214.
36. Fukada T, Kambe T. Molecular and genetic features of zinc transporters in physiology and pathogenesis. Metallomics. 2011; 3(7): 662-674.
37. Haase H, Rink L. Zinc signals and immune function. Biofactors. 2014; 40(1): 27-40.
38. Lu Q, Haragopal H, Slepchenko KG, Stork C, Li YV. Intracellular zinc distribution in mitochondria, ER and the Golgi apparatus. Int J Physiol Pathophysiol Pharmacol. 2016; 8(1): 35-43.
39. Gwak J, Hwang SG, Park HS, Choi SR, Park SH, Kim H, et al. Small molecule-based disruption of the Axin/beta-catenin protein complex regulates mesenchymal stem cell differentiation. Cell Res. 2012; 22(1): 237-247.
40. Maschio DA, Oliveira RB, Santos MR, Carvalho CP, Barbosa-Sampaio HC, Collares-Buzato CB. Activation of the Wnt/β-catenin pathway in pancreatic beta cells during the compensatory islet hyperplasia in prediabetic mice. Biochem Biophys Res Commun. 2016; 478(4): 1534-1540.

Original Article

Mesenchymal Stromal Cell Therapy Improves Refractory Perianal Fistula in Crohn's Disease: Case Series Clinical Interventional Study

Massoud Vosough, M.D., Ph.D.[1#*], Sepideh Nikfam, M.D.[2#], Shukoofeh Torabi, Ph.D.[1#], Bahareh Sadri, M.Sc.[1], Hadi Ahmadi Amoli, M.D.[3], Ali Basi, M.D.[4], Maryam Niknejadi, M.D.[5], Nikoo Hossein-Khannazer, Ph.D.[6], Seyedeh-Esmat Hosseini, Ph.D.[1], Soura Mardpour, Ph.D.[1], Vajiheh Azimian, Ph.D.[1], Neda Jaroughi, M.Sc.[1], Nasser Aghdami, Ph.D.[1], Hamid Reza Amirzehni, M.D.[2], Amir Anushirvani, M.D.[2], Reza Malekzadeh, M.D.[2], Hossein Baharvand, Ph.D.[7, 8*], Mehdi Mohamadnejad, M.D.[2*]

1. Department of Regenerative Medicine, Cell Science Research Center, Royan Institute for Stem Cell Biology and Technology, ACECR, Tehran, Iran
2. Liver and Pancreatobiliary Diseases Research Center, Digestive Diseases Research Institute, Tehran University of Medical Sciences, Tehran, Iran
3. Sina Trauma and Surgery Research Center, Tehran University of Medical Sciences, Tehran, Iran
4. Department of Hematology Oncology, Iran University of Medical Sciences, Tehran, Iran
5. Department of Reproductive Imaging, Reproductive Biomedicine Research Center, Royan Institute for Reproductive Biomedicine, ACECR, Tehran, Iran
6. Department of Immunology, School of Medicine, Shahid Beheshti University of Medical Sciences, Tehran, Iran
7. Department of Stem Cells and Developmental Biology, Cell Science Research Center, Royan Institute for Stem Cell Biology and Technology, ACECR, Tehran, Iran
8. Department of Developmental Biology, School of Basic Sciences and Advanced Technologies in Biology, University of Science and Culture, Tehran, Iran

 # These authors contributed equally to this work.

**Corresponding Addresses: P.O.Box: 16635-148, Department of Regenerative Medicine, Cell Science Research Center, Royan Institute for Stem Cell Biology and Technology, ACECR, Tehran, Iran*
P.O.Box: 16635-148, Department of Stem Cells and Developmental Biology, Cell Science Research Center, Royan Institute for Stem Cell Biology and Technology, ACECR, Tehran, Iran
P.O.Box: 1665659911, Liver and Pancreatobiliary Diseases Research Center, Digestive Diseases Research Institute, Tehran University of Medical Sciences, Tehran, Iran
Emails: masvos@royaninstitute.org, Baharvand@royaninstitute.org, mehdi.nejad@gmail.com

Received: 20/February/2021, Accepted: 09/May/2021

Abstract

Objective: Perianal fistulas in Crohn's disease (CD) are the main challenges in inflammatory bowel diseases (IBDs). Some of the fistulas are refractory to any therapeutic strategy. The aim of this study was to evaluate the therapeutic effects of mesenchymal stromal cells (MSCs) as a novel promising modality for the treatment of fistulizing CD.

Materials and Methods: This case series clinical interventional study was conducted from 2014 to 2017 at Shariati Hospital, an IBD referral center in Tehran, Iran. Refractory adult patients with CD who had draining perianal fistulas were enrolled in this study. All patients were examined by a colorectal surgeon and the fistula imaging studies were performed by pelvic magnetic resonance imaging (MRI). After autologous bone marrow (BM) aspiration and MSCs isolation, the cells were cultured and passaged under current good manufacturing practice (cGMP) conditions. Four intra-fistula injections of cells, each containing 40×10^6 MSCs suspended in fibrin glue, were administered by an expert surgeon every 4 weeks. Procedure safety, feasibility and closure of the perianal fistulas at week 24 were assessed. Clinical examination and MRI findings were considered as the primary end points.

Results: In total, 5 patients (2 males and 3 females) were enrolled in this study. No adverse events were observed during the six-month follow-up in these patients. Both the Crohn's Disease Activity Index (CDAI) and Perianal Disease Activity Index (PDAI) scores decreased in all patients after cell injections and one patient achieved complete remission with closure of fistulas, discontinuation of fistula discharge, and closure of the external opening.

Conclusion: Local injection of MSCs combined with fibrin glue is potentially a safe and effective therapeutic approach for complex perianal fistulas in patients with CD.

Keywords: Cell Therapy, Crohn's Disease, Mesenchymal Stromal Cells, Perianal Fistulas

Cell Journal(Yakhteh), Vol 24, No 2, February 2022, Pages: 62-68

Citation: **Vosough M, Nikfam S, Torabi Sh, Sadri B, Ahmadi Amoli H, Basi A Niknejadi M, Hossein-Khannazer N, Hosseini SE, Mardpour S, Azimian V, Jaroughi N, Aghdami N, Amirzehni HR, Anushirvani A, Malekzadeh R, Baharvand H, Mohamadnejad M. Mesenchymal stromal cell therapy improves refractory perianal fistula in crohn's disease: case series clinical interventional study. Cell J. 2022; 24(2): 62-68. doi: 10.22074/cellj.2022.7981.**

Introduction

Crohn's disease (CD) is a chronic inflammatory condition characterized by transmural involvement of the gastrointestinal tract and fistula formation. Patients may suffer from fissures, canal stenosis and fistulas with or without abscess (1, 2). Perianal fistulas are one of the most disabling complications and a source of morbidity for CD patients. The cumulative incidence of perianal fistulas in patients with CD ranges from 18 to 43% (3, 4).

Understanding the pathogenesis of CD has revealed that unresolved chronic inflammation triggers the recruitment of activated immune cells including lymphocytes and macrophages over time. Production of tumour necrosis factor alpha (TNF-α), interleukin-12 (IL-12), IL-17 and IL-23 inflammatory cytokines in addition to impairments in healing mechanisms can cause epithelial defects and fistula formation (5-7). Adversely, diagnosis and optimal management of perianal fistulizing CD is challenging, as many patients do not respond to approved and available medical therapies that include administration of antibiotics, immunomodulators, and biological agents (8). Patients with perianal fistulas unresponsive to conventional medical or biological treatments should undergo surgical therapy. However, only one third of patients with complex perianal fistula achieve durable remission with either medical or surgical treatments (9). These limitations have encouraged considerable attention in investigating new alternative treatment options for perianal fistulizing CD.

Recently, stem cell therapy has become a highly promising approach to address important challenges in CD patients in general (10, 11). Several studies suggest that mesenchymal stromal cell (MSC) therapy could be an option to improve CD and Crohn's fistula (12, 13). MSCs are multipotent adult stem cells derived from various tissues such as bone marrow (BM), adipose tissue, umbilical cord, and placenta. MSCs are involved in anti-inflammatory events and tissue repair through their immunomodulatory, anti-fibrotic, and pro-angiogenic properties. MSCs suppress the proliferation of CD4+ and CD8+ T lymphocytes and natural killer cells (NK), stimulate the proliferation of regulatory T cells, and suppress immunoglobulin production through secretion of various bioactive molecules and cytokines (14, 15). MSC therapy has shown encouraging results in the treatment of refractory fistulizing CD. Clinical applications of MSCs have demonstrated their efficacy and safety as a promising alternative for the currently available treatments of perianal fistulas in CD. Moreover, local administration of autologous MSCs have shown significantly higher healing rate (HR) compared to the allogenic MSCs (16, 17).

Advances in cell replacement therapies have resulted in development of advanced therapy medicinal products (ATMPs) for the treatment of inflammatory bowel disease (IBD) patients. The advantages of MSCs for tissue repair and regeneration make them promising tools for treatment of inflammatory diseases. Recently, three adipose tissue-derived (AD)-MSC-based cell therapy products received approval for treatment of fistula in CD. Cupistem®, which is the first approved autologous AD-MSCs product, was developed by Anterogen Company (South Korea) and approved by the South Korea Ministry of Food and Drug Safety (MFDS) in 2012. Alofisel (darvadstrocel), which was an allogeneic product co-developed by TiGenix (USA) and Takeda (UK) pharmaceutical Companies, was approved by the European Medicines Agency (EMA) in 2018, and finally, Ryoncil (remestemcel-L) was developed by Mesoblast Company and is currently in an ongoing phase 1/2 clinical trial (18). The aim of this study was to evaluate the safety, feasibility and efficacy of intrafistula injection of autologous BM-MSCs suspended in fibrin glue into perianal CD fistulas that were refractory to conventional medical therapy.

Materials and Methods

Mesenchymal stromal cells isolation, expansion and characterization

In this case series clinical interventional study, BM-MSCs were isolated and expanded according to our previous report (19). Briefly, after approval from the Ethics Committee of the research council of digestive disease research institute (DDRI) at Tehran University of Medical Sciences (FWA00001331), each patient signed an informed consent for participation in the study and underwent general physical examination and virus screening, followed by BM aspiration, approximately four weeks before the first cell injection. BM aspiration (100-150 ml) was performed under local anesthesia from the posterior iliac crests of the patients. BM was placed in aseptic blood collection bag and washed with phosphate-buffered saline (PBS, Gibco, USA). Mononuclear cells (MNCs) were isolated by layering them on top of a density gradient solution (Ficol-Hypaque, 1.077 g/ml, Lymphodex; Inno-Train, Kronberg im Taunus, Germany) and were washed twice with PBS buffer. Then, the resuspended MNCs were seeded at a density of 1×10^6 cells/cm^2 in Alpha Modified Eagle's Medium (α-MEM, Life Technologies, USA) supplemented with 10% fetal bovine serum (FBS, Hyclone, USA) and 2 mM L-glutamine (Gibco, USA) in T175 tissue culture flasks. On day 4, the medium was refreshed and nonadherent cells were transferred to new T175 flasks that contained 15 ml fresh medium, in which they were allowed to culture for an additional four days. The medium was refreshed every four days. Once they reached 80% confluency, the MSCs were harvested using trypsin/EDTA (Gibco,

USA) and seeded at a density of 2×10^5 cells/cm^2 in the same condition as before. The cells were passaged 3-4 times consecutively to provide enough cells for administration. After reaching 2×10^8 cells, MSCs were harvested and cryopreserved in 10% dimethyl sulfide (Sigma Aldrich, USA) at -80°C until the time of transplantation.

Quality control evaluation of the MSCs was performed by assessments of cell morphology and viability, immune phenotyping, and cytogenetic analysis, mycoplasma contamination, endotoxin tests using LAL test kit (Lonza, Walkersville, MD, USA; http://www.lonza.com) and microbial contamination test using BACTEC instrument (BD BACTEC; BD Diagnostics, Franklin, NJ, USA; http://www.bd.com).

The expression patterns of MSC specific surface markers (CD90, CD73, CD105, CD44 and CD29) and absence of hematopoietic specific markers (CD34 and CD45) were evaluated by flow cytometry (BD FACSCalibur™ cytometer and FlowJo 7-6-1 software). Table S1 lists the antibodies used in this assessment (See Supplementary Online Information at www.celljournal.org).

Fibrin glue preparation

Fibrin glue/gel is a two-component adhesive material composed of fibrinogen (sealant) and thrombin (catalyst), which is used to adhere tissues together and seal tissue defects. The fibrin glue was prepared from cord-blood-derived platelet rich plasma (PRP). The fibrinogen was precipitated from the PRP by ethanol precipitation at low temperature. The thrombin solution in the fibrin glue was obtained from diluted plasma through adjustment of the pH and centrifugation. Preparation of the fibrin glue was initiated (between 10 to 20 seconds) after mixing the fibrinogen and thrombin in the presence of $CaCl_2$ to convert prothrombin to thrombin. Fibrin Glue is commercially available from Royan Stem Cell Technology Co.

Patient criteria and treatment

This case series clinical interventional study was registered at www.clinicaltrials.gov. The registration number is: NCT01874015. Five patients (two males and three females) with refractory CD and active and persistent perianal fistulas were enrolled in this study.

Each patient signed a written informed consent prior to the study. Inclusion criteria consisted of: 18 years of age or older, confirmed diagnosis of CD for at least six months and presence of active and persistent refractory perianal fistula. Refractory fistula was defined as fistulas unresponsive to immunosuppressive therapy (e.g. azathioprine, 6-mercaptoputine and methotrexate) and/or anti-TNF therapy. The patients received 5-ASA, azathioprine, 6-mercaptoputine, methotrexate, or corticosteroids for at least eight weeks prior to their enrollment. Anti-TNF therapy must have been discontinued at least eight weeks before the enrollment. The exclusion criteria were the diagnosis of of fibrostenotic CD, any history of surgery four weeks prior to enrollment and previous history of any malignancies. Pelvic magnetic resonance imaging (MRI) was used to delineate the anatomy of the fistula track. The primary end point of the study was defined as closure of the treated perianal fistulas at week 24 post-transplantation, as assessed by both clinical examination and MRI. The secondary end points were reductions in Perianal Disease Activity Index (PDAI) and Crohn's Disease Activity Index (CDAI). Fistula closure was defined as the absence of discharge from the external orifice of the fistula after application of manual pressure along with re-epithelialization of the external orifice. Complete response was defined as closure of all fistulas and the absence of collections larger than 2 cm of the treated peri-anal fistulas as evaluated by MRI (9). Partial response was defined as a significant reduction of fistula discharge and a decrease in its diameter based on MRI imaging.

Cell transplantation

A total number of 4×10^7 MSCs were harvested and washed with PBS and re-suspended in sterile normal saline supplemented with 1% human serum albumin (HAS, Octapharma AG, Lachen, Switzerland, http://www.octapharma.com). A mixture of MSCs and fibrinogen, thrombin and calcium chloride (fibrin glue) was infused using a dual syringe injection system to fill both the peri-fistula and inside the fistula tract wall. The cells were injected every four weeks and four injections were performed per subject.

Injection procedure

After enrollment, all patients were examined by a colorectal surgeon. If a perianal abscess was detected, drainage was performed using seton placement and antibiotics were administered (oral ciprofloxacin and metronidazole) for two weeks before the first MSC injection. The injections were performed under local anesthesia and sterile conditions. The MSC suspension was mixed with fibrin glue and injected into the lumen and the walls of the fistula track. An average of 4×10^7 MSCs were transferred at each injection. The patients were monitored for possible adverse reactions such as fever for six hours after the procedure. CDAI (20) and PDAI (21) were calculated for each patient at baseline and at the end of the follow-up. The patients were examined three weeks after each injection, and the subsequent injections were performed every four weeks for up to four injections (Fig.1).

Ethical considerations

After receiving approval from the Ethics Committee of the research council of digestive disease research institute (DDRI) at Tehran University of Medical Sciences, the study conducted accordingly (FWA00001331).

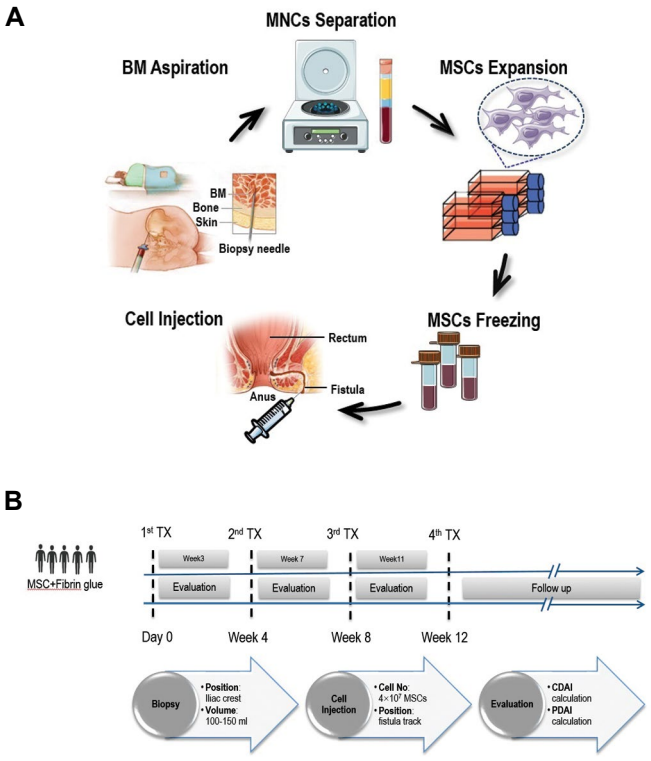

Fig.1: Steps of the injection of autologous BM-MSCs in CD patients. **A.** Isolation, expansion, characterization and intra-fistula injection of BM-MSCs in CD patients. **B.** The process time line of MSC therapy in CD patients. BM-MSCs; Bone marrow-derived mesenchymal stromal cells, CD; Crohn's disease, and MNCs; Mononuclear cells.

Statistical analysis

The student's t test for paired data was used to compare CDAI and PDAI before and after the treatment. The $P<0.05$ was considered as significant.

Results

Table 1 summarizes the patients' baseline characteristics.

Cell characteristics

MSCs from all patients were characterized in terms of cytogenetic integrity (karyotype analysis) identity (morphology), purity (surface marker expression patterns) and viability, according to the guidelines by the International Society for Cellular Therapy (ISCT) for MSCs. The isolated MSCs had a spindle-shaped morphology and expressed the general specific surface markers of MSCs including [CD90 (98.5%), CD73 (90.1%), CD105 (98.3%), CD44 (92%) and CD29 (96.4%)]. However, these cells did not express the hematopoietic stem cell markers [CD34 (1.59%), CD45 (0.06%) or CD11 (0.293%, (Fig.2A-F)]. Karyotype analysis of the expanded MSCs at passage 4 indicated normal karyotype without chromosomal aberrations (Fig.2F). Furthermore, MSCs from all CD patients met all other quality control criteria that included viability by more than 90% and absence of possible microbial contaminations before infusion. Table 2 lists the detailed results of the MNCs and MSC viability and cell count for all the patients.

Table 1: Baseline characteristics of the patients with Crohn's disease and refractory fistulas

Patient number	Age (Y)	Gender	Disease duration (Y)	Disease location	CDAI	PDAI	Previous surgery	Immunosuppressive	Biologics
1	48	F	15	Rectum left colon	169	5	No	Azathioprine	IFX
2	24	M	10	Ileum	99	7	No	Mesalazine	IFX
3	31	F	-	Rectum	166	6	No	Mesalazine	NA
4	31	F	4	Ileum	173	6	No	Azathioprine	NA
5	43	M	3	Ileum	167	9	No	Azathioprine	IFX

CDAI; Crohn's Disease Activity Index, PDAI; Perianal Disease Activity Index, NA; Not applicable, and IFX; Infliximab.

Table 2: Quantity and viability of MNCs and MSCs

Patient	MNC count (viability)	1st MSC count (viability)	2nd MSC count (viability)	3rd MSC count (viability)	4th MSC count (viability)	Mean ± SD
1	2.1×10^9 (94%)	3.8×10^7 (95%)	4.2×10^7 (95%)	4.2×10^7 (95%)	4.0×10^7 (95%)	$4.05\times10^7 \pm 1.77\times10^6$
2	1.8×10^9 (100%)	4×10^7 (96%)	4.7×10^7 (95%)	4.5×10^7 (96%)	4.2×10^7 (97%)	$4.35\times10^7 \pm 2.87\times10^6$
3	1.4×10^9 (94%)	4×10^7 (96%)	3.8×10^7 (94%)	4×10^7 (93%)	3.6×10^7 (93%)	$3.85\times10^7 \pm 1.77\times10^6$
4	2.5×10^9 (96%)	4×10^7 (95%)	4×10^7 (93%)	3.4×10^7 (92%)	3.2×10^7 (95%)	$3.65\times10^7 \pm 3.81\times10^6$
5	1×10^9 (100%)	4×10^7 (92%)	4×10^7 (93%)	4.2×10^7 (97%)	4.5×10^7 (92.5%)	$4.17\times10^7 \pm 2.18\times10^6$

MNCs; Mononuclear cells and MSCs: Mesenchymal stromal cells.

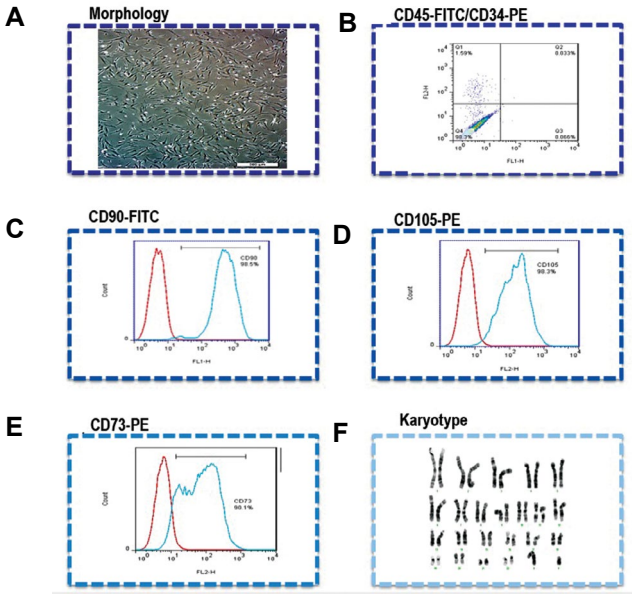

Fig.2: Detailed characterization of mesenchymal stromal cells (MSCs) from CD patients. **A.** Morphological examination revealed that MSCs were spindle-shaped and fibroblast-like cells in appearance. **B-E.** Immunophenotypic characterization of MSCs showed that these cells expressed general specific surface markers of MSCs [CD90 (98.5%), CD73 (90.1%), CD105 (98.3%), CD44 (92%) and CD29 (96.4%)], but did not express hematopoietic specific markers [CD34 (1.59%), CD45 (0.06%) and CD11 (0.293%)]. **F.** Normal diploid karyotype patterns of the isolated MSCs. MSCs; Mesenchymal stromal cells and CD; Crohn's disease.

Clinical assessment and follow-up

There were no adverse outcomes after the local injections and during the follow-up treatments in all five patients. One patient achieved complete remission during the six months of follow-up with fistula closure, cessation of fistula discharge, and closure of the external opening. A total number of three patients had partial responses with significant reductions of fistula discharge and decreased fistula diameters according to MRI imaging (Fig.3). One patient had no response to the treatment in terms of fistula closure, and a new perianal fistula track was observed during follow-up.

CDAI decreased to the mean of 118.4 points at the end of the treatment (154.8 to 36.4, P=0.004). There was also a significant decline in the PDAI after the treatment (6.6 to 4.6, P=0.04). Table 3 presents PDAI and CDAI scores before and after the intrafistula MSCs injections (Fig.4).

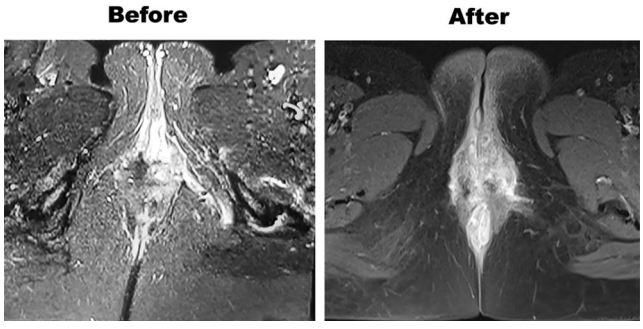

Fig.3: Short inversion recovery and T1-weighted, fat-suppressed (STIR T1W-FS) sequence with contrast injection of axial pelvic images before and after three weeks. Injection of mesenchymal stromal cells (MSCs) showed fistula tract closure on the left side at the 2 o'clock position of the anus. Decreased enhancement and shortening of the fistula tract with clinically reduced discharge was observed after treatment with MSCs.

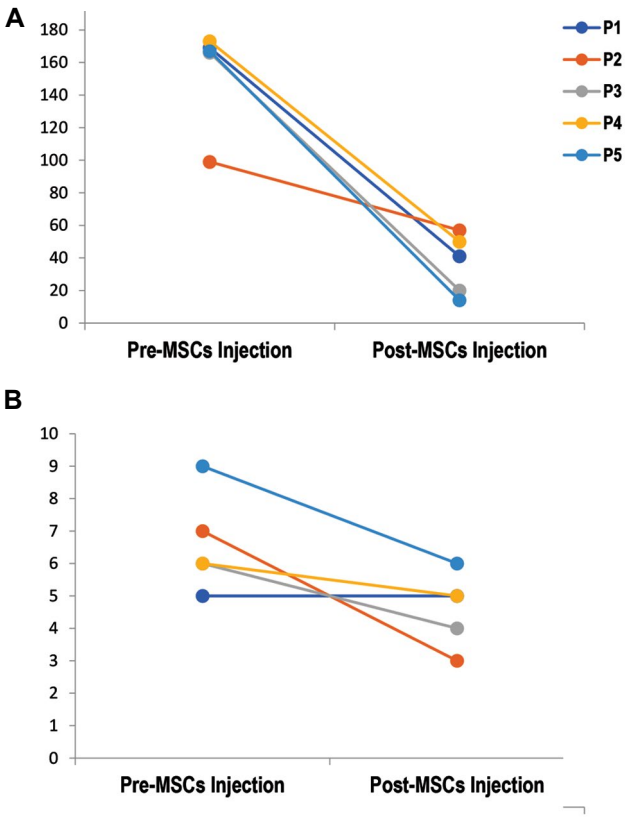

Fig.4: Perianal Disease Activity Index (PDAI) and Crohn's Disease Activity Index (CDAI) scores before and six months after intra-fistula mesenchymal stromal cells (MSCs) injections. **A.** CDAI scores before and after intra-fistula MSCs injection, **B.** PDAI scores before and after intra-fistula MSCs injection. Patients experienced clinical remission with the average of (CDAI<118.4) and (PDAI<4.6) scores by 6 months after local administration of MSCs.

Discussion

Using commercially available biological agents is the most frequent treatment strategy in 50% of IBD patients. However, long term therapy and many adverse event reports have caused serious limitations for this approach. Over the past few years, stem cell therapy has emerged as a promising option to treat soft-tissue injuries (22). Several studies have investigated the role of cell-based therapy with different types of stem cells, including HSCs, BM-MSCs and AD-MSCs from autologous or allogeneic sources for refractory CD. The results of such studies have successfully demonstrated the safety of this approach and the lack of serious adverse outcomes (23, 24).

MSCs have been extensively investigated and applied in regenerative medicine, tissue repair, and immunomodulation and are proposed to exert beneficial effects in fistulizing CD. Previous studies have shown the safety and effectiveness of a single injection of AD-MSCs in the treatment of fistulas in CD (25). The long-term evaluation of safety and efficacy of allogeneic BM-MSCs in CD patients has revealed that BM-MSC therapy is safe, as it resulted in successful fistula closure rates of 63, 100, and 43% after 4 years in three different MSC-based cohort studies (26). Moreover, a recent meta-

analysis study evaluated the efficacy and safety of local administration of MSCs for complex perianal fistula. The results have shown that application of MSCs alone or in combination with fibrin glue is effective with no serious adverse events.

Moreover, application of fibrin glue had a synergistic effect on the fistula closure (27). In this case series study we evaluated the safety and efficacy of intra-fistula injections of autologous BM-MSCs combined with fibrin glue for treating refractory fistulas in five CD patients. Our data indicated significant improvements in both CDAI and PDAI scores; however, only one patient showed complete closure and 60% of the subjects had a partial response. A randomized double-blinded placebo-controlled trial was conducted in 2016 to compare the impact of AD-MSCs and normal saline on fistula closure. Although the data showed significant improvement in PDAI scores, the CDAI scores did not notably differ between the two groups (28). In another study, patients with refractory CD had local injection of 2×10^6 autologous AD-MSCs plus fibrin glue or fibrin glue alone. The results showed more than 70% improvement in patients who received AD-MSCs plus fibrin glue compared to 16% in the fibrin glue-alone group ($P<0.001$) (29). Furthermore, a follow-up study was done by this research group for 49 patients for 42 months. Complete closure was seen in 12 of 21 patients who received autologous AD-MSCs plus fibrin glue and in 3 of 13 who received only fibrin glue (30). In 2013, Lee et al. (31) evaluated the effects of autologous AD-MSCs injection in 33 patients with fistulizing CD; almost 80% of the patients showed complete closure of the fistula tract after just a single injection and approximately 90% of them had no evidence of recurrence after 12 months. In another study, five out of six patients showed incomplete closure with 50% reduction in fistula drainage. Data from another randomized, double-blinded, placebo-controlled study that used allogeneic BM-MSCs in 21 patients with refractory perianal fistulizing CD, demonstrated that patients had healed perianal fistulas by week 12 after the BM-MSCs injection that persisted up to week 24, compared to those that received placebo. No significant adverse effects were observed (32).

Currently, the most common challenge reported for stem cell therapy in CD studies is patient recruitment. Furthermore, compared to biological agents, the only disadvantage for the cell-based therapeutic strategy is the invasiveness of local administration of MSCs. In addition, this procedure has no extra risk for an anal sphincter injury (25). Altogether, it seems that patients with refractory fistulizing CD might have benefited from BM-MSCs treatment. Nonetheless, short term follow-up and the low number of patients were the most notable limitations of this study. Larger sample size or repeated injections of MSCs may lead to more improved results in future studies.

Conclusion

We conclude that intra-fistula injection of BM-MSCs with fibrin glue is safe and effective in treating refractory fistulas in CD patients.

Acknowledgments

The authors express their gratitude to their fellow colleagues at the Department of Regenerative Medicine, Royan Institute, Tehran, Iran and the Research Center for Gastroenterology and Liver Diseases, Tehran University of Medical Sciences (TUMS), Shariati Hospital, Tehran, Iran. The authors declare that they have no financial or personal conflicts of interest. This study was funded by grants from Royan Institute (No. 91000170) and the Research Center for Gastroenterology and Liver Disease, Tehran University of Medical Sciences.

Authors' Contributions

R.M., S.N., N.A., H.B., M.V., H.R.A., M.M., A.A.; Participated in study design, drafting the manuscript, proofreading, and final approval and overall supervision of the study. M.V., H.A.A., S.T., B.S., N.H.-K.; Participated in data collection and analysis, drafting, and editing the manuscript for submission. A.B., S.-E.H., N.J., S.M., V.A.; Performed MSC isolation, expansion and characterization. M.N., A.A., M.V., M.M.; Contributed in data interpretation and finalization of the data. All authors read and approved the final manuscript.

References

1. Torres J, Mehandru S, Colombel JF, Peyrin-Biroulet L. Crohn's disease. Lancet. 2017; 389(10080): 1741-1755.
2. Le Berre C, Ananthakrishnan AN, Danese S, Singh S, Peyrin-Biroulet L. Ulcerative colitis and crohn's disease have similar burden and goals for treatment. Clin Gastroenterol Hepatol. 2020; 18(1): 14-23.
3. de Groof EJ, Sahami S, Lucas C, Ponsioen CY, Bemelman WA, Buskens CJ. Treatment of perianal fistula in Crohn's disease: a systematic review and meta-analysis comparing seton drainage and anti-tumour necrosis factor treatment. Colorectal Dis. 2016; 18(7): 667-675.
4. Park SH, Aniwan S, Scott Harmsen W, Tremaine WJ, Lightner AL, Faubion WA, et al. Update on the natural course of fistulizing perianal Crohn's disease in a population-based cohort. Inflamm Bowel Dis. 2019; 25(6): 1054-1060.
5. Petagna L, Antonelli A, Ganini C, Bellato V, Campanelli M, Divizia A, et al. Pathophysiology of Crohn's disease inflammation and recurrence. Biol Direct. 2020; 15(1): 1-10.
6. Moschen AR, Tilg H, Raine T. IL-12, IL-23 and IL-17 in IBD: immunobiology and therapeutic targeting. Nat Rev Gastroenterol Hepatol. 2019; 16(3): 185-196.
7. Scharl M, Rogler G. Pathophysiology of fistula formation in Crohn's disease. World J Gastrointest Pathophysiol. 2014; 5(3): 205-212.
8. Panés J, Rimola J. Perianal fistulizing Crohn's disease: pathogenesis, diagnosis and therapy. Nat Rev Gastroenterol Hepatol. 2017; 14(11): 652-664.
9. Molendijk I, Nuij VJ, van der Meulen-de Jong AE, van der Woude CJ. Disappointing durable remission rates in complex Crohn's disease fistula. Inflamm Bowel Dis. 2014; 20(11): 2022-2028.
10. Hossein-khannazer N, Torabi S, Hosseinzadeh R, Shahrokh S, Asadzadeh Aghdaei H, Memarnejadian A, et al. Novel cell-based therapies in inflammatory bowel diseases: the established concept, promising results. Hum Cell. 2021; 34(5): 1-12.
11. Al-Maawali AKS, Nguyen P, Phang PT. Modern treatments and stem cell therapies for Perianal Crohn's fistulas. Can J Gastroenterol Hepatol. 2016; 2016: 1651570.
12. Wang R, Yao Q, Chen W, Gao F, Li P, Wu J, et al. Stem cell therapy for Crohn's disease: systematic review and meta-analysis of preclinical and clinical studies. Stem Cell Res Ther. 2021; 12(1): 463.

13. Ocansey DKW, Qiu W, Wang J, Yan Y, Qian H, Zhang X, et al. The achievements and challenges of mesenchymal stem cell-based therapy in inflammatory bowel disease and its associated colorectal cancer. Stem Cells Int. 2020; 2020: 7819824.
14. Singer NG, Caplan AI. Mesenchymal stem cells: mechanisms of inflammation. Annu Rev Pathol. 2011; 6: 457-478.
15. DelaRosa O, Dalemans W, Lombardo E. Mesenchymal stem cells as therapeutic agents of inflammatory and autoimmune diseases. Curr Opin Biotechnol. 2012; 23(6): 978-983.
16. Gallo G, Tiesi V, Fulginiti S, De Paola G, Vescio G, Sammarco G. Mesenchymal stromal cell therapy in the management of perianal fistulas in crohn's disease: an up-to-date review. Medicina (Kaunas). 2020; 56(11): 563.
17. Cheng F, Huang Z, Li Z. Mesenchymal stem-cell therapy for perianal fistulas in Crohn's disease: a systematic review and meta-analysis. Tech Coloproctol. 2019; 23, 613-623.
18. Ramezankhani R, Torabi S, Minaei N, Madani H, Rezaeiani S, Hassani SN, et al. Two decades of global progress in authorized advanced therapy medicinal products: an emerging revolution in therapeutic strategies. Front Cell Dev Biol. 2020; 8.
19. Vosough M, Moossavi S, Mardpour S, Akhlaghpoor S, Azimian V, Jarughi N, et al. Repeated intraportal injection of mesenchymal stem cells in combination with pioglitazone in patients with compensated cirrhosis: a clinical report of two cases. Arch Iran Med. 2016; 19(2): 131-136.
20. Best WR, Becktel JM, Singleton JW, Kern F Jr. Development of a crohn's disease activity index. national cooperative crohn's disease study. Gastroenterology. 1976; 70(3): 439-444.
21. Sandborn WJ, Fazio VW, Feagan BG, Hanauer SB. American gastroenterological association clinical practice committee. AGA technical review on perianal Crohn's disease. Gastroenterology. 2003; 125(5): 1508-1530.
22. Saberi S, Karamzadeh R, Moghadam P, Kadivari M, Behbahani BE, Heydari Z, et al. Research performance in stem cell science and regenerative medicine in Iran: a national comprehensive observation. Arch Iran Med. 2019; 22(6): 318-327.
23. Irhimeh MR, Cooney J. Management of inflammatory bowel disease using stem cell therapy. Curr Stem Cell Res Ther. 2016; 11(1): 72-77.
24. Thomas A, Lodhia N. Advanced therapy for inflammatory bowel disease: a guide for the primary care physician. JABFM. 2014; 27(3): 411-420.
25. Nagaishi K, Arimura Y, Fujimiya M. Stem cell therapy for inflammatory bowel disease. J Gastroenterol. 2015; 50(3): 280-286.
26. Barnhoorn MC, Wasser MN, Roelofs H, Maljaars PJ, Molendijk I, Bonsing BA, et al. Long-term evaluation of allogeneic bone marrow-derived mesenchymal stromal cell therapy for Crohn's disease perianal fistulas. J Crohns Colitis. 2020; 14(1): 64-70.
27. Cheng F, Huang Z, Li Z. Efficacy and safety of mesenchymal stem cells in treatment of complex perianal fistulas: a meta-analysis. Stem Cells Int. 2020; 2020: 8816737.
28. Panés J, García-Olmo D, Van Assche G, Colombel JF, Reinisch W, Baumgart DC, et al. ADMIRE CD study group collaborators. expanded allogeneic adipose-derived mesenchymal stem cells (Cx601) for complex perianal fistulas in Crohn's disease: a phase 3 randomised, double-blind controlled trial. Lancet. 2016; 388(10051): 1281-1290.
29. Garcia-Olmo D, Herreros D, Pascual I, Pascual JA, Del-Valle E, Zorrilla J, et al. Expanded adipose-derived stem cells for the treatment of complex perianal fistula: a phase II clinical trial. Dis Colon Rectum. 2009; 52(1): 79-86.
30. Guadalajara H, Herreros D, De-La-Quintana P, Trebol J, Garcia-Arranz M, Garcia-Olmo D. Long-term follow-up of patients undergoing adipose-derived adult stem cell administration to treat complex perianal fistulas. Int J Colorectal Dis. 2012; 27(5): 595-600.
31. Lee WY, Park KJ, Cho YB, Yoon SN, Song KH, Kim DS, et al. Autologous adipose tissue-derived stem cells treatment demonstrated favorable and sustainable therapeutic effect for Crohn's fistula. Stem Cells. 2013; 31(11): 2575-2581.
32. Molendijk I, Bonsing BA, Roelofs H, Peeters KC, Wasser MN, Dijkstra G, et al. Allogeneic bone marrow-derived mesenchymal stromal cells promote healing of refractory perianal fistulas in patients with crohn's disease. Gastroenterology. 2015; 149(4): 918-927.e6.

Original Article

Trehalose An Additive Solution for Platelet Concentrate to Protect Platelets from Apoptosis and Clearance during Their Storage at 4°C

Vahid Baghdadi, Ph.D.[1], Reza Ranjbaran, Ph.D.[2], Fatemeh Yari, Ph.D.[1]*, Mohammad Hessam Rafiee, Ph.D.[1]

1. Blood Transfusion Research Center, High Institute for Research and Education in Transfusion Medicine, Tehran, Iran
2. Diagnostic Laboratory Sciences and Technology Research Center, School of Paramedical Sciences, Shiraz University of Medical Sciences, Shiraz, Iran

Corresponding Adrress: P.O.Box: 14665-1157, Blood Transfusion Research Center, High Institute for Research and Education in Transfusion Medicine, Tehran, Iran
Email: f.yari@ibto.ir

Received: 02/December/2020, Accepted: 11/May/2021

Abstract

Objective: Although cold storage of platelets (PLTs) could decrease the risk of bacterial growth, it could affect on the PLTs viability and hemostatic function. At cold temperatures, trehalose can be used to substitute water, inhibit the solid-liquid transition phase of the PLT membrane, and stop Glycoprotein Ibα (GPIbα) polymerization. In this study, we evaluated the potential of trehalose for reducing the negative effects of cold storage on the apoptosis and the clearance rates of PLTs after long-term storage at cold.

Materials and Methods: In this experimental study, PLT concentrates (PCs) were maintained for five days in the different circumstances. PLTs were subsequently counted by using an automated hematology analyzer. Also water-soluble tetrazolium salt (WST-1) assay was performed to estimate the viability of PLTs. The activity of lactate dehydrogenase enzyme (LDH) was determined by a biochemical analyzer. And human active caspase-3 levels were measured by using enzyme-linked immunosorbent assay (ELISA) method. Also, we applied flow cytometry technique.

Results: PLTs count and viability were higher, while LDH amount was lower in trehalose-treated PLTs when compared with two other groups (P=0.03). The highest increase in the amount of caspase-3 levels in the PLTs was observed at 4°C. However, trehalose-treated and 4°C PLTs had a lower amount of active caspase-3 in comparison with 4°C PLTs. The level of PS expression on PLTs was lower in the trehalose-treated PLTs in compared with the two other groups (P=0.03). PLTs ingestion by HepG2 cells was enhanced in the 4°C-stored PLTs. However, the ingestion rate was significantly reduced in the trehalose-treated PLTs on day 5 of storage (P=0.03).

Conclusion: Trehalose can moderate the effects of cold temperature on the apoptosis, viability, and the survival rate of PLTs. It also decreases the ingestion rate of refrigerated PLTs *in vitro*.

Keywords: Cold Storage, HepG2, Platelet Transfusion, Trehalose

Cell Journal(Yakhteh), Vol 24, No 2, February 2022, Pages: 69-75

Citation: **Baghdadi V, Ranjbaran R, Yari F, Rafiee MH. Trehalose an additive solution for platelet concentrate to protect platelets from apoptosis and clearance during their storage at 4°C. Cell J. 2022; 24(2): 69-75. doi: 10.22074/cellj.2022.7886.**

Introduction

Today, platelet (PLT) concentrates can be stored at 22°C for less than five days before transfusion (1). This short shelf life is because of the increase in bacterial contamination risk (2, 3). Another significant issue is correlated with the room temperature storage of PLTs' that resulted in the PLTs' loss of function and PLTs' structure changes, what is referred to the PLT storage lesion (PSL) (4, 5). Cold storage of PLTs can resolve several issues associated with 22°C- storage of them (6). Investigations have shown that cold storage of PLTs decreases the chance of bacterial contamination, reduces PLT metabolic activity, and minimizes the release of biological response modifiers (7-9). Many *in vivo* studies demonstrated that cold stored PLTs have the better function in the decreasing the bleeding time of patients with thrombocytopenia and functional disorders when in comparison with room temperature kept PLTs (10). However, due to the rapid removal of PLTs from the patients' bloodstream, use of cold-stored PLTs has been stopped since the 1970s (11, 12). Studies have indicated that storage of PLTs at a cold temperature for short-term (<4 hours) leads to clustering of GPIb receptors. Thereupon, and β2 integrins on the hepatic macrophages (Kupffer cells) selectively recognize uncovered βGlcNAc on the glycans within GPIb (13, 14). Moreover, prolonged cold storage of PLTs (48 hours at 4°C) has resulted in many changes such as increased galactose-terminated glycans on the GPIb, which are bound to the asialoglycoprotein receptors on the hepatocytes and thereby mediate PLTs clearance (15-17).

New methods may help to prevent PLT phagocytosis and protect the functional activity of refrigerated PLTs. Trehalose is a non-reducing disaccharide that is found in large amount in the nature. Some bacteria, fungi, plants and invertebrate animals produce it as a source of energy.

Trehalose could preserve phospholipids, proteins, and cells from damage (18). Trehalose is extensively utilized as a biomacromolecular protective agent, which is decomposed into the two molecules of glucose (GLU) and has no side or toxic effects (19). At low temperatures, trehalose can be used to replace water, prevent the solid-liquid transition phase of the PLT membrane, and halt GPIba polymerization. Hence, Trehalose is considered a satisfactory, potential, and protective agent for PLTs low temperature

storage (20). This sugar has been used as a cryoprotectant to stabilize PLT membranes through lyophilization. In the presence of Trehalose, lyophilized PLTs showed a longer shelf life and a better recovery upon restoration (21-23).

Recent investigations revealed that Trehalose could inhibit phagocytosis of cold temperature storage-PLTs by THP-1 cells (24). However, the impact of Trehalose on the phagocytosis and clearance of long-term stored-PLTs has remained unclear. Accordingly, in this study, we evaluated the effect of Trehalose on the ingestion rate of long-term stored-PLTs by HepG2 cells as a model for hepatocyte cells *in vitro*. Also, the survival and apoptosis rates of PLTs were also analyzed to evaluate the effects of Trehalose on the PLTs stored at cold.

Materials and Methods

Collection and preparation of platelet concentrates

This experimental investigation was confirmed by the College's Bioethics Ethics Committee (IR.TMI.REC.1396.004). In this study, PLT concentrates (PC) bags (24 bags) (Macopharma, France) with sodium citrate anticoagulant were collected by the Tehran Blood Transfusion Center (TBTC), Tehran, Iran.

Different parameters including, PLT enumeration, mean PLT volume (MPV), PLT distribution width (PDW), lactate dehydrogenase (LDH), water-soluble tetrazolium salts (WST-1), human active caspase-3, phosphatidylserine (PS), and the ingestion rate of PLTs by HepG2 cells were evaluated before adding Trehalose to the bags. Subsequently, utilizing a digital balance (Sartorius, Germany) and a Terumo Sterile Connecting Device (TSCD - II, Terumo Tubing welder, Japan), each PC bag was divided into three equal parts. Trehalose (Sigma-Aldrich, USA) with a concentration of 40 mg/ml was added to one of the bags. The Trehalose-containing bag and the control bag (without Trehalose) were transported to the refrigerator (4°C) while the bag without Trehalose (third bag) was kept at 22°C in a shaker- incubator. Since the usual storage temperature for PLTs is 22°C, one of the controls was kept at 22°C. It is worth mentioning that the second control bags, (4°C+without Trehalose), and third control bags, (22°C), did not receive any concentration of Trehalose.

Determination of the effective Trehalose concentration

Saccharomyces cerevisiae-derived Trehalose was purchased from Sigma-Aldrich, USA. Trehalose powder was mixed with saline, and several concentrations of Trehalose (20, 30, 40, 50, and 60 mg/ml) were added to PC bags. The PC bags were subsequently stored at 4°C for five days without agitation. The aforementioned PLT parameters were determined during the 5-day storage of PLT concentrates.

Determination of PLT count, MPV and PDW

PCs were diluted in the phosphate-buffered saline (PBS, M.P. Biomedicals, LLC, 1:2 dilution) and subsequently applied for assessment of PLT count, MPV, and PDW by an automated hematology analyzer (Sysmex XT-2000i, Kobe, Japan).

Evaluation of platelet bags for bacterial contamination

To examine probable bacterial contamination on day 1, the samples of all the bags were placed in a 37°C incubator in the Thioglycollate medium for one week. Then all samples were cultured on the blood agar.

Assessment of the PLT metabolic activity using WST-1 assay

WST-1 cell proliferation assay kit (WST-1, Cayman, USA) was used to measure the activity of cellular mitochondrial dehydrogenases in the PLTs. In this test, the tetrazolium salt is changed to formazan by viable PLTs; therefore, the result indicates PLTs viability rate. Following diluted with PBS, 10×10^6 PLTs (100 µl) were added into each well. Accordingly, 10 µl of the WST-1 mixture was added to each well, and the plate was incubated at 37°C in an incubator for 4 hours. The absorbance of the samples was measured at 450 nm in a microplate reader (Asys Expert 96, UK).

Lactate dehydrogenase measurement

LDH enzyme was used as a PLTs lysis marker. Utilizing the pyruvate-lactate method, the LDH enzyme levels were measured at 340 nm through a biochemical analyzer (Hitachi 911, Japan) and LDH kit (Pars Azmoon, Iran). The results of this parameter were analyzed by using the relative standard curve method.

Human active caspase-3 evaluation

The human active Caspase-3 level was evaluated with an enzyme-linked immunosorbent assay kit (Invitrogen, USA). The kit sensitivity was 1.25 ng/ml. Based on the producer instructions, cell extraction buffer was mixed with 5×10^8 PLTs and then washed three times with the PBS. The cell extraction buffer was then added to the pellet and suspensions were incubated at room temperature for 15 minutes. After centrifugation at 4000g for 10 minutes, the supernatant was collected in a clean tube. The ELISA steps were performed according to the kit instructions. After completing the reactions, the optical density of the each sample was read at 450 nm and the concentration of the samples as well as controls was ultimately determined by using the standard curve of the kit.

Evaluation of phosphatidylserine surface exposure

Using Annexin V-FITC (Fluorescein isothiocyanate) assay kit (Biolegend, USA) the surface exposure level of PS was determined. Briefly, 1.5×10^6 PLT cells were incubated in the 300 µl of annexin V binding buffer. Adding 5 µL of FITC-labeled annexin V all samples were incubated at 22°C for 20 minutes. Using the CyFlow Space (Partec, Germany) all samples were evaluated by flow cytometry technique.

Preparation of mepacrine-labeled platelets

Mepacrine (Sigma-Aldrich, USA) is an Acridine derivative whose emission wavelength is within the range of FITC. PLTs labeling, 20 µl of 20 mg/mL mepacrine was added to the 5×10^7 PLTs to 30 µl PBS solution and incubated for 30 minutes at ambient temperature. Afterward, the PLTs were washed three times with PBS by centrifugation at 1200 g for 15 minutes. Ultimately, PLTs were prepared for adding to cultured HepG2 cells.

Ingestion of platelets by HepG2 cells *in vitro*

HepG2 cells (IBRC, Iran) were cultured in DMEM-F12 medium (Sigma, USA) supplemented with 10% fetal bovine serum (FBS, Gibco, US). After the growth of the HepG2 cells, they incubated for 30 minutes in a serum-free medium. Then, mepacrine-labeled PLTs (5×10^7) were added to the each wells and incubated at 37°C for 30 minutes. Subsequently, the wells were washed three times with PBS, and HepG2 cells were detached from the culture plates by treatment with trypsin at 37°C for 2 minutes. The ingestion of mepacrine-labeled PLTs by HepG2 cells was evaluated by flow cytometry technique. HepG2 cells containing the ingested PLTs were identified by their green fluorescence related to mepacrine, and the PLT adherence to HepG2 cells was differentiated from ingested PLTs through PE- labeled anti-CD42b.

Statistical analysis

All data were statistically analyzed and processed by using commercially available SPSS software (Version 22, IBM Corporation, USA). Statistical analysis was performed by Paired t test. $P<0.05$ were considered significant.

Results

Determining the effective dose of Trehalose

The best dose of Trehalose was 40 mg/ml. In this dose, PS exposure was less on the PLTs at all days of storage in comparison to other doses. Also, according to the WST-1 assay, higher viability of PLTs was obtained at this dose of Trehalose (Table 1).

Platelets count, size and width distribution

The count of PLTs reduced in all the study groups. The rate of decrease in the PLTs count was less in the presence of Trehalose. During storage, the order of PLTs count was as follows: Trehalose treated PLTs (4°C) >Non-treated PLTs (4°C) >Non-treated PLTs (22°C). The differences between Trehalose-treated PLTs (4°C) and non-treated PLTs (4°C) were not statistically significant, whereas, the differences between non-treated PLTs (4°C) and (22°C) were statistically significant (day 3, P=0.03, and day 5, P=0.01, Fig.1, Table 2).

MPV and PDW parameters significantly raised in the non-treated PLTs (4°C) group and Trehalose-treated (4°C) group in compared with the non-treated PLTs (22°C) group. The differences between Trehalose-treated PLTs (4°C) and non-treated PLTs (4°C) groups were statistically significant on the fifth day of storage (P=0.03). At the 22°C, however, the mean of MPV significantly reduced on the both days (3 and 5 days) of storage in comparison with the first day ($P<0.05$, Fig.1, Table 2).

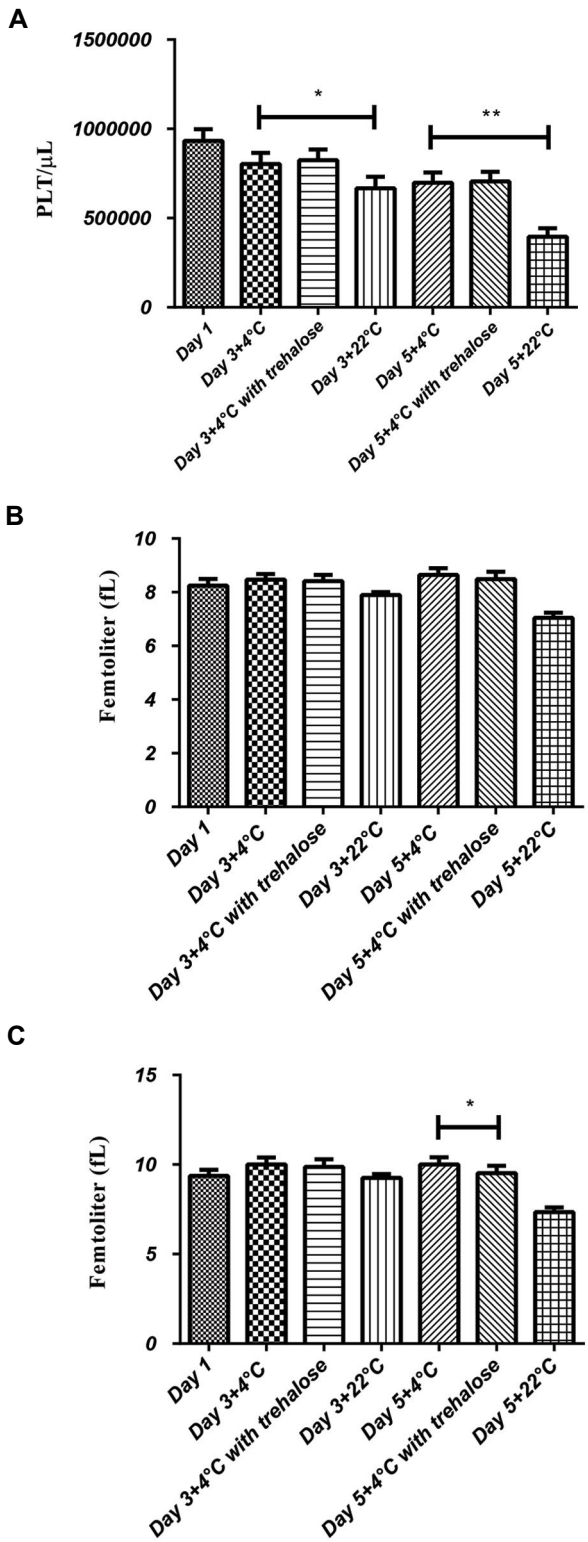

Fig.1: Comparative effect of cold, room temperature, and Trehalose on the PLTs count, MPV, and PDW. **A.** The count of PLTs was reduced during stored in all groups of investigation. Only, the differences between 4°C PLTs and 22°C PLTs were statistically significant (day 3, P=0.03, and day 5, P=0.01). **B.** Different amount of MPV. **C.** Different amount of PDW. The differences between Trehalose (4°C) PLTs and 4°C PLTs were statistically significant on the fifth day of storage (P=0.03). PLTs; Platelets, MPV; Mean PLT volume, PDW; PLT distribution width, *; P=0.03, and **; P=0.01.

Table 1: Determine the effective Trehalose concentration

Trehalose concentration (mg/ml) n=4	Storage days	Platelet count (10^3/µL)		MPV (fL)		PDW (fL)		Phosphatidyl- serine (%)		WST-1 (OD_{450} nm)	
		4°C	4°C+trehalose	4°C	4°C+trehalose	4°C	4°C+trehalose	4°C	4°C+trehalose	4°C	4°C+trehalose
20	3	685 ± 101	714 ± 111	7.9 ± 0.908	7.7 ± 0.945	8.2 ± 0.866	8.1 ± 0.901	25.9 ± 3.92	24.5 ± 3.17	0.285 ± 0.063	0.252 ± 0.059
	5	720 ± 193	788 ± 149	8.2 ± 0.918	8 ± 0.961	8.3 ± 0.958	8 ± 0.983	13.2 ± 3.72	11.6 ± 2.75	0.324 ± 0.096	0.349 ± 0.103
30	3	675 ± 109	685 ± 118	7.9 ± 0.752	7.8 ± 0.805	8.2 ± 0.784	8.1 ± 0.815	19.8 ± 4.15	17 ± 3.64	0.295 ± 0.084	0.314 ± 0.095
	5	705 ± 122	781 ± 133	9.7 ± 0.958	9.5 ± 0.999	10.8 ± 0.805	10.7 ± 0.819	12.9 ± 3.01	9.2 ± 2.65*	0.684 ± 0.213	0.874 ± 0.169*
40	3	669 ± 99	975 ± 121*	9.4 ± 0.837	9.3 ± 0.858	10.5 ± 0.818	10.3 ± 0.858	20.8 ± 4.75	11.7 ± 3.01*	0.512 ± 0.145	0.800 ± 0.141*
	5	725 ± 135	915 ± 141*	8.1 ± 0.901	7.9 ± 0.927	8.5 ± 0.912	8.3 ± 0.939	11.4 ± 3.28	9.7 ± 2.55*	0.519 ± 0.139	0.608 ± 0.128*
50	3	725 ± 97	747 ± 82	7.9 ± 0.799	7.7 ± 0.817	8.2 ± 0.738	8.1 ± 0.768	26.8 ± 3.95	24.7 ± 3.32	0.342 ± 0.103	0.380 ± 0.088
	5	842 ± 105	856 ± 93	8.4 ± 0.808	8.2 ± 0.818	8.7 ± 0.795	8.6 ± 0.804	19 ± 2.96	17.2 ± 3.10*	0.459 ± 0.111	0.526 ± 0.111*
60	3	682 ± 117	703 ± 101	8.1 ± 0.933	7.9 ± 0.957	7.9 ± 0.902	7.7 ± 0.937	31.5 ± 4.05	28.9 ± 3.88*	0.301 ± 0.097	0.352 ± 0.102
	5	685 ± 125	714 ± 121	7.9 ± 0.989	7.7 ± 0.991	8.2 ± 0.967	8.1 ± 0.998	25.9 ± 3.54	24.5 ± 3.67	0.285 ± 0.072	0.252 ± 0.069

Data are presented as mean ± SD. All data were statistically analyzed and processed by using commercially available SPSS software (version 22). MPV; Mean platelet volume, PDW; Platelet distribution width, and WST1; Water soluble tetrazolium salt, and *; P=0.03.

Table 2: The mean ± standard deviation for different parameters of platelets during the storage at different days and conditions

Study variables (n=12)	Day 1	Day 3 (4°C)	Day 3 (4°C+Trehalose)	Day 3 (22°C)	Day 5 (4°C)	Day 5 (4°C+Trehalose)	Day 5 (22°C)
Platelet count (10^3/µL)	933 ± 240	803 ± 234	823 ± 141	667 ± 240	697 ± 216	705 ± 202	396 ± 180
MPV (fL)	8.24 ± 0.958	8.47 ± 0.785	8.41 ± 0.880	7.89 ± 0.402	8.64 ± 0.951	8.48 ± 1.037	7.04 ± 0.731
PDW (fL)	9.36 ± 1.295	10 ± 1.454	9.87 ± 1.581	9.25 ± 0.810	10 ± 1.488	9.52 ± 1.533	7.34 ± 0.985
LDH (U/L)	295 ± 42.10	394 ± 47.53	352 ± 54.64	1990 ± 499	485 ± 40.89	439 ± 55.52	3087 ± 635
WST1 (OD 450 nm)	0.718 ± 0.256	0.594 ± 0.281	0.631 ± 0.274	0.26 ± 0.939	0.438 ± 0.81	0.504 ± 0.113	0.221 ± 0.74
Phosphatidylserine (%)	5.33 ± 2.22	10.69 ± 3.75	9.53 ± 3.84	54.79 ± 16.09	19.91 ± 5.22	16.82 ± 7.05	75.83 ± 7.30
active caspase-3 (ng/ml)	0.579 ± 0.172	1.657 ± 0.492	1.377 ± 0.668	0.958 ± 0.538	2.181 ± 0.722	1.930 ± 0.586	1.267 ± 0.593
HepG2 ingest (%)	19.79 ± 15.45	36.32 ± 18.01	38.61 ± 23.33	31.71 ± 20.85	37.58 ± 15.88	30.33 ± 12.06	32.35 ± 12.10

MPV; Mean platelet volume, PDW; Platelet distribution width, LDH; Lactate dehydrogenase, and WST1; Water soluble tetrazolium salt.

Evaluation of platelet bags for bacterial contamination

The results of bacterial culture on the Thioglycollate and Blood agar media were evaluated showed no effect of contamination.

The metabolic activity of platelets by WST-1 assay

The metabolic activity was proportional to the PLTs viability. It was diminished during storage in the all groups, and the highest decrease was observed in the PLTs storage at 22°C. The metabolic activity of PLTs was well maintained in the presence of Trehalose (4°C) compared with 4°C-kept PLTs, and the differences were statistically significant (P=0.03, Fig.2, Table 2).

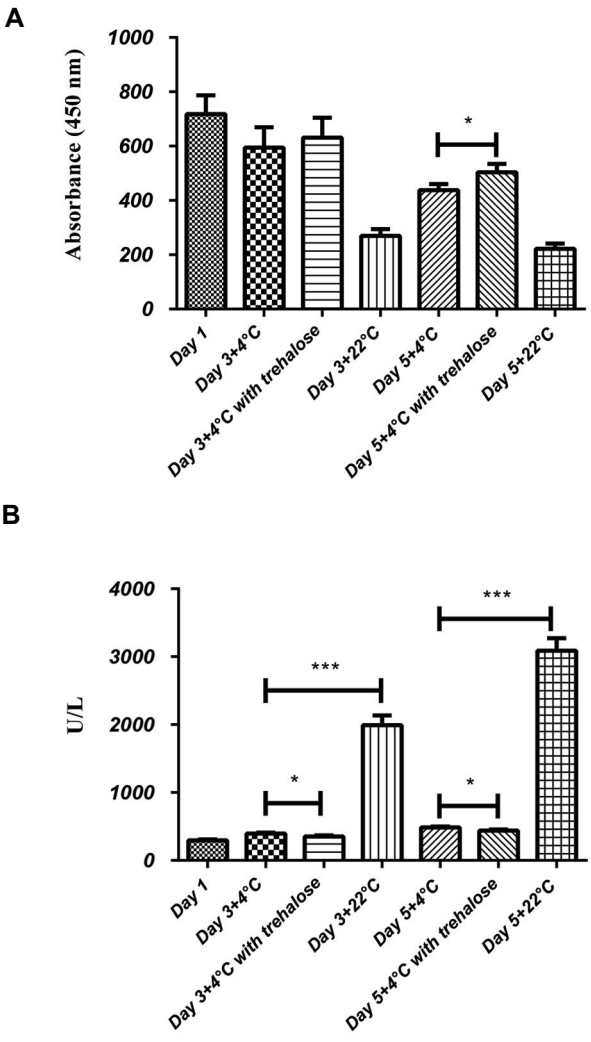

Fig.2: Effect of cold, room temperature and Trehalose on the lactate dehydrogenase (LDH) activity and the metabolic activity and the survival (WST1) amount of the platelets in different days of storage. **A.** The differences Wst1 results between Trehalose (4°C) PLTs and 4°C PLTs were statistically significant (P=0.03). **B.** LDH level was higher at room temperature (22°C) in comparison with 4°C (P<0.05). LDH in the PC bags was lower in the presence of Trehalose at 4 °C; the difference with 4°C groups was statistically significant (P=0.03). *; P=0.03 and ***; P=0.001.

The platelets lactate dehydrogenase levels

The LDH value of PC bags was increased during storage in the all groups, and it was significantly higher at room temperature (22°C) in comparison with non-treated PLTs (4°C) and Trehalose-treated (4°C) groups (P=0.001). It is important to regard that the lowest value of LDH was observed in the Trehalose-treated PLTs (4°C) and the difference was statistically significant in comparison with non-treated PLTs storage at 4°C (P=0.03, Fig.2, Table 2).

Human active caspase-3 levels in the platelets

The level of human active caspase-3 was increased in the PLTs in all groups. Also, a higher increase was observed in the non-treated PLTs (4°C) group. There was a significant difference in active caspase-3 levels between PLTs stored at 4°C in the presence and absence of Trehalose on the fifth day of storage (P=0.03, Fig.3, Table 2).

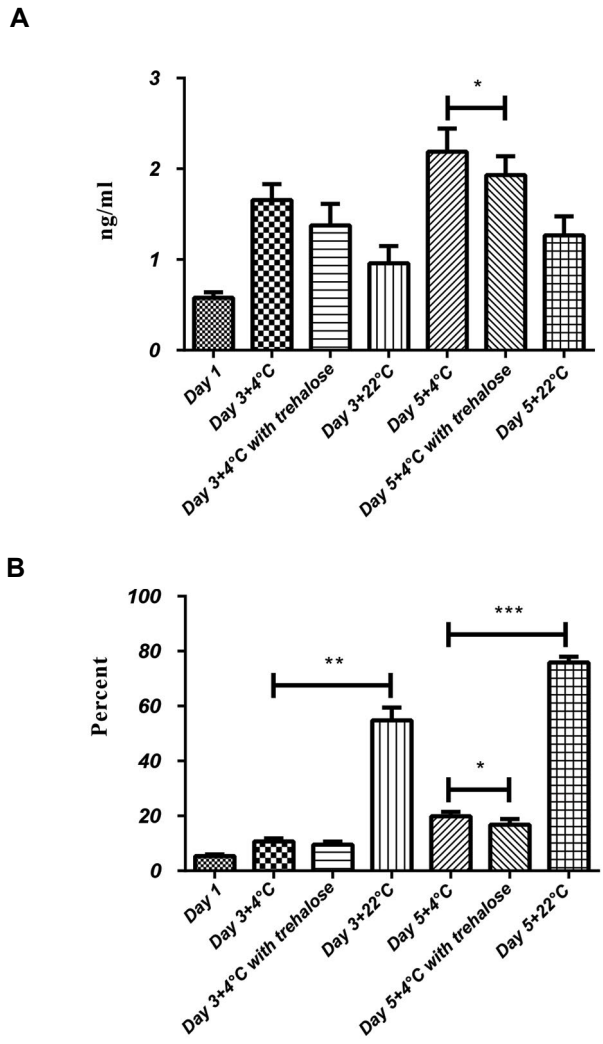

Fig.3: Effect of the temperature and Trehalose presence on the active caspase-3 levels and the exposure level of PS in the platelets during storage. **A.** There was a significant difference in active caspase-3 levels between 4°C PLTs stored with and without Trehalose at the fifth day of storage (P=0.03). **B.** The exposure level of PS was significantly lower in the presence of Trehalose (4°C) on day 5 in comparison with 4°C groups (P=0.03). PS; Phosphatidylserine, PLTs; Platelets, *; P=0.03, **; P=0.01, and ***; P=0.001.

The exposure level of phosphatidylserine on the platelets

During the storage time, the surface exposure of PS increased in the all groups. The level of PS exposure was significantly lower in the Trehalose-treated PLTs (4°C) on the 5th day in comparison with the non-treated PLTs (4°C, P=0.03). Also, the differences in the PS exposure between PLTs storage at 22°C group and other groups were statistically significant (P=0.001, Fig.3, Table 2).

Ingestion of the refrigerated platelets by HepG2 cells

PLTs storage at cold temperature caused an increase in the PLTs ingestion rate by HepG2 cells in comparison with PLTs stored in 22°C during 5-day storage. Trehalose caused a lower clearance rate for 4°C storage PLTs by HepG2 cells in compared with 4°C storage PLTs in the absence of Trehalose, and the differences were significant on the fifth day of storage (P=0.03, Fig.4, Table 2).

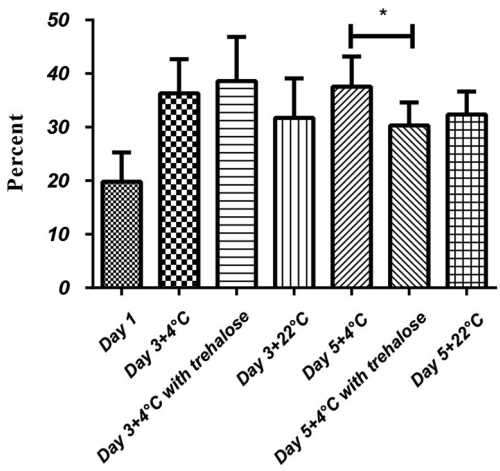

Fig.4: Trehalose effect on the ingestion of platelets by HepG2 cells during storage in the different groups of study [22°C, non-treated PLTs (4°C) and Trehalose-treated (4°C)]. The differences were significant at the fifth day of storage (P=0.03). *; P=0.03.

Discussion

In this investigation, the impact of Trehalose on the viability, apoptosis, and the clearance rate of PLTs was evaluated during 5-day PCs storage. We found that Trehalose could provide protective effects on the 4°C-storage PLTs. Trehalose could reduce the ingestion rate of the refrigerated PLTs by HepG2 cells through preventing PS exposure and caspase-3 activity. It was also able to keep better the viability and metabolic activity of the refrigerated PLTs.

Based on the results of this study, PLTs enumeration reduced during storage in the all of our groups. However, the highest reduction in the PLTs counts was observed in the PLTs stored at 22°C. In Trehalose-treated PLTs, the PLTs counts were higher and better preserved than our other groups. However, the differences were not statistically significant. The results of this study were consistent with the results reported in our previous research as well as findings published by Handigund et al. (25-27). They showed that PLTs count diminished in both room temperature and 4°C during storage (25). Additionally, it was in line with the results obtained by Wang et al. which showed PLTs treated with PLT additive solution and Trehalose had a high count during storage at 10°C (28).

According to this study, PLT survival decreased during storage. The lowest viability was observed in the PLTs maintained at room temperature, whereas the highest viability was seen in the Trehalose-treated PLTs (4°C). The results of this investigation showed that Trehalose could preserve the survival rate of PLTs.

Additionally, in this study, we indicated that the LDH activity was lower in Trehalose-treated PLTs (4°C) compared to non-treated PLTs (4°C) and room temperature (22°C) PLTs. The highest enzyme activity was observed in PLTs maintained at 22°C on the both days (3 and 5 days) of storage. One of the essential agents in preserving the quality and survival of PLTs in PCs is the low amount of LDH released into the bag during storage (29). The results of this study are consistent with findings of Dasgupta et al. (30) research regarding the effects of cold temperature and Trehalose on the reducing LDH levels in the stored PLTs.

As Marini et al. (12) reported, PS exposure on PLTs is an essential indicator of apoptosis. The result of this study showed that exposure of PS in the Trehalose-treated PLTs was lower than those of other groups of study. In consistent with our findings, Liu et al. (24) demonstrated that Trehalose could reduce PS expression levels on the PLTs when maintained at low temperature.

This study also showed an increase in the caspase-3 levels in the all groups during the 5-day storage of PLTs. This finding corroborates the results obtained by Quach et al. (29) and Perrotta et al. (31). In the PLTs treated with Trehalose, the level of caspase-3 was lower than other groups. These results were also consistent with the findings of Liu et al. (24).

We also investigated the effect of Trehalose and cold storage on the ingestion rate of PLTs by HepG2 cells. According to our findings, PLTs ingestion increased in the all groups during storage. However, the lowest increase in the PLT ingestion was related to the PLTs stored at 22°C. This finding was consistent with the previous reports (14, 32). We observed an increase in the PLTs ingestion by HepG2 cells during 5-day storage in the cold temperature.

However, the Trehalose-treated PLTs had a lower uptake than the non-treated PLTs. This might be due to the protective effect of Trehalose on the phospholipids, proteins, and cells against cold storage-mediated damages (18).

Our results were in line with the study of Liu and co-workers (24). Although Liu et al. stored PLTs for a short period in the cold temperature, they showed that removal of PLTs by THP1 cells reduced in the presence of Trehalose. These findings support the protective effects of Trehalose for the PLTs in the PCs during storage at 4°C.

Conclusion

Trehalose could moderate the effects of cold temperature on the apoptosis and survival of PLTs. It also decreased the ingestion rate of long-time refrigerated PLTs *in vitro*. Further studies with more sample numbers are required to demonstrate the effect of trehalose on the reducing the clearance rate of PLTs.

Acknowledgments

This study was the result of a Ph.D. thesis, financially supported by Blood Transfusion Research Center, High Institute for Research and Education in Transfusion Medicine, Iranian Blood Transfusion Organization, Tehran, Iran. The authors have disclosed no conflicts of interest.

Authors' Contributions

V.B.; Performed all of experimental work, contributed to the design of the study, interpretation and manuscript drafting and reviewing as a Ph.D. student. R.R.; Contributed to data and statistical analysis, and interpretation of data. F.Y.; Was responsible for overall supervision of the Ph.D. thesis and contributed to the study conception and design. M.H.R.; Contributed to conception and design. All authors read and approved the final manuscript.

References

1. Reddoch-Cardenas KM, Montgomery RK, Lafleur CB, Peltier GC, Bynum JA, Cap AP. Cold storage of platelets in platelet additive solution: an in vitro comparison of two food and drug administration-approved collection and storage systems. Transfusion. 2018; 58(7): 1682-1688.
2. Babic AM, Josefsson EC, Bergmeier W, Wagner DD, Kaufman RM, Silberstein LE, et al. In vitro function and phagocytosis of galactosylated platelet concentrates after long-term refrigeration. Transfusion. 2007; 47(3): 442-451.
3. Wood B, Johnson L, Hyland RA, Marks DC. Maximizing platelet availability by delaying cold storage. Vox Sang. 2018; 113(5): 403-411.
4. Mittal K, Kaur R. Platelet storage lesion: An update. Asian J Transfus Sci. 2015; 9(1): 1-3.
5. Cho J, Kim H, Song J, Cheong JW, Shin JW, Yang WI, et al. Platelet storage induces accelerated desialylation of platelets and increases hepatic thrombopoietin production. J Transl Med. 2018; 16(1): 199.
6. Stubbs JR, Tran SA, Emery RL, Hammel SA, Haugen AL, Zielinski MD, et al. Cold platelets for trauma-associated bleeding: regulatory approval, accreditation approval, and practice implementation-just the "tip of the iceberg". Transfusion. 2017; 57(12): 2836-2844.
7. Johnson L, Tan S, Wood B, Davis A, Marks DC. Refrigeration and cryopreservation of platelets differentially affect platelet metabolism and function: a comparison with conventional platelet storage conditions. Transfusion. 2016; 56(7): 1807-1818.
8. Nair PM, Pandya SG, Dallo SF, Reddoch KM, Montgomery RK, Pidcoke HF, et al. Platelets stored at 4°C contribute to superior clot properties compared to current standard-of-care through fibrin-crosslinking. Br J Haematol. 2017; 178(1): 119-129.
9. Johnson L, Tan S, Jenkins E, Wood B, Marks DC. Characterization of biologic response modifiers in the supernatant of conventional, refrigerated, and cryopreserved platelets. Transfusion. 2018; 58(4): 927-937.
10. Reddoch KM, Pidcoke HF, Montgomery RK, Fedyk CG, Aden JK, Ramasubramanian AK, et al. Hemostatic function of apheresis platelets stored at 4°C and 22°C. Shock. 2014; 41 Suppl 1: 54-61.
11. Murphy S, Gardner FH. Effect of storage temperature on maintenance of platelet viability--deleterious effect of refrigerated storage. N Engl J Med. 1969; 280(20): 1094-1098.
12. Marini I, Aurich K, Jouni R, Nowak-Harnau S, Hartwich O, Greinacher A, et al. Cold storage of platelets in additive solution: the impact of residual plasma in apheresis platelet concentrates. Haematologica. 2019; 104(1): 207-214.
13. Sørensen AL, Hoffmeister KM, Wandall HH. Glycans and glycosylation of platelets: current concepts and implications for transfusion. Curr Opin Hematol. 2008; 15(6): 606-611.
14. Hoffmeister KM, Felbinger TW, Falet H, Denis CV, Bergmeier W, Mayadas TN, et al. The clearance mechanism of chilled blood platelets. Cell. 2003; 112(1): 87-97.
15. Morell AG, Gregoriadis G, Scheinberg IH, Hickman J, Ashwell G. The role of sialic acid in determining the survival of glycoproteins in the circulation. J Biol Chem. 1971; 246(5): 1461-1467.
16. Jansen AJ, Josefsson EC, Rumjantseva V, Liu QP, Falet H, Bergmeier W, et al. Desialylation accelerates platelet clearance after refrigeration and initiates GPIbα metalloproteinase-mediated cleavage in mice. Blood. 2012; 119(5): 1263-1273.
17. Rumjantseva V, Grewal PK, Wandall HH, Josefsson EC, Sørensen AL, Larson G, et al. Dual roles for hepatic lectin receptors in the clearance of chilled platelets. Nat Med. 2009; 15(11): 1273-1280.
18. Ohtake S, Wang YJ. Trehalose: current use and future applications. J Pharm Sci. 2011; 100(6): 2020-2053.
19. Crowe JH, Crowe LM, Oliver AE, Tsvetkova N, Wolkers W, Tablin F. The trehalose myth revisited: introduction to a symposium on stabilization of cells in the dry state. Cryobiology. 2001; 43(2): 89-105.
20. Italiano JE Jr, Bergmeier W, Tiwari S, Falet H, Hartwig JH, Hoffmeister KM, et al. Mechanisms and implications of platelet discoid shape. Blood. 2003; 101(12): 4789-4796.
21. Crowe JH, Carpenter JF, Crowe LM. The role of vitrification in anhydrobiosis. Annu Rev Physiol. 1998; 60: 73-103.
22. Wolkers WF, Walker NJ, Tablin F, Crowe JH. Human platelets loaded with trehalose survive freeze-drying. Cryobiology. 2001; 42(2): 79-87.
23. Crowe JH, Tablin F, Wolkers WF, Gousset K, Tsvetkova NM, Ricker J. Stabilization of membranes in human platelets freeze-dried with trehalose. Chem Phys Lipids. 2003; 122(1-2): 41-52.
24. Liu Q, Xu L, Jiao SX, Wang TX, Song Y, Wen ZK. Trehalose inhibited the phagocytosis of refrigerated platelets in vitro via preventing apoptosis. Transfusion. 2009; 49(10): 2158-2166.
25. Handigund M, Bae TW, Lee J, Cho YG. Evaluation of in vitro storage characteristics of cold stored platelet concentrates with N acetylcysteine (NAC). Transfus Apher Sci. 2016; 54(1): 127-138.
26. Baghdadi V, Yari F, Rezaei N, Rafiee MH. The surface markers and survival rate of platelets during storage at 4°C: the influence of sodium octanoate. Iran J Ped Hematol Oncol. 2019, 9(2): 105-116.
27. Baghdadi V, Yari F, Nikougoftar M, Rafiee MH. Platelets apoptosis and clearance in the presence of sodium octanoate during storage of platelet concentrate at 4˚C. Cell J. 2020; 22(2): 212-217.
28. Wang X, Fan Y, Shi R, Li J, Zhao S. Quality assessment of platelets stored in a modified platelet additive solution with trehalose at low temperature (10 °C) and in vivo effects on rabbit model of thrombocytopenia. Platelets. 2015; 26(1): 72-79.
29. Quach ME, Chen W, Li R. Mechanisms of platelet clearance and translation to improve platelet storage. Blood. 2018; 131(14): 1512-1521.
30. Dasgupta SK, Argaiz ER, Mercado JE, Maul HO, Garza J, Enriquez AB, et al. Platelet senescence and phosphatidylserine exposure. Transfusion. 2010; 50(10): 2167-2175.
31. Perrotta PL, Perrotta CL, Snyder EL. Apoptotic activity in stored human platelets. Transfusion. 2003; 43(4): 526-535.
32. Li Y, Fu J, Ling Y, Yago T, McDaniel JM, Song J, et al. Sialylation on O-glycans protects platelets from clearance by liver kupffer cells. Proc Natl Acad Sci USA. 2017; 114(31): 8360-8365.

Original Article

Upregulation of hsa-miR-625-5p Inhibits Invasion of Acute Myeloid Leukemia Cancer Cells through ILK/AKT Pathway

Sahar Samieyan Dehkordi, M.Sc.[1], Seyed Hadi Mousavi, Ph.D.[1]*, Marzieh Ebrahimi, Ph.D.[2, 3]*, Shaban Alizadeh, Ph.D.[1], Amir Abbas Hedayati Asl, MD.[2, 3], Monireh Mohammad, M.Sc.[2], Bahareh Aliabedi, M.Sc.[1]

1. Department of Hematology, School of Allied Medical Sciences, Tehran University of Medical Sciences, Tehran, Iran
2. Department of Stem Cells and Developmental Biology, Cell Science Research Center, Royan Institute for Stem Cell Biology and Technology, ACECR, Tehran, Iran
3. Department of Regenerative Biomedicine, Cell Science Research Center, Royan Institute for Stem Cell Biology and Technology, ACECR, Tehran, Iran

**Corresponding Addresses: P.O.Box: 14177-44361, Department of Hematology, School of Allied Medical Sciences, Tehran University of Medical Sciences, Tehran, Iran*
P.O.Box: 16635-148, Department of Stem Cells and Developmental Biology, Royan Institute for Stem Cell Biology and Technology, ACECR, Tehran, Iran
Emails: hmousavi@tums.ac.ir, m.ebrahimi@royan-rc.ac.ir

Received: 08/June/2020, Accepted: 8/December/2020

Abstract

Objective: Acute myeloid leukemia (AML) is characterized by abnormalities of differentiation and growth of primary hematopoietic stem cells (HSCs) in the blood and bone marrow. In many studies, miR-625-5p has been shown to inhibit downstream pathways from affecting the metastasis and invasion of the integrin-linked kinase (ILK) signaling pathway. It has been proved that the expression of miR-625-5p decreases in AML cell lines. This study aimed to investigate the effect of miR-625-5p upregulation on the invasion of KG1 ell line *in vitro*.

Materials and Methods: In this experimental study, we investigated the impact of upregulation of miR-625-5p on invasion via the ILK/AKT pathway in the KG1 cell line. After transfection using the viral method, the cellular invasion was assessed by invasion assay and the levels of miR-625-5p genes and protein were evaluated by quantitative polymerase chain reaction (qPCR) and western blotting. Moreover, CXCR4 level was assessed by flow cytometry.

Results: The invasion significantly reduced in MiR-625-5p-transfected KG1 cells (P<0.01) that was concomitant with remarkably decreasing in the expression levels of *ILK, NF-κB*, and *COX2* genes compare with the control group (P<0.01). Incontrast, *MMP9, AP1*, and *AKT* significantly increased (P<0.01, P<0.001 and P<0.01, respectively) and GSK3β did not change significantly in MiR-625-5p-transfected KG1 cells. The protein level of NF-κB decreased (P<0.01) and MMP9 increased, however it was not significant. Moreoever, the expression of CXCR4 was significantly lower (P<0.01) in comparison with the control group.

Conclusion: miR-625-5p leads to a reduction in cell invasion in the AML cell line through ILK pathway. Therefore, it could be a breakthrough in future AML-related research. However, further studies are needed to support this argument.

Keywords: Acute Myeloid Leukemia, COX2, Integrin-Linked Kinase, Invasion, MMP9

Cell Journal(Yakhteh), Vol 24, No 2, February 2022, Pages: 76-84

Citation: Samieyan Dehkordi S, Mousavi SH, Ebrahimi M, Alizadeh Sh, Hedayati Asl AA, Mohammad M, Aliabedi B. Upregulation of hsa-miR-625-5p inhibits invasion of acute myeloid leukemia cancer cells through ilk/akt pathway. Cell J. 2022; 24(2): 76-84. doi: 10.22074/cellj.2022.7658.

Introduction

Acute myeloid leukemia (AML) is a heterogeneous class of aggressive hematopoietic malignancies with abnormal hematopoietic stem cells (HSCs) in the blood and bone marrow. AML leads to dysregulation and activation of cellular cascades such as invasion and migration. Invasiveness and resistance to therapy are two main issues that challenge research and treatment of refractory cancer (1). Some mechanisms of invasion and migration are cell migration and motility, extracellular matrix (ECM) destruction, and interaction with stromal and other cells (2).

The main problem is that the tumor cells, unlike normal cells, do not stop the signaling pathways to end this process, leading to the emergence of invasion (3). The majority of patients are not treated fully, and therefore identification of the mechanisms involved in AML invasion may culminate in innovative therapeutic methods, improve the treatment rate and reduce the rate of recurrence. Many studies have been conducted on AML, but the complex molecular mechanisms of the disease invasion and progression have not yet been adequately identified and further studies are needed to investigate this subject (4).

Much evidence has revealed dysregulation of microRNAs expression in cancer cells, so that miRNAs serve as tumor suppressors or oncogenes in cancer (5).

MiR-625-5p dysfunction has been identified in many diseases, often with reduced expression of the microRNA. This molecule can suppress various tumors, such as hepatocellular carcinoma, breast cancer, gastric cancer, and acute lymphocytic lukemia (ALL) (6). The increased expression of this miR can inhibit the proliferation and invasion of cancer cells. It has been confirmed that miR-625-5p expression decreases in AML cell lines (7).

Upregulation of miR-625-5p in gastric cancer significantly suppresses cell invasion and metastasis. ILK is a target gene of miR-625-5p that regulates cell invasion and metastasis. The integrin signaling pathway plays a crucial role in mediating the interaction between cells and the ECM. The ligand of ILK binds to the integrin and initiates out-to-inside signals by modulating the changes in various intracellular pathways including the expression of the genes MMP9 and NF-κB contributed in cell migration and invasion (8, 9).

ILK contributes substantially to regulating anchorage cell survival and growth, cell cycle progression, the epithelial-mesenchymal transition, invasion, and migration as well ascell movement. The invasion of the ILK signaling pathway occurs through two pathways: the GSK3β-Ap1-MMP9 signaling pathway and the AKT- NF-κB-COX2 pathway (10).

ILK activity increases in many cancers, and therefore ILK inhibitors have been identified that contribute to cancer treatment by inhibiting cell invasion, proliferation and survival so far (11, 12). It has also been demonstrated that this miR y, can control the downstream pathways by influencing the ILK signaling pathway and thus involved in the invasion and metastasis of cancers (8, 13).

Increased expression of miR-625-5p leads to induction of apoptosis and reduction in migration and invasion in AML by decreasing oncogenes. Studies on ILK gene expression throughout miR-625-5p's exerting effect on AML cell and changes in the expression of proteins involved in invasion and metastasis have increased our understanding of how this miR and its target genes in various processes lead to leukemia in the bone marrow.

This study investigated the effect of miR-625-5p upregulation on the invasion of AML cell *in vitro*. Finally, the mechanism of effect of miR-625-5p of KG1 cell line invasion is evaluated, and mRNA and protein levels of factors involved in the invasion, are measured through the ILK signaling pathway, including COX2, NF-ƙB, GSK3β, MMP9, AP1, and ILK.

Materials and Methods

Cell lines and cell cultures

In this experimental study, mycoplasma-negative KG1 human cells were purchased from the Pasteur Institute (Tehran, Iran). The KG1 cell line was taken from a patient with erythroleukemia in the myeloblastic phase and has the phenotype and function of myeloblasts. Human embryonic kidney 293 T cells were obtained from the Royan Institute (Tehran, Iran).

KG1 cell lines were cultured in RPMI1640 medium (Gibco-BRL, Eggenstein, Germany) containing10% fetal bovine serum (FBS, Gibco BRL, USA) and 1% penicillin/streptomycin and 2mm L-glutamine (Gibco, Germany) and in the presence of 5% CO_2 at 37°C.

HEK cells were cultured in Dulbecco's Modified Eagle Medium (DMEM ,Gibco-BRL, Eggenstein, Germany) with 15% FBS at 37°C and 5% CO_2. Every two days, the cell lines medium was changed.

This study was ethically coded and approved by Tehran University of Medical Sciences (IR.TUMS.SPH.REC.1395.837) and Royan Institute (IR.ACECR.ROYAN.REC.1397.41).

Plasmid construct and extraction

The pLentiIII-premiR-625-5p-GFP expression vector constructs and pLentiIII-Backbone-GFP were purchased from the Bonyakhte Institute (Tehran, Iran). Vector-harboring E. coliDH5α strain was grown in an incubator for 24 hours to produce a single colony on an LB agar medium (Thermo Fisher Scientific, USA) containing ampicillin at a concentration of 50 mg/ml of culture medium. One hundred µl of the culture containing bacteria purchased in Falcon tube was cultured in 300 ml of LB Broth (Thermo Fisher Scientific, USA) containing antibiotics and ampicillin, and placed inside a shaker incubator at 37°C for 12-16 hours. The plasmid was extracted by using Gene All Exprep™ Plasmid Kit (Gene All, Dongnam, Songpa-gu, Macherey-Nagel, Korea).

Confirmation of plasmid structure of pLentiIII-miR-625-5p-GFP and pLenti-backbone-GFP

To confirm the presence of miR-625-5p, we first retrieved the sequence file for miR-625-5p and the backbone using the Snap Gene program and the gene bank. miR-625-5p restriction enzymes, called BamH1 and EcoR1(Bonyakhte, Iran). Solutions contain of vector and enzymes that were first placed in a 37°C incubator for 4-6 hours run On the 1% electrophoresis gel (Merck, Germany). Then the plasmids were electrophoresed with a 1 kb marker size (Gibco BRL, USA) on 1% agar gel. After 45 minutes, plasmids were digested and identified by a gel document (Syngen, England).

Transient transfection

The concentration of fresh KG1 cells was maintained at 0.5-1.5×10^6 cells/ml. 5.0×10^6 from the cell subcultures were transfected with 5 µg miR-625-5p and Backbone vector using the viral transfection according to the respective protocol. First, we added gelatin 1% into the plate and placed it in the incubator at 37°C for 1 hours. After the removal of gelatin, the complete medium was added. 293T cells were counted and added drop by drop on the culture medium inside the plate,the supernatant was removed after a night and the new medium was added. At this step, we produced a transfection solution such as DMEM low glucose media, packaging vector PD and PS (Bonyakhte, Iran), miR-625-5p or backbone plasmid, PEI

(Bonyakhte, Iran) and incubated at room temperature. We added the transfection solution to the cells, and after 6-12 hours, removed the supernatant and added preheated media. Twenty four hours later, the first virus was extracted and the complete medium was added to the cells again. 48 hours later, the second step of the virus production was performed. At this step, we centrifuged the viruses at 37565 g and 4°C for 2 hours and dissolved them in RPMI1640 media. The virus was finally added to KG1 cell line and 48 hours after transfection, the Survival rate efficiency was investigated by flow cytometry. Transfection was performed on two cell groups (Backbone and Mir-625-5p) with three replications. After 48 hours of transfection, the transfected cells were collected for further assay.

Sorting green fluorescent protein expressing cells

First, the supernatant was isolated from the cells using centrifugation at 250 g for 5 minutes. Then, the cells were rinsed with dulbecco's phosphate-buffered saline (D-PBS)$^-$ solution and finally centrifuged at 250 g for 5 minutes. Then PBS with 1% bovine serum albumin (BSA) was added, and the cells expressing GFP were isolated using Ariya FACS sorting (Becton Dickinson, Belgium),

Functional assay

Invasion assay *in vitro*

We applied transwell inserts (24 well inserts, 8 μm pore size Millipore, USA) to gain the effect of miR-625-5p on the invasion of AML cells *in vitro*. the inserts were coated with ECM gel (BD Biosciences, Bedford, MA) for one night. Briefly, 2×10^5 cells were resuspended in serum-free medium and were dumped in the upper chambers as duplicates. The bottom chamber was incubated via RPMI1640 containing 20% FBS as absorbent (chemotactic) overnight to perform an invasion test.

Upon completion of the experiment, the cells that have remained on the upper surface of the membranes were removed and finally, the invasion cells to the bottom chamber were centrifuged at 250 g for 5 minutes.Then, the supernatant was removed and were counted on the neo-bar slide that were approximately 7×10^3.

The underlying cells of the insert were also fixed with 4% paraformaldehyde and stained with 0.1% crystal violet. Randomly five visual fields were counted from each insert using an optical microscope (14).

Flow cytometry

A total of 2-3×10^5 cells were rinsed with D-PBS solution and then incubated with CXCR4-PE (Santa Cruz Biotechnology. Inc, USA). Identical iso-type antibodies were used as a control (IgG2ακ, PE-conjugated, Santa Cruz Biotechnology. Inc, USA) for 30 minutes at 4°C.

Cells were analyzed using a FACS flow cytometer (Becton-Dickinson). Analysis of CXCR-4 expression in GFP-positive KG1 gametes, GFP-positive KG1 cells were gated in a SSC/FL-3 dot plot.

A FL-1/FL-2 dot plot was applied for further analysis of GFP-positive KG1 cells. Mean fluorescence intensity was measured with reference to the fluorescence histogram and presented as corresponding units (15).

RNA extraction and cDNA synthesis

Total RNA was extracted from the KG1 cell line using Trizol (Invitrogen, Carlsbad, CA, USA) reagent 48 hours after transfection based on the manufacturer's protocol. RNA quality was then determined by electrophoresis and DNA extraction was performed using a fermentase kit (Fermentas, Lithuania) to remove any remaining DNA according to the manufacturer's protocol. cDNA of the whole RNA was synthesized by cDNA synthesis kit (Royan Biotech, Tehran, Iran) and miR-625-5p by another CDNA synthesis kit (Bonyakhte Tehran, Iran) (16).

Quantitative polymerase chain reaction for miR-625-5p expression

The reverse and forward primers with the stem-loop primers were designed for cDNA synthesis and miR-625-5p qPCR according to the procedure of Chen et al. (17).

The expression level of miRNA was assessed by miRNA diagnostic kit (Bonyakhte, Iran) using the qRT-PCR stem-loop method. U6 RNA (snord47) was used for normalization. Finally, the relative expression ratio of miR-625-5p was determined by $2^{-\Delta\Delta CT}$in triplicate (13).

Quantitative polymerase chain reaction for genes expression

ILK and *NF-κB* as direct targets and *AKT, GSK3β, AP1 (c-FOS), MMP-9, COX2* as indirect targets of miR-625-5p, were determined using the miRNAs target prediction site (http//: miRtarbase.mbc.nctu.edu.tw) and according to the study of Wang et al. (8). Gene primers were then designed and blasted for using Primer Premier 5 software (Premier Biosoft International, USA) and Gen Runner software (ver.5.1). *GAPDH* was used a reference gene (Table 1).

To detect *ILK, AKT, GSK3β, AP1, MMP-9, NF-κB, COX2,* and *GAPDH* transcription levels, cDNA was made from the total RNA using SuperScript III First-Strand Synthesis System and then measured using Takara SYBR PCR Green Kit (Takara Bio Inc., Shiga, Japan).

The expression levels of *ILK, AKT, GSK3β, AP1, MMP-9, NF-κB and COX2* mRNA were normalized to

GAPDH mRNA level. Target genes relative expression ratio was calculated by the $2^{-\Delta\Delta CT}$ method in triplicate.

To plot the standard curve of the primers, we prepared their 1:5 to 5 titrations in distilled water and placed them in the ABI StepOnePlus device to determine the CT. The qRT-PCR reaction (ABI StepOnePlus) was used to measure gene expression changes (8).

Western blotting analysis

After 48 hours, cell lines transfected with miR-625-5p and backbone vector were cultured and rinsed three times with cold PBS solution.

Total protein was extracted from cells by trisol (Invitrogen, Carlsbad, CA, USA) and cell lysis buffer (Biyuntian Biotechnological Co., USA). The protein concentration of the lysate was calculated from the standard line of BSA.

First 5 µl protein was boiled at 95°C for 5 minutes and then cooled on ice. Then it was run on an SDS-PAGE gel (Millipore, USA) to determine its quality and electrotransferred to PVDF membrane (Life Science, Amersham, Braunschweig, Germany). Membranes were blocked by non-fat dry milk (w/v) and then immunoblotted with anti-NF-κB-p65 (Abcam, Inc., Cambridge, MA, USA) and anti-MMP-9 (Santa Cruz Biotechnology. Inc, USA) at 4°C overnight (dilutions 1: 200 and 1: 700, respectively), followed by horseradish peroxidase-conjugated rabbit (Abcam, Inc., Cambridge, MA, USA) and goat (Santa Cruz Biotechnology. Inc, USA) secondary antibodies (dilution1:3000) incubated at room temperature for one hour. NF-κB and MMP-9 protein bands were visualized with ECL (Kodak Image Station; New Haven, CT, USA). The band densities were analyzed to use Image J software (n=3) (18).

Table 1: The list of primers used in quantitative real time polymerase chain reaction analysis

Genes	Primer sequence (5´-3´)	Length	Annealing temp.(°C)	Reference
miR-625-5p	StemloopRT: AGGGUAGAGGGAUGAGGGGGAAAGUUCUAUAGUCCUGUAAUU AGAUCUCAGGACUAUAGAACUUUCCCCCUCAUCCCUCUGCCCU	503	60	http://www.mirbase.org/
	F: CTCTGCTTGACTGTGCTG			
	R: TACCAGAACCTAACCAACTG			
SNORD 47	StemloopRT: GTCGTATGCAGAGCAGGGTCCGAGGTAT TCGCACTGCATACGACAACCTC	71	60	Designed by AlleleID and oligo sofware
	F: ATCACTGTAAAACCGTTCCA			
	R: GAGCAGGGTCCGAGGT			
GAPDH	F: AGGGTCTCTCTCTTCCTCTTGTGC TCT	224	60	Designed by AlleleID and oligo sofware
	R: CCAGGTGGTCTCCTCTGACTTCAA CAG			
ILK	F: CACCTGCTCCTCATCCTACTC	209	60	Designed by AlleleID and oligo sofware
	R: CTCATCAATCATTACACTACGGCT			
AKT	F: AACGAGTTTGAGTACCTGAAGC	204	60	Designed by AlleleID and oligo sofware
	R: GTACTTCAGGGCTGTGAGGA			
GSK3β	F: AGTGGTGAGAAGAAAGATGAGGT	207	60	Designed by AlleleID and oligo sofware
	R: GAGGTTCTGCGGTTTAATATCCC			
MMP-9	F: CAAGGATGGGAAGTACTGGC	117	60	Designed by AlleleID and oligo sofware
	R: TCCTCAAAGACCGAGTCCAG			
NF-κB	F: ACTGCCCAATTTAACAACCTG	220	60	Designed by AlleleID and oligo sofware
	R: CATCACTGGCTCTAAGGAAGG			
COX2	F: ACCAATTGTCATACGACTTGCAG	197	60	Designed by AlleleID and oligo sofware
	R: AAGGATTTGCTGTATGGCTGAG			
C-FOS (AP1)	F: TCGGGCTTCAACGCAGAC	85	60	Designed by AlleleID and oligo sofware
	R: GAGTGGTAGTAAGAGAGGCTATCC			

Statistical analysis

In this study, the GraphPad Prism software (V.7, GraphPad Software, Inc., San Diego, CA) was employed to conduct statistical analysis. The results of our tests were analyzed with t test and ANOVA. The data were expressed as mean ± standard deviation (SD). The significance level P<0.05 was considered statistically significant. In the charts, the P<0.05 shown with a star (*), P<0.01 shown with two stars (**), P<0.001 shown with three stars (***), and P<0.0001 shown with four stars (****). All the experiments were repeated three times.

Results

Transfected and overexpression of miR-625-5p in KG1 cells

To study the impact of miR-625-5p on the regulation of *ILK, AKT, GSK3β, AP1(C-FOS), MMP-9, NF*-κB, *COX2*, and finally invasion in KG1 cells, the cells were first transfected with premiR-625-5p and backbone expression vectors construct by viral transfection followed by detection of invasion.

Fluorescent microscope (Fig.1A) and flow cytometry analysis confirmed the efficacy of transfection after 48 hours (Fig.1B) where around 60% of the cells were transfected. The qRT-PCR showed a significantly increased miR-625-5p expression in the cells after 48 hours of transfection (Fig.1C). MiR-625-5p expression was approximately 27-fold higher than that of backbone vector-transfected cells (P=0.01).

miR-625-5p expression reduced cell counts after transfection

After adjoining the virus to the cells, the number o cells, and cell viability were studied after 24 and 48 hours of the transfection. After 48 hours, it was observed that the average number of cells and viability percentage reduced in miR-625-5p-transfected cells compared to the backbone group (P<0.01).

The association of miR-625-5p expression with the invasive activity of acute myeloeid leukemia cell line

To figure out the association of miR-625-5p with cell invasion, cellular invasion in the KG1 cells was evaluated by transwell insert 48 hours after transfection. As illustrated in Figure 2A and B, the count of cells attached to the filter bottom decreased in cells treated with miR-625-5p. The number of miR-625-5p transfected KG1 cell line was lower than that of Backbone transfected cells. The count of these cells was approximately 0.6% fold lower than control (Fig.2C, P<0.01).

Overexpression of miR-625-5p reduced CXCR-4 expression in the surface of the KG1 cell

The CXCR-4 surface marker was examined using flow cytometry with an antibody attached to the PE as a marker of invasion. As illustrated in Figure 3A and B, the count of miR-625-5p transfected KG1 cell line was lower than that in backbone transfected cells. The count of cells transfected with pre miR-625-5p expressing CXCR was around 13.7% lower than Backbone vector-transfected cells (Fig.3C).

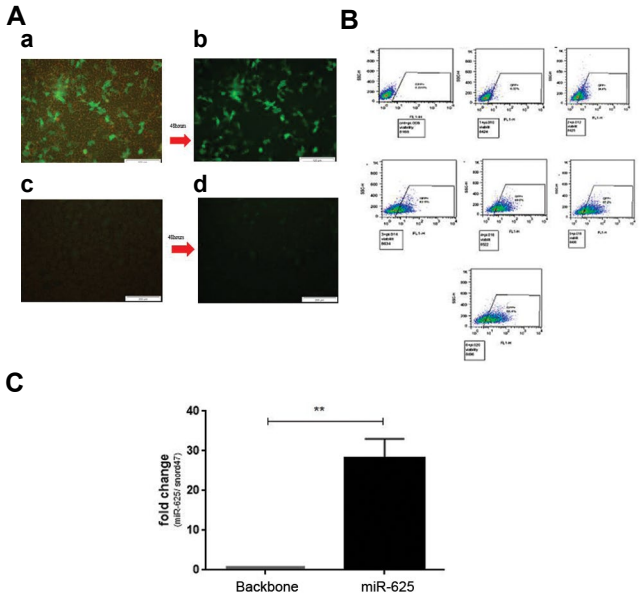

Fig.1: GFP expression in 293T cell and KG1**. A.** GFP expression in 293Tcell and KG1 after 48 hours by Fluorescent microscope**.** 293T cells as controls for GFP expression (a, b), KG1 cells without and with GFP expression (c), KG1 cells expressing GFP positive (d). **B.** Virus-free control cells with 82% viability (a) and cells with 10 µl of concentrated virus and 7% GFP expression (b). Cells with 20µl of concentrated virus and 34% GFP expression (c). Cells with 50 µl of concentrated virus and 43% GFP expression (d). Cells with 70 µL of concentrated virus and 66% GFP expression (e). Cell with 90 µl concentrated virus and 67% GFP expression (f) and cell with 120 µl concentrated virus and 66% GFP expression (g). Based on the percentage of expression GFP, the amount of concentrated virus was found to have a constant expression at 70, 90 and 120 µl. **C.** Confirmation of miR-625-5p expression in KG1 cells after transfection by qRT-PCR. KG1 cells were transfected with pre miR-625-5p expression vector construct or Backbone. The expression of the miR-625-5p in the KG1 cells transfected with the recombinant vector was considerably higher than Backbone after 48 hours (**P<0.01). GFP; Green fluorescent protein and qRT-PCR; Quantitative real time polymerase chain reaction.

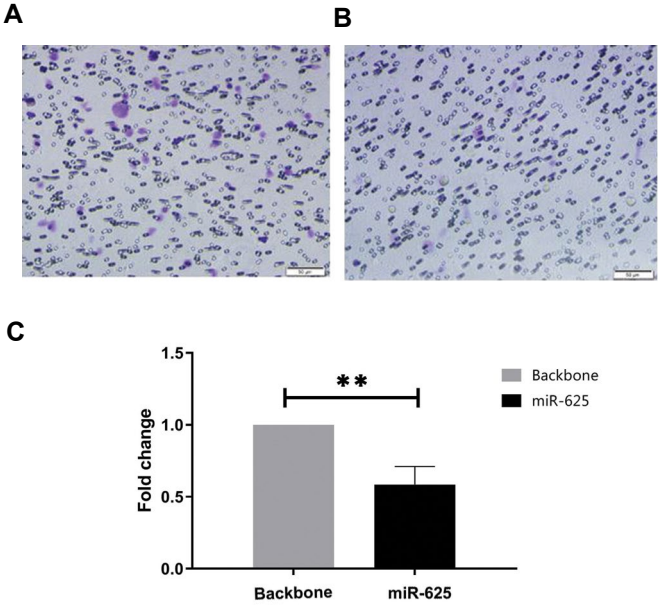

Fig.2: Effect of miR-625-5p overexpression on invasion in kG1 cells 48 hours post-transfection. The transfected KG1 cells were treated with invasion assay (transwell insert) and followed by count. Invasive cells and connected to bottom the filter. **A.** Cells transfected with backbone (scale bar: 100 µm). **B.** Cells transfected with miR-625-5p (scale bar: 100 µm). Overexpression of miR-625-5p in KG1 cells significantly decreased the invasive cell compared to Backbone. **C.** There was a significant 0/6% reduction in the invasive cells transfected with miR-625-5p construct (**P<0.01).

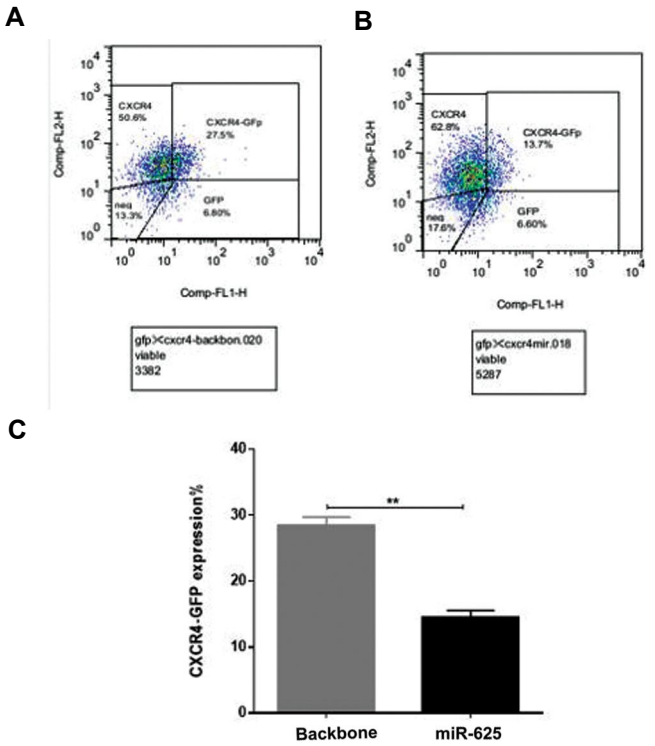

Fig.3: Effect of miR-625 overexpression on cells expressing CXCR-4 in KG1 cells 48 hours post-transfection. The transfected KG1 cells were treated with Antibody CXCR-4-PE and followed by flow cytometry analysis. **A.** In the KG1 cells transfected with pre miR-625-5p-GFP construct, approximately 13.7% of cells became CXCR-4-PE positive. **B.** About 27.5% of KG1 transfected cells with Backbone-GFP showed CXCR-4-PE positive. **C.** Overexpression of miR-625-5p in KG1 cells significantly decreased cells expressing CXCR-4compared to Backbone (**P<0.01).

ILK and NF-κB are potential downstream targets of miR-625-5p

To figure out the miR-625-5p-mediated invasion molecular mechanism in KG1 cells, we identified the targets of miR-625-5p. The sequence analysis of ILK demonstrated that ILK harbored potential miR-625-5p target sites at 136-143nt, which are the ILK 3′UTR, and the sequence analysis of NF-κB indicated that NF-κB harbored potential miR-625-5p target site 3′UTR of the microRNA.org site. Regarding the correlation of miR-625-5p to ILK, the ILK and downstream oncogenes mRNA levels were measured in the KG1 cell line. Cell mRNA was used 48 hours after transfection to evaluate changes in the expression of *ILK, AKT, GSK3β, C-FOS (AP1), MMP-9, NF*-κB genes using qRT-PCR (Fig.4). Our results from qRT-PCR demonstrated that the expression of ILK, as the main target at the mRNA level, was dramatically reduced in KG1 compared with the Backbone-transfected KG1 cell line. The expression of *ILK* in these cells caused a significant decrease (0.53 times lower than Backbone group) (P<0.01). The expression of the *NF*-κB and *COX2* genes decreased [0.55 (P<0.01), 0.32 (P<0.001), respectively] and the expression of genes *MMP-9, C-FOS (AP1)* and *AKT* increased [1.36 (P<0.01), 3 (P<0/001) and 1.43 (P<0.01), respectively]; however *GSK3β* did not show a significant change (0.85 with P>0.05).

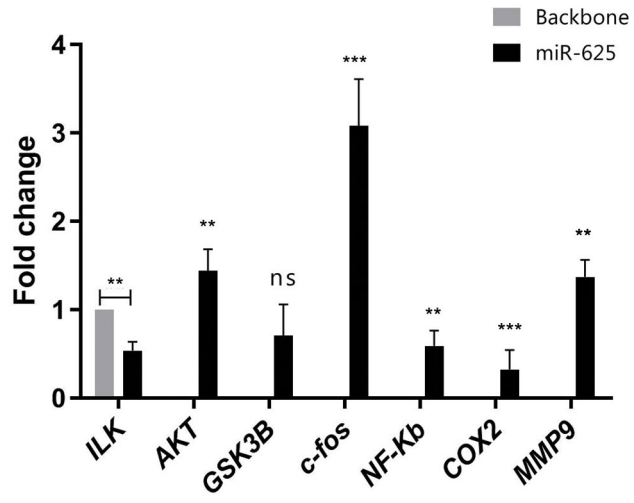

Fig.4: Expression of *ILK, AKT, GSK3β, AP1, MMP-9, NF*-κB genes by qPCR. KG1 cells transfected either with the premiR-625-5p construct or Backbone vector followed by expression evaluation *ILK, AKT, GSK3β, AP1, MMP-9, NF*-κB genes 48 hours after transfection. Overexpressed miR-625-5p resulted in downregulation of *ILK, NF*-κB and *COX2* expression and upregulation of *AKT, MMP-9* and *C-FOS* (*AP1*) but caused no alteration in *GSK3β* expression (P<0.01, P<0.001). In the diagrams, P<0.01 and P<0.001 are shown with ** and ***, respectively. qPCR; Quantitative real time polymerase chain reaction and ns; Not significant.

Overexpression MiR-625-5p reduction of NF-κB expression of protein

The western blotting was performed to evaluate the expression of NF-κB, MMP-9 and β-Actin proteins in invasion KG1 cells compared with the Backbone cells 48 hours after transfection. As illustrated in Figure 5A, the NF-kB protein showed a significant reduction of 0.6% fold (P<0.01) when it transfected with miR-625-5p versus the backbone group and MMP9 protein expression that did not show a significant change (Fig.5B). The results showed that miR-625-5p could inhibit cell invasion by inhibiting ILK and NF-κB as well as the COX-2 signaling pathway.

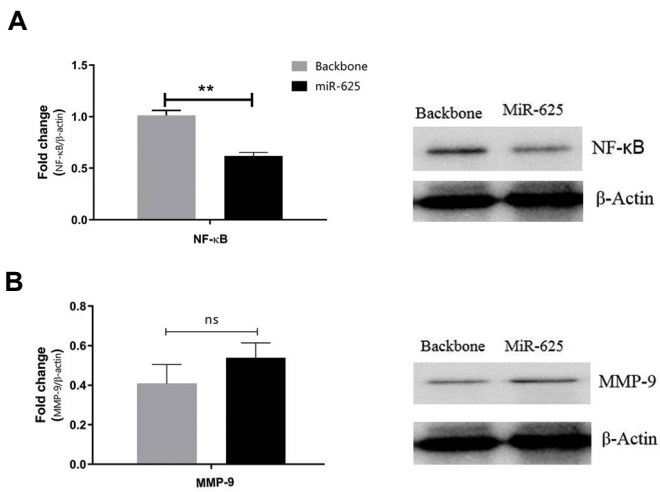

Fig.5: Western blot and Densitometry analysis of NF-κB and MMP-9 protein expression in KG1 cells transfected by either premiR625-5p construct or Backbone vector 48 hours post-transfection. **A.** miR-625-5p downregulated (0.6 fold lower) NF-κB protein. **B.** miR-625-5p caused no alteration in MMP-9 expression. Densitometry analysis of bands by ImageJ software. β-actin was used as loading control (P<0.01). In the diagrams, P<0.01 is shown with (**).

Discussion

The unnatural expression of miRNAs has already been investigated in different cancers, focusing on the understanding of the role and function of miRNAs in cancer progression (19). Here, we assessed miR-625-5p-mediated invasion molecular mechanism in AML cells (20). MiR-625-5p-transfected KG1 cells of invasion significantly decreased. The expression levels of ILK, NF-κB, and COX2 genes significantly decreased while MMP9, AP1, and AKT significantly increased, whereas GSK3β did not change significantly. At the protein level, NF-κB, decreased and MMP9 increased but not significantly. The expression of CXCR4 was also significantly lower.

Our results also showed that miR-625-5p inhibited cell invasion and migration in AML cells. Surprisingly, we found ILK as a possible target for miR-625-5p. We observed that miR-625-5p exhibited its tumor-suppressing function in the downregulation of cell invasion by regulating the ILK-NF-ƙB-COX2 pathways. Our study may therefore offer a new strategy for AML treatment through the upregulation miR-625-5p level.

AML is a heterozygous disease in which cell proliferation is high and apoptosis is low, and therefore its treatment is challenging due to the unknown pathogenic and intrinsic biological agents (21). The identification of AML invasion mechanisms may culminate in innovative therapeutic methods, an increase in treatment rate, and a decrease in the recurrence rate (4). Various types of miR-RNAs play part in AML and other cancers. For example, miR-625-5p is a potential biomolecule playing part in regulating cell survival and differentiation. Studies have shown miR-625-5p expression is often reduced and acts as a tumor suppressor in various tumors, including hepatocellular carcinoma, breast cancer, and malignant melanoma (22). It has also been demonstrated that miR-625-5p expression decreases in AML cell lines (23).

The expression of this miR can inhibit the proliferation and invasion of cancer cells (7). In the study Ma et al. (14) increased expression of mir-625-5p led to decreased apoptosis and cellular metastasis in patients with AML. In another study, Wang et al. (8) showed that miR- 625-5p upregulation in gastric cancer resulted in a decrease in invasion through interfering with the regulation of the ILK signaling pathway. Our findings revealed that invasion was significantly decreased in KG1 cells following overexpression of miR-625-5p. In the current study, we addressed the potential anticancer effect of miR-625-5p to assist in the treatment of AML (11).

According to a previous study, the expression of ILK has constitutive activation in AML (12). Inhibition of ILK by compound-22 causes inhibition of migration, invasion, and proliferation in CML, AML, and ALL (24). ILK is a direct target of miR-625-5p, and miR-625-5p upregulation in KG1 cells results in ILK expression downregulation (8) followed by downregulation of AKT of NF-κB and COX2, resulting in invasion (25, 26). AKT1 activates the proliferation and invasion pathways in breast tumors, colorectal cancer, and leukemia (27). AKT1 seems to play an essential yet passive part in oncogenesis. AKT is activated directly via PIP3 and ILK (10). In reality, the PI3K/AKT signaling pathway contributes greatly to regulating cellular processes by which cancer is characterized, such as cell proliferation, survival, and migration (28). AKT can activate NF-κB and therefore NF-κB is an important marker in cancer cells involved in growth-independent propagation, apoptosis prevention, infiltrate replication, invasion, and tissue metastasis. ILK also leads to the activation of COX2 via the ILK-AKT-NF-κB pathway (25, 29). Previous studies have shown that the expression of COX2 increases in AML (30). Our results also showed that overexpression of miR-625-5p resulted in the downregulation of ILK, NF-κB, and COX2 because of miR-625-5p, according to microRNA.org, directly inhibited ILK and NF-κB and subsequently invasion. Overexpression of miR-625-5p led to the upregulation of AKT because AKT was separately activated via PIP3.

Ample evidence demonstrates that ILK activates the GSK3β-AP1-MMP9 signaling pathway. GSK3β contributes substantially to the cytoskeletal organization, cell polarity, and migration in organogenesis and wound healing physiological processes (2). GSK3β also contributes to cancer cell motility, migration, and invasion via a pharmacological inhibitor and, through the interference of RNA, reduces the capacity of migration and invasion of pancreatic cancer glioblastoma cells, resulting in the decrease of MMP-2 expression (31). AKT positively regulates these targets through the inhibition of GSK3 as well (32). Then, the increase in the expression of c-fos (AP1), in addition to AP1-related target genes, has been observed in many cancers. The expression of ILK induces expression of MMP-9 through the activation of AP1 transcription, causing the increase of migration and invasion. MMPs are indeed a family of endopeptidases that are functionally and structurally zinc-dependent and are responsible for the destruction of ECM components, and thus regulate metastasis and invasive tumor cells. The expression of MMPs is controlled by upstream regulation of sequences and has a connection point for AP1. MMP-9 expression increases in malignant cancers (33). In our study the miR-625-5p expression did not change the expression level of MMP-9.

Lou et al. (34) investigated osteosarcoma (OS) and its miR-625 related effects. miR-625 expression enhanced by mimic-miR-625 substantially decreased the invasion and proliferation of OS cells through the *YAP-1* gene, an important target for the treatment of OS. Wang et al. (8) studied the expression of miR-625, which contributes importantly to cancer progression. By inducing and increasing the expression of this miR in gastric cancer cells, they found that metastasis and tumor invasion were inhibited by the ILK signaling pathway and ILK was miR-625-5p's direct target.

Generally, in agreement with the results of Wang et al. (8) and Lou et al. (34). the current study indicated that

miR-625's inhibitory effect on invasion was similar to its oncogenic effects (35). In our study, similar to the findings of previous studies the overexpression of miR-625-5p altered the expression level of ILK, NF-κB, and COX2. The results of our study regarding ILK expression and invasion are consistent with the this study.

CXCR-4 is a chemokine receptor coupled to G proteins, which are expressed on the HSCs. Indeed, CXCL-12 is coupled to the CXCR-4 receptor on the surface of HSCs, which is a chemokine playing a highly important role in maintaining bone marrow, silence, implantation, survival, leading to the maintenance of the function of HSCs and gene expression, and cell migration by downstream B kinase (AKT)/(MAPK) signaling pathway activity (35). In AML patients, CXCR4 expression is significantly up-regulated and has a poor prognosis. In leukemia, CXCR4 causes the adhesion of leukemia cells to bone marrow stromal cells, resulting in resistance to chemotherapy and extramedullary infiltration into organs expressing SDF-1 (36). Metastasis of cancer cells occurs through the activation of CXCR-4 and the migration of cancer cells towards the organs expressing CXCL-12. Also, SDF-1a regulates leukemia cell trafficking through binding its cognate receptor CXCR4 on leukemia cells. In the BM, disturbance and destruction of cell anchorage by SDF1-CXCR-4 via proteolytic enzymes such as MMP-9 can lead to cellular development in the bloodstream. The CXCR-4-CXCL-12 axis is powered by AML and is a regulator of cell invasion, mobilization, implantation, and maintenance of leukemia stem cells during the onset and progression of the disease (37, 38). Panneerselvam et al. (39) reported that IL-24 disrupted the SDF-1/CXCR4 signaling axis and reduced CXCR4 expression and finally inhibited the invasion and migration of lung cancer cells. The study of Zuo et al. (40) indicated that CXCR4 overexpression enhanced cell motility and invasion by producing EGFR and MMP-9 in lung cancer (NSCLC). The results of our study regarding the expression of CXCR-4 are consistent with the studies of Panneerselvam et al. (39) and Zuo et al. (40) in which miR-625-5p overexpression caused CXCR-4 expression reduction.

Conclusion

The upregulation of the miR-625-5p expression leads to a reduction in cellular invasion in AML cell lines via the ILK pathway signaling via AKT-NF-κB-COX2 pathway. Based on the findings, that show that miR-625-5p leads to a reduction in cell invasion in the AML cell line by ILK pathway, this strategy could be a breakthrough in future AML-related research. However, further studies are needed to achieve this goal.

Acknowledgments

The current research was obtained from an M.Sc. Thesis funded at Tehran University of Medical Sciences (Grant no.: 32831), Royan Institute and Royan Stem Cell Technology Cord Blood Bank. The authors are thankful for the collaboration of Royan Institute to support experiments. The authors do not have any conflicts of interest to report.

Authors' Contributions

S.H.M, M.E.; Contributed to conception, design, statistical analysis, interpretation of data, and were responsible for overall supervision. S.S.D; Contributed to all of the experimental works, drafted the manuscript and designed the figures which was revised by S.H.M, Sh.A., A.A.H.A. Sh.A., A.A.H.A.; Also contributed to the interpretation of the results. B.A., M.M.; Contributed to some experimental works and did transfection. All authors read and approved the final manuscript.

References

1. Ye Q, Liao X, Fu P, Dou J, Chen K, Jiang H. Portulacerebroside A inhibits adhesion, migration, and invasion of human leukemia HL60 cells and U937 cells through the regulation of p38/JNK signaling pathway. Onco Targets Ther. 2016; 9: 6953.
2. Domoto T, Pyko IV, Furuta T, Miyashita K, Uehara M, Shimasaki T, et al. Glycogen synthase kinase-3β is a pivotal mediator of cancer invasion and resistance to therapy. Cancer Sci. 2016; 107(10): 1363-1372.
3. Stuelten CH, Parent CA, Montell DJ. Cell motility in cancer invasion and metastasis: insights from simple model organisms. Nat Rev Cancer. 2018; 18(5): 296-312.
4. Ye Q, Fu P, Dou J, Wang N. Downregulation of PDIA3 inhibits proliferation and invasion of human acute myeloid leukemia cells. Onco Targets Ther. 2018; 11: 2925-2935.
5. Gupta GP, Massagué J. Cancer metastasis: building a framework. Cell. 2006; 127(4): 679-695.
6. Li JY, Liang ZA, Zheng J. MicroRNA-625 serves as a tumor suppressor in non-small cell lung cancer through targeting SOX4. Int J Clin Exp Med. 2018; 11(4): 3225-3234.
7. Lou X, Qi X, Zhang Y, Long H, Yang J. Decreased expression of microRNA-625 is associated with tumor metastasis and poor prognosis in patients with colorectal cancer. J Surg Oncol. 2013; 108(4): 230-235.
8. Wang M, Li C, Nie H, Lv X, Qu Y, Yu B, et al. Down-regulated miR-625 suppresses invasion and metastasis of gastric cancer by targeting ILK. FEBS Lett. 2012; 586(16): 2382-2388.
9. Wu C. PINCH, N(i)ck and the ILK: network wiring at cell-matrix adhesions. Trends Cell Biol. 2005; 15(9): 460-466.
10. Faes S, Dormond O. PI3K and AKT: unfaithful partners in cancer. Int J Mol Sci. 2015; 16(9): 21138-21152.
11. Krenn PW, Hofbauer SW, Pucher S, Hutterer E, Hinterseer E, Denk U, et al. ILK induction in lymphoid organs by a TNFα-NF-κB-regulated pathway promotes the development of chronic lymphocytic leukemia. Cancer Res. 2016; 76(8): 2186-2196.
12. Alasseiri M, Ahmed AU, Williams BRG. Mechanisms and consequences of constitutive activation of integrin-linked kinase in acute myeloid leukemia. Cytokine Growth Factor Rev. 2018; 43: 1-7.
13. Wang Z, Qiao Q, Chen M, Li X, Wang Z, Liu C, et al. miR-625 down-regulation promotes proliferation and invasion in esophageal cancer by targeting Sox2. FEBS Lett. 2014; 588(6): 915-921.
14. Ma L, Wang YY, Jiang P. LncRNA LINC00909 promotes cell proliferation and metastasis in pediatric acute myeloid leukemia via miR-625-mediated modulation of Wnt/β-catenin signaling. Biochem Biophys Res Commun. 2020; 527(3): 654-661.
15. Zheng J, Fu L, Li Z, Shi Q, Li J, Chen S. RNA interfering of CXCR4 inhibits the adhesion, invasion, and tumorigenicity of acute monocytic leukemic cells in vivo. Int J Clin Exp Pathol. 2018; 11(1): 68-75.
16. Khosravi MA, Abbasalipour M, Concordet JP, Berg JV, Zeinali S, Arashkia A, et al. Expression analysis data of BCL11A and γ-globin genes in KU812 and KG-1 cell lines after CRISPR/Cas9-mediated BCL11A enhancer deletion. Data Brief. 2019; 28: 104974.
17. Chen C, Ridzon DA, Broomer AJ, Zhou Z, Lee DH, Nguyen JT, et al. Real-time quantification of microRNAs by stem-loop RT-PCR. Nucleic Acids Res. 2005; 33(20): e179.
18. Pan L, Li Y, Zhang HY, Zheng Y, Liu XL, Hu Z, et al. DHX15 is associated with poor prognosis in acute myeloid leukemia (AML) and regulates cell apoptosis via the NF-kB signaling pathway. Onco-

target. 2017; 8(52): 89643-89654.
19. Landgraf P, Rusu M, Sheridan R, Sewer A, Iovino N, Aravin A, et al. A mammalian microRNA expression atlas based on small RNA library sequencing. Cell. 2007; 129(7): 1401-1414.
20. Vidigal JA, Ventura A. The biological functions of miRNAs: lessons from in vivo studies. Trends Cell Biol. 2015; 25(3): 137-147.
21. Stone RM, Mandrekar SJ, Sanford BL, Laumann K, Geyer S, Bloomfield CD, et al. Midostaurin plus chemotherapy for acute myeloid leukemia with a FLT3 mutation. N Engl J Med. 2017; 377(5): 454-464.
22. Li JY, Liang ZA, Zheng J. MicroRNA-625 serves as a tumor suppressor in non-small cell lung cancer through targeting SOX4. Int J Clin Exp Med. 2018; 11(4): 3225-32134.
23. Xiong Q, Yang Y, Wang H, Li J, Wang S, Li Y, et al. Characterization of miRNomes in acute and chronic myeloid leukemia cell lines. Genomics Proteomics Bioinformatics. 2014; 12(2): 79-91.
24. de la Puente P, Weisberg E, Muz B, Nonami A, Luderer M, Stone RM, et al. Identification of ILK as a novel therapeutic target for acute and chronic myeloid leukemia. Leuk Res. 2015; 39(11): 1299-1308.
25. Hsu HC, Fong YC, Chang CS, Hsu CJ, Hsu SF, Lin JG, et al. Ultrasound induces cyclooxygenase-2 expression through integrin, integrin-linked kinase, Akt, NF-kappaB and p300 pathway in human chondrocytes. Cell Signal. 2007; 19(11): 2317-2328.
26. Xia M, Duan ML, Tong JH, Xu JG. MiR-26b suppresses tumor cell proliferation, migration and invasion by directly targeting COX-2 in lung cancer. Eur Rev Med Pharmacol Sci. 2015; 19(24): 4728-4737.
27. Zeng Z, Sarbassov dos D, Samudio IJ, Yee KW, Munsell MF, Ellen Jackson C, et al. Rapamycin derivatives reduce mTORC2 signaling and inhibit AKT activation in AML. Blood. 2006; 109(8): 3509-3512.
28. Kumar A, Rajendran V, Sethumadhavan R, Purohit R. AKT kinase pathway: a leading target in cancer research. ScientificWorldJournal. 2013; 2013: 756134.
29. Li C, Li F, Zhao K, Yao J, Cheng Y, Zhao L, et al. LFG-500 inhibits the invasion of cancer cells via down-regulation of PI3K/AKT/NF-κB signaling pathway. PLoS One. 2014; 9(3): e91332.
30. Iachininoto MG, Nuzzolo ER, Bonanno G, Mariotti A, Procoli A, Locatelli F, et al. Cyclooxygenase-2 (COX-2) inhibition constrains indoleamine 2,3-dioxygenase 1 (IDO1) activity in acute myeloid leukaemia cells. Molecules. 2013; 18(9): 10132-10145.
31. Koul D, Shen R, Bergh S, Lu Y, de Groot JF, Liu TJ, et al. Targeting integrin-linked kinase inhibits Akt signaling pathways and decreases tumor progression of human glioblastoma. Mol Cancer Ther. 2005; 4(11): 1681-1688.
32. Manning BD, Toker A. AKT/PKB signaling: navigating the network. Cell. 2017; 169(3): 381-405.
33. Hannigan G, Troussard AA, Dedhar S. Integrin-linked kinase: a cancer therapeutic target unique among its ILK. Nat Rev Cancer. 2005; 5(1): 51-63.
34. Luo Z, Wu G, Zhang D, Liu J, Ran R. microRNA-625 targets Yes-associated protein 1 to suppress cell proliferation and invasion of osteosarcoma. Mol Med Rep. 2018; 17(1): 2005-2011.
35. Domanska UM, Kruizinga RC, Nagengast WB, Timmer-Bosscha H, Huls G, de Vries EG, et al. A review on CXCR4/CXCL12 axis in oncology: no place to hide. Eur J Cancer. 2013; 49(1): 219-130.
36. Matsuo H, Nakamura N, Tomizawa D, Saito AM, Kiyokawa N, Horibe K, et al. CXCR4 overexpression is a poor prognostic factor in pediatric acute myeloid leukemia with low risk: a report from the japanese pediatric leukemia/lymphoma study group. Pediatr Blood Cancer. 2016; 63(8): 1394-1399.
37. Rashidi A, DiPersio JF. Targeting the leukemia-stroma interaction in acute myeloid leukemia: rationale and latest evidence. Ther Adv Hematol. 2016; 7(1): 40-51.
38. Cao T, Ye Y, Liao H, Shuai X, Jin Y, Su J, et al. Relationship between CXC chemokine receptor 4 expression and prognostic significance in acute myeloid leukemia. Medicine (Baltimore). 2019; 98(23): e15948.
39. Panneerselvam J, Jin J, Shanker M, Lauderdale J, Bates J, Wang Q, et al. IL-24 inhibits lung cancer cell migration and invasion by disrupting the SDF-1/CXCR4 signaling axis. PLoS One. 2015;10(3):e0122439.
40. Zuo J, Wen M, Li S, Lv X, Wang L, Ai X, et al. Overexpression of CXCR4 promotes invasion and migration of non-small cell lung cancer via EGFR and MMP-9. Oncol Lett. 2017; 14(6): 7513-7521.

Original Article

Melittin Prevents Metastasis of Epidermal Growth Factor-Induced MDA-MB-231 Cells through The Inhibition of The SDF-1α/CXCR4 Signaling Pathway

Fatemeh Salimian, M.Sc., Mohammad Nabiuni, Ph.D.*, Ensieh Salehghamari, Ph.D.

Department of Cell and Molecular Biology, Faculty of Biological Sciences, Kharazmi University, Tehran, Iran

**Corresponding Address: P.O.Box: 31979-37551, Department of Cell and Molecular Biology, Faculty of Biological Sciences, Kharazmi University, Tehran, Iran*
Email: devbiokharazmi@gmail.com

Received: 18/May/2020, 26/September/2020

Abstract

Objective: Melittin is one of the natural components of bee venom (*Apis mellifera*), and its anticancer and antimetastatic properties have been well established, but the underlying mechanism remains elusive. The MDA-MB-231 is a triple-negative cell line that is highly aggressive and invasive. Besides, many critical proteins are involved in tumor invasion and metastasis. In this study, we investigated whether melittin inhibits the migration and metastasis of epidermal growth factor (EGF)-induced MDA-MB-231 cells via the suppression of SDF-1α/CXCR4 and Rac1-mediated signaling pathways.

Materials and Methods: In this experimental study, cells were treated with melittin (0.5-4 μg/ml), and the toxicity of melittin was assessed by the MTT assay. Afterward, the migration assay was conducted to measure the degree of the migration of EGF-induced cells. The western blot technique was performed to analyze the rate of Rac1, p-Rac1, SDF-1α, and CXCR4 expression in different groups.

Results: The results demonstrated that melittin markedly suppressed the migration of EGF-induced cells and decreased the expression of p-Rac1, CXCR4, and SDF-1α proteins.

Conclusion: The results of the present study suggested that the anti-tumor properties of melittin could be through the blocking of the SDF-1α/CXCR4 signaling pathway, which is beneficial for the reduction of tumor migration and invasion.

Keywords: CXCR4, Melittin, Rac1, SDF-1α

Cell Journal(Yakhteh), Vol 24, No 2, February 2022, Pages: 85-90

Citation: **Salimian F, Nabiuni M, Salehghamari E. Melittin prevents metastasis of epidermal growth factor-induced MDA-MB-231 cells through the inhibition of the SDF-1α/CXCR4 Signaling Pathway. Cell J. 2022; 24(2): 85-90. doi: 10.22074/cellj.2022.7626.**

Introduction

Bee venom consists of a variety of biologically active peptides, including melittin, apamin, adolapin, and mast cell degranulating peptide (MCDP) (1). Melittin is a major constituent of bee venom, which is a 26-amino acid polypeptide containing 40-60% of the whole bee venom (2). It belongs to amphipathic, α-helical, and cell-penetrating peptides, possessing anti-inflammatory, anti-bacterial, anti-thrombosis, and anti-tumor properties (3).

Organs have restricted boundaries that are identified by the basement membrane that can surround the cells with a particular matrix (4). Metastasis is known as the dissemination of cancer cells from a specific organ or region to another location that is not generally connected to it (5). The process of metastasis occurs via the blood vessels or lymphatic system or both (6). It is now known that cell migration is a critical step in metastasis and tumor invasion, and the regulation of this process can control the pathogenesis of cancer. The understanding of the molecular mechanism underlying the process of cancer cell migration and metastasis is a prerequisite for designing new therapies for the elimination of cancer cells.

The stromal cell-derived factor1α (SDF1α) and its cognate receptor, CXC chemokine receptor type 4 (CXCR4), play a crucial role in tumor metastasis (7). Chemokines are a group of peptides with molecular weights between 8 and 12 kDa (8). They are divided into four groups based on the position of the cysteine motif at the NH2 terminus (9). CXCL-12 (SDF-1) is the most significant member of this family in numerous types of cancer, which exists in two forms, namely SDF-1α/CXCL-12a and SDF-1β/CXCL-12b (10). The binding of CXCL-12 to CXCR-4 can activate multiple molecular signaling pathways (11). Through one of these pathways, the association of SDF-1 with CXCR-4 could activate the Rho family GTPases, such as Rac1, which plays a critical role in tumor progression and modulation of other signaling pathways, such as cell-cell adhesion (12). In this way, the GTP-bound form of the Rac1 protein binds to the PAK family and induces the kinase activity of these types of proteins. PAKs phosphorylate and activate actin-binding LIM kinases present in two types, namely LIMK1 and LIMK2. These kinases can phosphorylate cofilin, which leads to the deactivation of this protein. The activity of cofilin, which participates in the actin cytoskeleton formation, is essential for tumor cell

metastasis and migration (13). Indeed, actin cytoskeleton reorganization is considered a principal mechanism for triggering cell motility, and necessary for numerous kinds of cell migration (14). Rac1 also causes dissociation of the WAVE-1 protein from its regulatory complex to drive Arp2/3 complex-mediated actin polymerization, and it induces the formation of the lamellipodium. Therefore, Rac1 regulates multiple elements involved in the invasion and metastasis of cancer cells (13).

Previous studies have demonstrated that EGF-induced cell migration is associated with Rac1 activation and promotes tumor cell motility and invasion (15). Besides, it was reported that interaction between the chemokine receptor CXCR4 and its ligand SDF 1α plays a significant role in cell proliferation, angiogenesis, tumorigenicity, and metastasis in various types of cancer cell lines, such as breast cancer cells (16). Likewise, it has been shown that EGF can increase the expression of CXCR4, thereby the PI-3 kinase pathway (17). To date, there is no report on the stimulation of EGF in response to SDF 1α expression.

In the past few years, the anticancer properties of melittin have attracted much attention (18). Thus, due to the side effects of conventional therapies, such as chemotherapy, natural components possessing fewer side effects and enormous anti-cancer properties are currently used as complementary therapies (19). Data obtained during previous studies confirmed that melittin inhibits tumor cell metastasis via the suppression of the Rac1-dependent pathway in different types of cancer cell lines; however, the precise mechanisms of this event are still unclear (18). Since MDA-MB-231 is a triple-negative cell line (20), the effect of melittin on ER, PR, and HER2 receptors is rejected. According to the significant role of SDF-1α and CXCR4 in the migration and metastasis of cancer cells, this study aimed to examine the effect of melittin on the possible inhibition of the CXCR4/ SDF-1α pathway in MDA-MB-231 cells stimulated by EGF.

In this study, the effects of melittin on the motility and migration of a triple-negative breast cancer cell line were investigated. It was observed that melittin suppresses the level of CXCR4, SDF-1α, and Rac1 expression. Therefore, the CXCR4/SDF-1α signaling pathway could be one of the main ways through which melittin puts its effects. To confirm this, the expression level of Rac1, one of the key proteins in this pathway, was also examined. Evidence showed that the phosphorylation rate of this protein is decreased parallel with an increase in the concentration of melittin.

Materials and Methods

Cells and materials

In this experimental study, the breast cancer cell line MDA-MB-231 was purchased from the Pasteur Institute of Tehran, Iran. Melittin, at a concentration of 2 μg/ml, was purchased from Sigma-Aldrich (Sigma Aldrich, St. Louis, MO, USA). The monoclonal antibodies against Rac1 and its phosphorylated form were obtained from Abcam (Abcam, Cambridge, MA). Antibodies against CXCR4 and SDF-1α were obtained from Santa Cruz Biotechnology (Santa Cruz Biotechnology, Santa Cruz, CA). The anti-β-actin and anti-IgG HRP-conjugated (as a secondary antibody) antibodies were procured from Abcam (United Kingdom). The study was approved by the Kharazmi University of Tehran (616/9415).

Cell culture

MDA-MB-231 cancer cells were first cultured in the RPMI-1640 medium (Gibco, USA) that was supplemented with 100 U/ml penicillin-streptomycin and 10% fetal bovine serum (FBS). The cells were incubated at 37°C in a 5% CO_2 -95% air atmosphere for 24 hours. The medium was replaced with the fresh cell culture medium every 48 hours when the color of the medium was changed.

Morphological observations

For the evaluation of the impact of melittin on the morphological alterations of MDA-MB-231 cells, approximately 5×10^4 cells were cultured in a 24-well plate. Upon reaching 65-70% confluence, cells were treated with various concentrations of melittin (0.5-4 μg/ml). After 24 hours, morphological changes were observed under an inverted microscope (Biomedia, EU) and compared to the control cells.

Cell viability assay

The toxicity of melittin against cancer cells was examined by the MTT assay. To this aim, cells were seeded onto a 24-well plate at the density of 30×10^3 cells per well in the RPMI-1640 medium and allowed to adhere for 24 hours and then treated with different concentrations of melittin for 24, 48, and 72 hours. Then, the medium was discarded, and the cells were incubated with 0.5 mg/ml of 3- [4, 5-dimethylthiazol-2-yl]-2, 5-diphenyltetrazolium bromide (MTT) (Sigma, USA). After 3-4 hours of the incubation period at 37°C and 5% CO_2 atmosphere, the number of formazan crystals was quantified at a wavelength of 570 nm.

Migration assay

The process of cell migration was examined by the migration assay. Briefly, cells were seeded onto a 6-well plate and incubated at 37°C for 24 hours until a monolayer is formed. Monolayers were gently and slowly scratched with a pipette tip across the center of the well. Then, they were treated with various concentrations of melittin for 6 hours, followed by incubation with EGF (20 ng/ml) and 1% FBS medium for 24 and 48 hours. After the incubation period, the process of cell migration was tracked at the 24 and 48 hours of incubation. The open area was calculated

with the T scratch software, a novel and simple tool for the automated analysis of monolayer migration assay.

Western blot analysis

The western blot technique was performed to analyze the relative expression of the desired proteins after 6 hours of incubation of MDA-MB-231 cells with melittin. Briefly, cells were seeded onto a 6-well plate at a density of 5×10^5 cells per well and then treated with various doses of melittin for 6 hours, followed by the stimulation in the absence or presence of EGF (20 ng/ml) for 2 hours. The cell lysate was centrifuged at 13000 rpm at 4°C for 15 minutes. The supernatant was collected, and the concentration of total protein was determined by the Bradford assay. Approximately 25 µg of the extracted proteins were used for the sodium dodecyl sulphate-polyacrylamide electrophoresis gel (SDS-PAGE). The protein mixture was electrophoretically separated on 15% polyacrylamide gel and then transferred onto the PVDF membrane. The membrane was soaked in 5% non-fat dry milk and Tris-buffered saline and 0.1% Tween-20 (TBST) to prevent the binding of non-specific antibodies. The membrane was subsequently incubated with proper amounts of primary antibodies. After three times washing with TBST, the membrane was probed with horseradish peroxidase (HRP)-conjugated secondary antibody. The membrane was rinsed again for an additional three times in TBST, and finally, DAB (3,3'-diaminobenzidine) was used to visualize the protein bands. The densitometry analysis of protein bands was performed using the ImageJ software.

Statistical analysis

The obtained values were analyzed by Graphpad prism version 7.0 (San Diego, California USA). One-way analysis of variance (ANOVA), followed by Tukey's post hoc test was employed for the comparison of differences between experimental groups. Data are expressed as the mean ± standard error of the mean. The level of the statistical significance was set at $P<0.05$.

Results

Morphological alterations in MDA-MB-231 cells in response to melittin

The morphological changes induced by 0.5-4 µg/ml melittin after 48 hours was observed and compared with untreated cells. As shown in Figure 1, this type of cells exhibit a typical spindle-shaped morphology. Cells were treated with 0.5, and 1 µg/ml melittin did not show a significant morphological alteration when compared with untreated cells. Cells treated with melittin at a concentration of 2 µg/ml underwent some cellular damages such as cell shrinkage. The results demonstrated that 4 µg/ml melittin caused a significant morphological change as compared with untreated cells, showing a significant degree of cell death exposed to melittin.

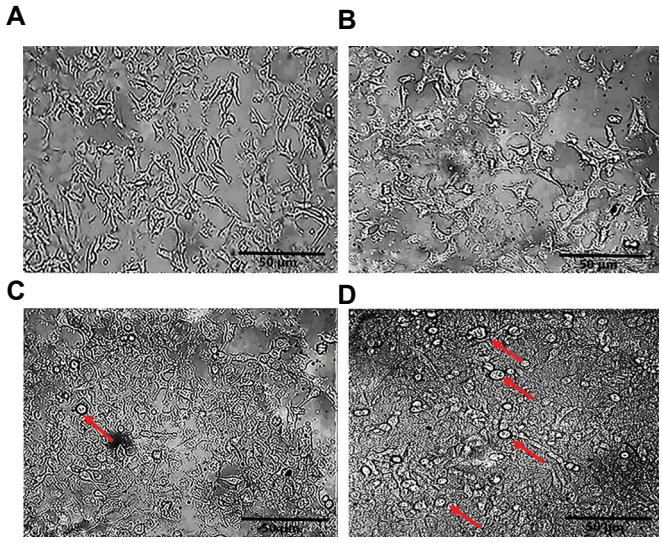

Fig.1: Morphological analysis of MDA-MB-231 cells in response to treatment with melittin after 48 hours. **A.** Untreated (control) cells, and **B.** treated with 1, **C.** 2, **D.** 4 µg/ml melittin (scale bar: 50 µm). Red arrows show dead cells (magnification ×10).

Melittin at low concentrations does not affect cell survival

Before the examination of migration and metastasis of cancer cells, the cell viability of the cultured cells, as well as the impact of melittin on cell survival was examined by the MTT assay. Melittin significantly caused cell death in MDA-MB-231 cells when used at a concentration of 4 µg/ml, and the cytotoxicity of the drug was mediated in a dose-dependent fashion. However, melittin, at concentrations lower than 2 µg/ml, cannot significantly change the cell survival of MDA-MB-231 cells compared with untreated cells (Fig.2). So, melittin was used at a lower concentration of 2 µg /ml for subsequent experiments.

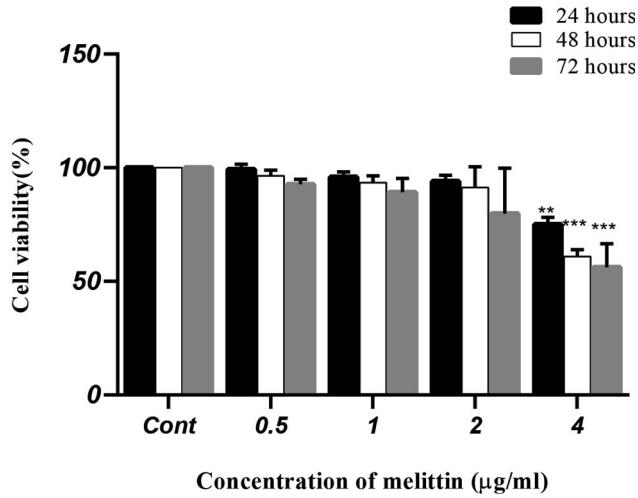

Fig.2: The percentage of the cell viability of MDA-MB-231 cells determined by the MTT assay. After 24, 48, and 72 hours, the impact of melittin on 0.5, 1, 2, and 4 µg/ml on the survival rate of breast cancer cells (MDA-MB-231) was measured. The graph shows that, in parallel with an increase in the concentration of melittin, the cell viability of MDA-MB-231 cells is markedly decreased. The data are expressed as the means and standard errors (mean ± SE) of three independent experiments. ***;* P<0.001, **;* P<0.01 compared to the untreated control (the first bar).

Inhibitory effect of melittin on the migration of the MDA-MB-231 cancer cell line

The cell migration assay was carried out to assess the preventive role of melittin in migration and cell motility of the MDA-MB-231 cancer cell line induced by EGF at 24 and 48 hours. As illustrated in Figure 3, along with an increase in the levels of melittin the rate of cell migration is decreased.

Melittin halts the invasion of the MDA-MB-231 cancer cell line induced by epidermal growth factor by reducing the expression of Rac1, CXCR4, and SDF-1α

The inhibitory effect of melittin on the expression of Rac1, p-Rac1, CXCR4, and SDF-1α was examined by the western blot analysis of whole-cell lysates of MDA-MB-231 cells treated with melittin for 6 hours, followed by stimulating with EGF (20 ng/ml) for 2 hours. As depicted in Figure 4., the results showed that the rate of the expression of the proteins mentioned above was substantially diminished in a dose-dependent manner in response to the treatment of EGF-induced MDA-MB-231 cancer cells with melittin.

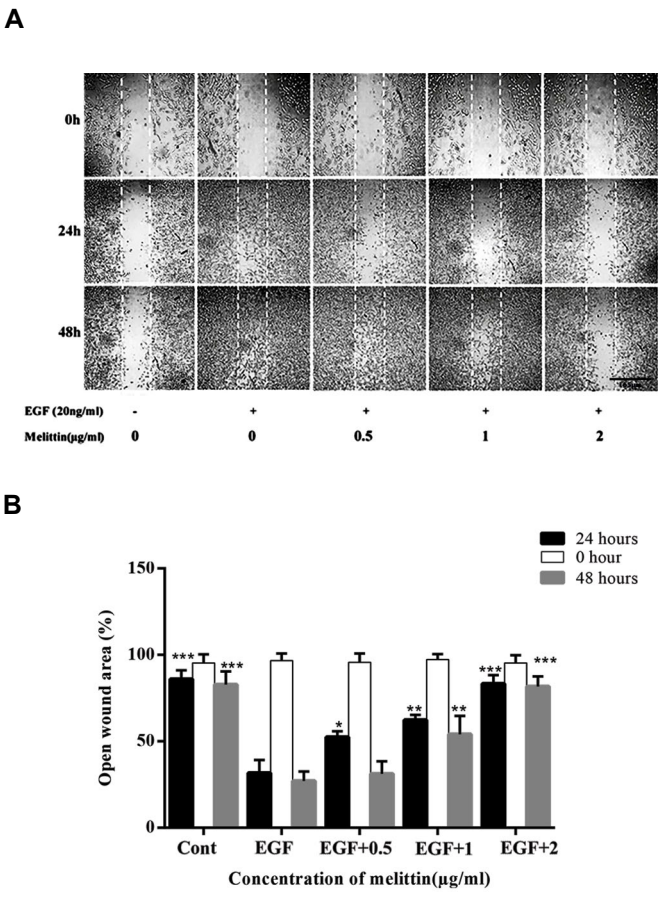

Fig.3: The inhibitory effect of different concentrations of melittin on the migration of epidermal growth factor (EGF)-induced MDA-MB-231 cells. **A.** The migration assay was carried out after 24 and 48 hours; then the migrated cells were imaged. **B.** Semi-quantification of protein bands in the migration assay (scale bar: 165 µm) (n=3, mean ± SE, ***; P<0.001, **; P<0.01, *; P<0.05, compared to the 0 hour (the white bars).

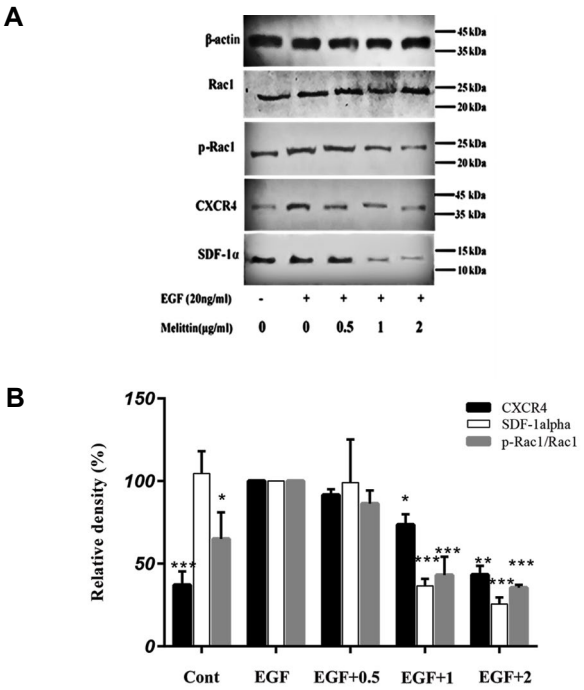

Fig.4: The inhibitory effect of melittin on epidermal growth factor (EGF)-induced Rac1, p-Rac1, CXCR4, and SDF-1α, in EGF-induced MDA-MB-231 cells. **A.** The western blot analysis indicated that melittin treatment reduces the expression of all metastasis-related proteins. β-actin was used as a loading control. **B.** Semi-quantification of the density of protein bands showed a significant decrease in the expression of all proteins in a dose-dependent manner (n=2, mean ± SE, ***; P<0.001, **; P<0.01 *; P<0.05, compared to the untreated control which is getting EGF and no melittin (the second group bar).

Discussion

Breast cancer is the most common type of cancer among women. In recent decades, the number of patients diagnosed with breast cancer, as well as the mortality of patients, has been significantly increased, implying that there is an urgent need to seek more efficient therapeutic strategies to cure patients who have breast cancer.

One of the main problems in breast cancer, especially in MDA-MB-231 cells, is the occurrence of metastasis. Several lines of evidence demonstrated that EGF is capable of promoting the migration of the MDA-MB-231 cancer cell line (21). EGF can stimulate F-actin polymerization, which leads to the formation of lamellipodia (22). Our results also confirmed that EGF stimulates the motility of MDA-MB-231 cells. The migration assay also revealed that this EGF-induced motility could be inhibited by melittin.

It has been indicated that a large number of genes contribute to the signaling pathways related to the metastasis process. Among those genes, Rac1, SDF-1α, and CXCR-4 have an undeniable impact on the function of cofilin, which contributes to stimulus-induced actin filament assembly during the formation of the lamellipodium.

The Rac1 protein belongs to the Rho family proteins, and it is one of the most common proteins, regulating the adhesion and migration of various types of cells. Rac1

is crucial for tumor growth, invasion, metastasis, and angiogenesis. This protein binds to either GDP or GTP, Rac1-GDP (inactive), and Rac1-GTP (activated) (23). The activation of the Rac1 leads to actin polymerization and lamellipodium formation during the migration of cells (24). Rac1 is overexpressed in numerous types of cancers, including testicular cancer, gastric, and breast cancers (25). Therefore, Rac1 may be a useful target for therapeutic purposes to halt the process of metastasis in cancer.

Chemokines are small proteins that interact with a large superfamily of the G protein-coupled receptors (8). Previous studies have shown that binding of SDF 1α and its cognate receptor, CXCR4, is essential for tumor progression, angiogenesis, metastasis, and survival (26). Thus, the inhibition of this chemokine and its cognate receptor can result in the prevention of tumor metastasis (27). Any interference with the expression of master genes involved in actin cytoskeleton formation can contribute to a decrease in the motility of cancer cells (28). Due to the severe side effects of chemotherapy and surgery, in recent years, the use of natural compounds with anticancer properties has been proposed since they possess much fewer adverse effects on the human body. Melittin is one of these natural components that the biological potential of this compound has been extensively studied (19). Melittin has only mild allergic side effects (29). Besides, melittin can cause massive hemolysis. This poses significant limitations in clinical studies. These days, the discovery of new methods of melittin delivery has solved this problem (30).

On the other hand, EGF treatment increased the expression of CXCR-4 and the active form of Rac1 (p-Rac1) proteins, but it was not able to alter the expression of SDF1α and total Rac1 (Rac1) significantly. These data are in conformity with the previous evidence that EGF induces CXCR4 activation in other cancer cells (16) and Rac1 expression in MDA-MB-231 cells (15) particularly Rac1 and Rac1b in TGF-β-induced epithelial-mesenchymal transition (EMT. But there is not any evidence on the role of EGF in the modulation of SDF1α.

A large body of evidence has shown that melittin could induce cell death in ovarian cancer cells via the stimulation of the expression of death receptors, as well as the inhibition of the STAT-3 pathway (29). This peptide inhibits metastasis through the hindrance of MMP-9 expression (30). In a study performed by Huh et al., they have demonstrated that melittin inhibits the VEGFR-2 and COX-2-mediated MAPK signaling pathways, which have anti-angiogenesis and anti-tumor activities (31). In a study conducted on AGS gastric cancer cell line and HeLa cervical cancer cell line, it was shown that melittin inhibited the proliferation of both types of cell lines (32, 33). In another study performed on the expression of Rac1 in gastric carcinoma, Wu et al. reported that Rac1 expression is associated with increased metastasis in gastric cancer (34). Studies have also shown that the suppression of Rac1 activity by melittin halts the process of metastasis in liver cancer cells in nude mice (35). Several lines of evidence indicated that the expression levels of the chemokine receptors are highly associated with the development of some cancers and have specific roles in cancer metastasis (36). It has been shown that melittin is capable of decreasing the expression of SDF1α and CXCR4 in the UMR-106 osteosarcoma xenograft mouse model (37). Another report showed that melittin could attenuate tumor invasion through the inhibition of the PI3K/AKT/mTOR signaling pathway in breast cancer cells (38). Our findings were in line with previous results showing that melittin is able to halt migration and invasion of the EGF-induced MDA-MB-231 cancer cells through mitigating the expression of *Rac1* and *CXCR4* genes. Although the comparison between the control group (receiving no treatment) and the EGF group (treated with EGF) shows that EGF was not capable of stimulating the expression of SDF1α, whereas melittin suppressed the expression of SDF1α in a dose-dependent fashion.

In summary, the present study indicated the anti-proliferative effect of melittin on EGF-induced MDA-MB-231cancer cells as a metastatic cell line. Our findings implicated that this natural compound is highly toxic and could impair the viability of MDA-MB-231 cells and reduce the migration of cancer cells in a dose-dependent manner.

Conclusion

In this study, it was shown for the first time that melittin can affect tumor cell migration through CXCR4/SDF-1α signaling pathway. All in all, we revealed that melittin, by blocking CXCR4 in the cell membrane and inhibiting the expression of SDF-1α, can exert an anti-motility potential. Altogether, further studies such as murine models of breast cancer will be required to unravel the inhibitory effects of melittin on the propagation of tumor cells.

Acknowledgments

This project was performed in the Laboratory of Cell and Developmental Biology at Kharazmi University, and the authors are thankful to all lab staff. The authors received no specific funding for this work. The authors have no conflicts of interest to declare.

Authors' Contributions

M.N.; Designed experiments, contributed to material preparation, and wrote the manuscript. F.S.; Performed experiments, analyzed the data, and wrote the manuscript. E.S.; Supervised the research, developed the theory, contributed to the final version of the manuscript, and read and approved the final manuscript. All authors read and approved the final manuscript.

References

1. Wehbe R, Frangieh J, Rima M, El Obeid D, Sabatier JM, Fajloun Z. Bee venom: overview of main compounds and bioactivities for therapeutic interests. Molecules. 2019; 24(16): 2997.
2. Chen J, Guan SM, Sun W, Fu H. Melittin, the major pain-producing

substance of bee venom. Neurosci Bull. 2016; 32(3): 265-272.
3. Wu Y, Han MF, Liu C, Liu TY, Feng YF, Zou Y, et al. Design, synthesis, and antiproliferative activities of stapled melittin peptides. RSC Adv. 2017; 7(28): 17514-17518.
4. Sekiguchi R, Yamada KM. Basement membranes in development and disease. Curr Top Dev Biol. 2018; 130: 143-191.
5. Fares J, Fares MY, Khachfe HH, Salhab HA, Fares Y. Molecular principles of metastasis: a hallmark of cancer revisited. Signal Transduct Target Ther. 2020; 5(1): 28.
6. Rahman M, Mohammed S. Breast cancer metastasis and the lymphatic system. Oncol Lett. 2015; 10(3): 1233-1239.
7. Kircher M, Herhaus P, Schottelius M, Buck AK, Werner RA, Wester HJ, et al. CXCR4-directed theranostics in oncology and inflammation. Ann Nucl Med. 2018; 32(8): 503-511.
8. Miller MC, Mayo KH. Chemokines from a structural perspective. Int J Mol Sci. 2017; 18(10): 2088.
9. Choi J, Selmi C, Leung PS, Kenny TP, Roskams T, Gershwin ME. Chemokine and chemokine receptors in autoimmunity: the case of primary biliary cholangitis. Expert Rev Clin Immunol. 2016; 12(6): 661-672.
10. Adelita T, Stilhano RS, Han SW, Justo GZ, Porcionatto M. Proteolytic processed form of CXCL12 abolishes migration and induces apoptosis in neural stem cells in vitro. Stem Cell Res. 2017; 22: 61-69.
11. Busillo JM, Benovic JL. Regulation of CXCR4 signaling. Biochim Biophys Acta. 2007; 1768(4): 952-963.
12. Lopez-Haber C, Barrio-Real L, Casado-Medrano V, Kazanietz MG. Heregulin/ErbB3 Signaling enhances CXCR4-driven Rac1 activation and breast cancer cell motility via hypoxia-inducible factor 1α. Mol Cell Biol. 2016; 36(15): 2011-2026.
13. Clayton NS, Ridley AJ. Targeting Rho GTPase signaling networks in cancer. Front Cell Dev Biol. 2020; 8: 222.
14. Zeng Y, Cao Y, Liu L, Zhao J, Zhang T, Xiao L, et al. SEPT9_i1 regulates human breast cancer cell motility through cytoskeletal and RhoA/FAK signaling pathway regulation. Cell Death Dis. 2019; 10(10): 720.
15. Ungefroren H, Witte D, Lehnert H. The role of small GTPases of the Rho/Rac family in TGF-β-induced EMT and cell motility in cancer. Dev Dyn. 2018; 247(3): 451-461.
16. Xu C, Zhao H, Chen H, Yao Q. CXCR4 in breast cancer: oncogenic role and therapeutic targeting. Drug Des Devel Ther. 2015; 9: 4953-4964.
17. Wang L, Li X, Zhao Y, Fang C, Lian Y, Gou W, et al. Insights into the mechanism of CXCL12-mediated signaling in trophoblast functions and placental angiogenesis. Acta Biochim Biophys Sin (Shanghai). 2015; 47(9): 663-672.
18. Rady I, Siddiqui IA, Rady M, Mukhtar H. Melittin, a major peptide component of bee venom, and its conjugates in cancer therapy. Cancer Lett. 2017; 402: 16-31.
19. Schirrmacher V. From chemotherapy to biological therapy: A review of novel concepts to reduce the side effects of systemic cancer treatment (Review). Int J Oncol. 2019; 54(2): 407-419.
20. Huang Z, Yu P, Tang J. Characterization of triple-negative breast cancer MDA-MB-231 cell spheroid model. Onco Targets Ther. 2020; 13: 5395-5405.
21. Park JH, Cho YY, Yoon SW, Park B. Suppression of MMP-9 and FAK expression by pomolic acid via blocking of NF-κB/ERK/mTOR signaling pathways in growth factor-stimulated human breast cancer cells. Int J Oncol. 2016; 49(3): 1230-1240.
22. Ho E, Dagnino L. Epidermal growth factor induction of front-rear polarity and migration in keratinocytes is mediated by integrin-linked kinase and ELMO2. Mol Biol Cell. 2012; 23(3): 492-502.
23. Haga RB, Ridley AJ. Rho GTPases: Regulation and roles in cancer cell biology. Small GTPases. 2016; 7(4): 207-221.
24. Kunschmann T, Puder S, Fischer T, Steffen A, Rottner K, Mierke CT. The small GTPase Rac1 increases cell surface stiffness and enhances 3D migration into extracellular matrices. Sci Rep. 2019; 9(1): 7675.
25. Porter AP, Papaioannou A, Malliri A. Deregulation of Rho GTPases in cancer. Small GTPases. 2016; 7(3): 123-138.
26. García-Cuesta EM, Santiago CA, Vallejo-Díaz J, Juarranz Y, Rodríguez-Frade JM, Mellado M. The role of the CXCL12/CXCR4/ACKR3 axis in autoimmune diseases. Front Endocrinol (Lausanne). 2019; 10: 585.
27. Gupta N, Duda DG. Role of stromal cell-derived factor 1α pathway in bone metastatic prostate cancer. J Biomed Res. 2016; 30(3): 181-185.
28. Gandalovičová A, Rosel D, Fernandes M, Veselý P, Heneberg P, Čermák V, et al. Migrastatics-anti-metastatic and anti-invasion drugs: promises and challenges. Trends Cancer. 2017; 3(6): 391-406.
29. Jo M, Park MH, Kollipara PS, An BJ, Song HS, Han SB, et al. Anticancer effect of bee venom toxin and melittin in ovarian cancer cells through induction of death receptors and inhibition of JAK2/STAT3 pathway. Toxicol Appl Pharmacol. 2012; 258(1): 72-81.
30. Park JH, Jeong YJ, Park KK, Cho HJ, Chung IK, Min KS, et al. Melittin suppresses PMA-induced tumor cell invasion by inhibiting NF-kappaB and AP-1-dependent MMP-9 expression. Mol Cells. 2010; 29(2): 209-215.
31. Huh JE, Kang JW, Nam D, Baek YH, Choi DY, Park DS, et al. Melittin suppresses VEGF-A-induced tumor growth by blocking VEGFR-2 and the COX-2-mediated MAPK signaling pathway. J Nat Prod. 2012; 75(11): 1922-1929.
32. Mahmoodzadeh A, Morady A, Zarrinnahad H, Pooshang Bagheri K, Ghasemi-Dehkordi P, Mahdavi M, et al. Isolation of melittin from bee venom and evaluation of its effect on proliferation of gastric cancer cells. Tehran Univ Med J. 2013; 70(12): 760-767.
33. Zarinnahad H, Mahmoodzadeh A, Pooshang Bagheri K, Mahdavi M, Shahbazzadeh D, Moradi A. Isolation of melittin from iranian honey bee venom and investigation of its effect on proliferation of cervical cancer- hela cell line. JSSU. 2013; 21(2): 226-238.
34. Wu YJ, Tang Y, Li ZF, Li Z, Zhao Y, Wu ZJ, et al. Expression and significance of Rac1, Pak1 and Rock1 in gastric carcinoma. Asia Pac J Clin Oncol. 2014; 10(2): e33-39.
35. Liu S, Yu M, He Y, Xiao L, Wang F, Song C, et al. Melittin prevents liver cancer cell metastasis through inhibition of the Rac1-dependent pathway. Hepatology. 2008; 47(6): 1964-1973.
36. Mollica Poeta V, Massara M, Capucetti A, Bonecchi R. Chemokines and chemokine receptors: new targets for cancer immunotherapy. Front Immunol. 2019; 10: 379.
37. Qin G, Chen Y, Li H, Xu S, Li Y, Sun J, et al. Melittin inhibits tumor angiogenesis modulated by endothelial progenitor cells associated with the SDF-1α/CXCR4 signaling pathway in a UMR-106 osteosarcoma xenograft mouse model. Mol Med Rep. 2016; 14(1): 57-68.
38. Jeong YJ, Choi Y, Shin JM, Cho HJ, Kang JH, Park KK, et al. Melittin suppresses EGF-induced cell motility and invasion by inhibiting PI3K/Akt/mTOR signaling pathway in breast cancer cells. Food Chem Toxicol. 2014; 68: 218.

Original Article

Circ_0000228 Promotes Cervical Cancer Progression via Regulating *miR-337-3p/TGFBR1* Axis

Yongqian Xu, Ph.D., Xiaona Dong, B.Sc., Baoli Ma, B.Sc., Pingping Mu, B.Sc., Xiang Kong, B.Sc.*, Dongmei Li, B.Sc.*

Department of Gynecology and Obstetrics, Shengli Oilfield Central Hospital, Dongying, Shandong, China.

Corresponding Address: Department of Gynecology and Obstetrics, Shengli Oilfield Central Hospital, Dongying, Shandong, China
Emails: drkongxiang@21cn.com, jibimibai18507@163.com

Received: 24/December/2020, Accepted: 24/June/2021

Abstract

Objective: This study aims to investigate the biological function of circular RNA (circRNA) *circ_0000228* in the cervical cancer (CC).

Materials and Methods: In this experimental study, the GSE113696 dataset was downloaded from the Gene Expression Omnibus (GEO). GEO2R was employed to obtain differentially expressed circRNA between CC tissues and matched paracancerous tissues. Quantitative real-time polymerase chain reaction (qRT-PCR) and Western blot were employed to detect *circ_0000228*, microRNA-337-3p *(miR-337-3p)* and transforming growth factor, beta receptor I (*TGFBR1*) expression levels in the CC tissues and cells. Following gain-of-function and loss-of-function models establishment, CCK-8 and BrdU tests were conducted to examine cell proliferation. Transwell experiment was executed to examine CC cells migration and invasion. A lung metastasis model was utilized to determine the ability of *circ_0000228* on the lung metastasis. Bioinformatics analysis, dual-luciferase reporter experiment and RNA immunoprecipitation (RIP) assay were applied to verify the targeting relationship among *miR-337-3p*, circ_0000228, and *TGFBR1*.

Results: *Circ_0000228* expression in the CC tissues and cells was up-modulated. *Circ_0000228* overexpression markedly enhanced cell proliferation, migration, and invasion, while knocking down *circ_0000228* remarkably repressed cell proliferation, migration, and invasion. *MiR-337-3p* could be adsorbed by circ_0000228. *TGFBR1* was identified as a target gene of *miR-337-3p* that indirectly and positively modulated by *circ_0000228* in the CC cells.

Conclusion: *Circ_0000228* up-modulates *TGFBR1* by targeting *miR-337-3p* to enhance CC cell proliferation, migration and invasion. Also, *Circ_0000228* is a promising therapeutic target for the CC.

Keywords: Cervical Cancer, miR-337-3p, *TGFBR1*

Cell Journal(Yakhteh), Vol 24, No 2, February 2022, Pages: 91-98

Citation: Xu Y, Dong X, Ma B, Mu P, Kong X, Li D. Circ_0000228 promotes cervical cancer progression via regulating miR-337-3p/TGFBR1 axis. Cell J. 2022; 24(2): 91-98. doi: 10.22074/cellj.2022.7914.

Introduction

Cervical cancer (CC), a common malignancy, seriously threatens women's health (1) and also, surgery, chemotherapy and radiation therapy are considered as approaches for CC treatment (2). Unfortunately, the majority of patients have reached an advanced stage by the time of diagnosis, resulting in losing the opportunity for radical surgery (3). It is of great clinical value to decipher the CC pathogenesis to reach target therapy, particularly in the advanced stage.

Circular RNAs (circRNAs) as a member of endogenous non-coding RNAs, are closed-loop RNA molecules that are formed by reverse splicing. There are not 5'-end cap and 3'-end poly A tail in their structure. Also, they can be stably present in the diverse eukaryotic cells (4). Previously, circRNAs were considered as a "noise" of gene transcription (5, 6). However, recently, their biological function has been revealed (5, 7). Some studies have shown, abnormal expression of circRNAs in the human malignancies with unfavorable prognosis (8-15). For instance, in gastric cancer, *circ-DONSON* promotes the proliferation, migration, and invasion of cancer cells, and impedes apoptosis (13). In CC, *circ_0000515* and *circ_0007534* facilitate proliferation, migration and invasion of CC cells and repress apoptosis (14, 15). Also, *circ_0000228* is generated from zinc finger E-box binding homeobox 1 (*ZEB1*) transcription. *ZEB1* has been reported to be up-regulated in the CC and acts as an oncogene (16). Nonetheless, the biological function and mechanism of *circ_0000228* in CC is undefined.

MicroRNA (miRNA, miR)-337-3p is down-modulated in the CC cells and suppresses proliferation, migration and invasion of these cells and induces apoptosis (17, 18). Also, *TGFBR1* is reported to be overexpressed in the CC, and can enhance CC cell malignancy (19). Bioinformatics analysis predicts that *miR-337-3p* targets the 3′UTR of transforming growth factor, beta receptor I (*TGFBR1*). Moreover, *circ_0000228* is predicted to be a potential molecular sponge for *miR-337-3p*. In this study, we probe function and mechanism of circ_0000228, *miR-337-3p* and *TGFBR1* in the CC progression. We aim to offer clues to improve clinical diagnosis and therapy of CC.

Materials and Methods

Specimens collection

The work was approved by the Ethics Committee of Shengli Oilfield Central Hospital (2018-06). Totally, 57 CC specimens and corresponding cervical paracancerous specimens were surgically obtained of patients who

referred to the Shengli Oilfield Central Hospital. The patients with pathologically diagnosed CC who are willing to provide written informed consents participated in this study. The specimens were stored in the liquid nitrogen. All subjects did not undergo radiotherapy, chemotherapy or other anti-cancer treatments before surgery. All subjects signed an informed consent form before the surgery and tissue collection.

Cell culture

Human cervical epithelial cells (HUCECs) and CC cell lines (SiHa, HeLa, CaSKi, and C33A) were purchased from the Cell Center of Chinese Academy of Sciences (Shanghai, China). All cell lines were cultured in Dulbecco's Modified Eagle Medium (DMEM) medium (Cat No. 11965-092, Invitrogen, Carlsbad, CA, USA) containing 10% fetal bovine serum (FBS, Cat No. 10270098, Gibco, Grand Island, NY, USA)+100 U/mL penicillin+100 μg/mL streptomycin (Cat No. 15140122, Hyclone, Logan, UT, USA). Then, all were incubated at 37°C, 5% CO_2, 95% humidity

Cell transfection

Small interfering RNA (siRNA) negative control (si-NC), siRNA against circ_0000228-1 (si-circ_0000228-1), siRNA against circ_0000228-2 (si-circ_0000228-2), pcDNA empty vector (NC), pcDNA-*circ_0000228* (*circ_0000228*), mimics negative control (mimics NC), miRNA inhibitors negative control (inhibitors NC), *miR-337-3p* mimics, and *miR-337-3p* inhibitors were available from GenePharma Co., Ltd (Cat No. MIN0000578, Shanghai, China).

HeLa and C33A cells were planted in 6-well plates (3×10^5 cells/mL) (Cat No. 353046, BD Biosciences, Bedford, MA, USA) and cultured at 37°C with 5% CO_2 for 24 hours. Then, cells were transfected using Lipofectamine® 3000 (Cat No. L3000015, Invitrogen, Carlsbad, CA, USA) according to the manufacture's instruction. Quantitative real-time polymerase chain reaction (qRT-PCR) was performed to detect the transfection efficiency.

Quantitative real-time polymerase chain reaction

Using TRIzol reagent (Cat No. 15596-018, Invitrogen, Carlsbad, CA, USA), total RNA was extracted from CC tissues and cells. Then, the PrimeScript™ RT Reagent kit (Cat No. RR037A, Takara Biotechnology Co., Ltd., Dalian, China) was utilized to reverse transcribe total RNA into cDNA. Next, qRT-PCR was implemented using SYBR®Premix-Ex-Taq™ (Cat No. 368706, Takara, Dalian, China) on the ABI7500 FAST Real-Time PCR system (Thermo Fisher Scientific, Waltham, MA, USA). *GAPDH* was regarded as an internal reference to quantify *circ_0000228* and *TGFBR1* mRNA expression levels, and *U6* was considered as an internal reference to detect *miR-337-3p* expression. *Circ_0000228*, *miR-337-3p*, and *TGFBR1* mRNA relative expression was calculated using the $2^{-\Delta\Delta CT}$ method. A PARIS™ Kit (Cat No. AM1556, Ambion, Austin, TX, USA) was employed for subcellular fractionation. After the cytoplasmic RNA and nuclear RNA were isolated respectively, qRT-PCR was executed to evaluate *circ_0000228* expression in cytoplasm and nuclei. The primer sequences used for qRT-PCR were as follows:

circ_0000228-

F: 5′-GAGGTGTGGGGTGTGAGAAC-3′
R: 5′- GCAGACAGTAGCCAAATCACA-3′

miR-337-3p-

F: 5′- CUCCUAUAUGAUGCCUUUCUUC-3′
R: 5′-GAAGAAAGGCAUCAUCUAGGAG-3′

TGFBR1-

F: 5′-CACAGAGTGGGAACAAAAAGGT-3′
R: 5′- CCAATGGAACATCGTCGAGCA-3′

U6-

F: 5′-GCCGTTGCAGCACATATACAATAAT-3′
R: 5′-CGCTACGTTAATGCTCGTGTCAT-3′

GAPDH-

F: 5′-AGAAGGCTGGGGCTCATTTG-3′
R: 5′-AGGGGCCATCCACAGTCTTC-3′

Colorimetric measurement of cell proliferation

After trypsinization, both cells, HeLa and C33A, were harvested. Then the cells were inoculated in a 96-well plate (2×10^3 cells/well) and incubated. After 24 hours, 10 μL of cell counting kit8 (CCK-8) solution (Cat No. HY-K 0301, MedChemExpress, Monmouth Junction, NJ, USA) was supplemented to each well and then the cell culture was continued for 1 hour. The absorbance (OD_{450nm} value) of each well was recorded using a Bio-Tek Synergy HT Microplate Reader (Bio-Tek Instruments, Winooski, VT, USA). Thereafter, with the same method, the absorbance of the cells was measured 48 hours and 72 hours later, respectively.

BrdU experiment

Cell proliferation was also assessed with the BrdU Cell Proliferation Assay kit (Cat No. 6813, Beyotime, Shanghai, China). The single-cell suspension was prepared with HeLa and C33A cells, and the cells were inoculated into 96-well plates (1×10^4 per well). Subsequently, 20 μl BrdU solution was added to each well and incubated for 24 hours. Subsequently, the culture medium was discarded and the cells were washed with PBS. Cells were fixed with 4% paraformaldehyde for 30 min at room temperature and washed again with PBS. Cells were incubated with anti-BrdU (Cat No. ab6326, Abcam, Shanghai, China) for 1 hour at room temperature. Then, cell nuclei were counterstained using Hoechst staining solution (Beyotime, Shanghai, China) at room temperature for 30 minutes. After PBS washing, the cells were incubated with pre-diluted detection antibody for 1 hour. Thereafter, the cells

were stained with Hoechst staining solution. The total number of cells and the number of BrdU-positive cells in 10 high magnification fields were counted randomly under the microscope, and the percentage of BrdU-positive cells was calculated.

Transwell experiment

In the migration experiments, HeLa and C33A cells were resuspended in the serum-free medium, and the cell density was modulated (2×10^5 cells / mL), and then 100 µL of the cell suspension was supplemented to the upper compartment of the Transwell system (Cat No. 3422, Corning, Corning, NY, USA). Then, 500 µl DMEM medium containing 10% FBS was supplemented to the lower compartment of the Transwell chamber. 24 hours' incubation at room temperature, the upper compartment cells that did not migrate were gently wiped off with cotton swabs, and the attached cells on the lower surface of the membrane were fixed with 4% paraformaldehyde (Cat No. J61899, Alfa Aesar, averhill, MA, USA). After that, the cells were stained with 0.1% crystal violet (Cat No. C0121, Beyotime, Shanghai, China) for 10 minutes. After the membranes were washed, five randomly selected microscopic fields per membrane was selected and the numbers of stained cells were counted. To perform the cell invasion assay, the Transwell inserts were pre-covered with 50 ml of the Matrigel matrix. DMEM medium containing 10% FBS was placed in the lower chamber as a chemoattractant. Twenty-four hours later, 0.1% crystal violet was used to stain the cells that had invaded through the membranes. Then, the cells were observed by a microscope.

Dual-luciferase reporter assay system

The dual-luciferase reporter assay system (Cat No. 11752250, Promega, Madison, WI, USA) was used in this experiment. HeLa and C33A cells were trypsinized, counted, and planted in a 24-well plate (1×10^4 cells/well), and cultured for 24 hours. When cell confluence reached 80-90%, the transfection was performed with Lipofectamine® 3000 (Invitrogen, Carlsbad, CA, USA). Wild-type *circ_0000228* (WT circ_0000228), wild-type *TGFBR1* (WT *TGFBR1*), mutant-type *circ_0000228* (MUT circ_0000228) and mutant-type *TGFBR1* (MUT *TGFBR1*) reporter vectors were co-transfected with mimics NC, *miR-337-3p* mimics and *miR-337-3p* inhibitors, respectively. After the cells were cultured for 48 hours, the cells were collected, lysed with lysis buffer, and the supernatant was collected. Following that, the luciferase substrate was added and the luciferase activity was examined by the luminometer (Glomax 96 Microplate Luminometer, Promega, Madison, WI, USA). Firefly luciferase activity was normalized to the Renilla luciferase activity.

RNA immunoprecipitation assay

Using Magna RIP™ RNA - Binding Protein Immunoprecipitation Ki (Cat No. 17-700, Millipore, Billerica, MA, USA), the interaction between circ_0000228 and miR-337-3p was evaluated. Both cells, HeLa and C33A, were lysed in the RIP lysis buffer, and 100 µL of cell lysates were incubated with magnetic beads coupling with anti-Argonaute2 (Ago2) antibody or negative control IgG in the RIP buffer. Then the specimens were incubated with Proteinase K (Cat No. 25530-031, Invitrogen, Carlsbad, CA, USA) to remove proteins and then RNA precipitation was obtained. The purified RNA was subjected to qRT-PCR analysis.

Western blot

48 hours after transfection, HeLa and C33A cells were lysed with RIPA lysis buffer (Cat# P0013B, Beyotime Biotechnology, Shanghai, China) containing protease inhibitors (Cat No. 11836170001, Roche Applied Science, Penzberg, Germany), and the supernatants were collected after high-speed centrifugation, and protein concentrations were determined by a BCA kit (Cat No. P0012S, Beyotime, Shanghai, China). The supernatant was mixed with loading buffer, and then heated in a water bath at 100°C for 10 minutes to denature the protein. Next, the total proteins were separated using sodium dodecyl sulfate-polyacrylamide gel electrophoresis (SDS-PAGE) and transferred to polyvinylidene difluoride (PVDF) membranes by electrotransfer. The membranes were then incubated with the specific primary antibodies overnight at 4°C. After rinsing with Tween-20 (TBST, Cat No. AAJ77500K8, Fisher Scientific, Houston, TX, USA), the membranes were then incubated with corresponding secondary antibodies for 2 hours at room temperature. The protein bands were visualized by electrochemiluminescence automatic chemiluminescence imaging analysis system (Tanon 5500, Tanon Science & Technology, Shanghai, China), and β-actin was regarded as an internal reference. The antibodies used in this work were available from Abcam (Shanghai, China), including primary antibodies: anti-TGFBR1 antibody (ab31013, 1:1000), anti-β-actin antibody (ab179467, 1:1000), and a secondary antibody (ab205718, 1:2000).

Lung metastasis experiment

The protocol of animal experiments was approved by the Institutional Animal Care and Use Committee of Shengli Oilfield Central Hospital. 12 male BALB/C nude mice (4 weeks old, Vital River Laboratory Animal Technology, Beijing, China) were utilized for lung metastasis experiments, to evaluate the metastatic ability of CC cells *in vivo*. Mice were housed under standard housing conditions (23°C, 40% humidity, 12 hours/12 hours light-dark cycle, food and water were available). Then, HeLa cells (1×10^7 cells/per mouse) transfected with *circ_0000228* overexpression or empty vector plasmid were injected into the tail veins of nude mice (6 mice/per group). After 4 weeks, the mice were euthanized and the lung tissues were obtained. Next, hematoxylin/eosin staining was performed to show the metastatic nodules.

Statistical analysis

All data were analyzed using GraphPad Prism 8 (GraphPad Software, La Jolla, CA, USA). Shapiro-Wilk

(SW) test was used to analyze the normal distribution of the data. All the measurement data were expressed as "mean ± standard deviation" (mean ± SD). Also, t test was adopted for comparison between two groups, and one-way ANOVA was used for comparison of the means among multiple groups. For skewed distributed data, the Wilcoxon signed-rank test was used. Counting data were expressed in contingency tables, and $\chi 2$ test was utilized to analyze differences between the two groups. Statistical significance was indicated by $P<0.05$.

Results

Circ_0000228 expression was up-modulated in cervical cancer

Detecting circRNA expression profile in the CC tissues, we observed that 122 circRNAs were down-modulated ($P<0.05$), while 34 circRNAs (including circ_0000228) were up-modulated (Fig.1A, B, $P<0.05$). Consistently, qRT-PCR indicated that circ_0000228 was up-modulated in the CC tissues (n=57) in comparison with the matched non-cancerous tissues (Fig.1C, $P<0.001$). Analyzing relationship between circ_0000228 expression in the CC tissues and clinical parameters, we observed that high circ_0000228 expression in the CC tissues was linked to lymph node metastasis and low differentiation of tumor tissues (Fig.1D, Table 1, $P<0.05$). Additionally, circ_0000228 expression was up-modulated in all of the 4 CC cell lines (SiHa, HeLa, CaSKi, C33A) relative to normal cervical epithelial cell line HUCEC cell (Fig.1E, $P<0.01$).

Circ_0000228 enhanced the proliferation, migration and invasion of cervical cancer cells

To examine the biological role of *circ_0000228* in the CC, HeLa cells were transfected with *circ_0000228* overexpression plasmid. Also, C33A cells were transfected with si-circ_0000228-1 and si-circ_0000228-2 (Fig.2A). CCK-8 colorimetric assay unveiled that *circ_0000228* overexpression facilitates the proliferation of HeLa cells ($P<0.001$), while knock down *circ_0000228* restrained C33A cell proliferation (Fig.2B, $P<0.001$). The data of BrdU experiments manifested, that the number of BrdU-positive cells was higher in the *circ_0000228* overexpression group in comparison with the control group ($P<0.001$). The BrdU-positive cells number was lower in the si-circ_0000228-1 and si-circ_0000228-2 groups (Fig.2C, $P<0.001$). And, Transwell experiment was executed to examine the effects of *circ_0000228* on the CC cell migration and invasion. The results demonstrated that *circ_0000228* overexpression facilitates migration of HeLa cell and invasion ($P<0.001$), while *circ_0000228* knockdown restrained C33A cells migration and invasion (Fig.2D, $P<0.001$). Finally, we used a lung metastasis model, *in vivo* model, to investigate the role of *circ_0000228* in the CC cells metastasis regulation. The results indicated that *circ_0000228* overexpression promoted lung metastasis *in vivo* (Fig.S1, See Supplementrary Online Information at www.celljournal.org, $P<0.001$).

Table 1: Correlation between clinicopathological features and expression of circ_0000228 in the CC tissues

Pathological parameters	Numbers	Circ_0000228 expression		$\chi 2$	P value
	(n=57)	High (n=28)	Low (n=29)		
Age (Y)				0.4220	0.5159
<45	33	15	18		
≥45	24	13	11		
Tumor size (cm)				1.4164	0.2340
<4	29	12	17		
>4	28	16	12		
FIGO stage				0.8884	0.3459
I	26	11	15		
II	31	17	14		
Lymph node metastasis				4.1352	0.0420*
No	24	8	16		
Yes	33	20	13		
Degree of differentiation				9.4270	0.0021*
Poor, moderate	31	21	10		
Well	26	7	19		

CC; Cervical cancer, FIGO; International federation of gynecology and obstetrics, and *; $P<0.05$.

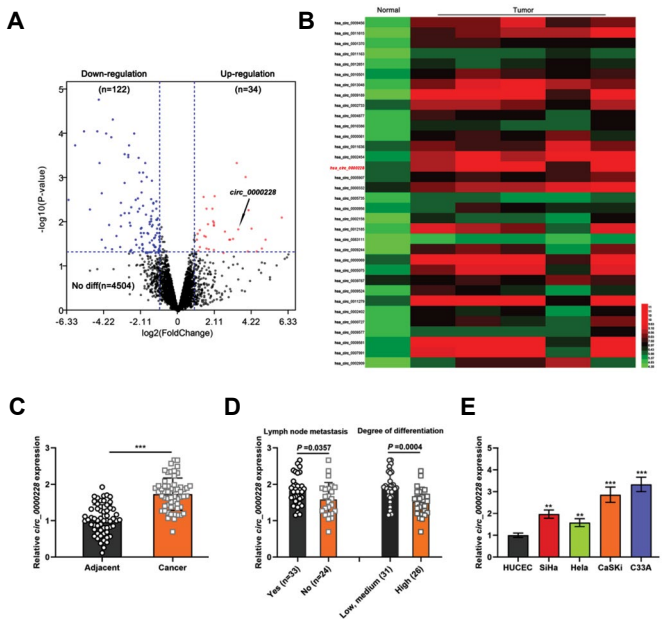

Fig.1: The expression characteristics of circ_0000228 in CC. **A, B.** Variations in the expression of circRNAs in the CC tissues were examined by analyzing dataset GSE113696. **C.** qRT-PCR was executed to examine *circ_0000228* expression in the 57 cases of CC tissues and matched paracancerous tissues. **D.** qRT-PCR was implemented to examine *circ_0000228* expression in the CC tissues of the patients with lymph node metastasis and without lymph node metastasis, different differentiation status, respectively. **E.** *Circ_0000228* expression in the HUCECs and CC cell lines (SiHa, HeLa, CaSKi and C33A) was measured by qRT-PCR. CC; cervical cancer, qRT-PCR; Quantitative real-time polymerase chain reaction, HUCECs; Human cervical epithelial cells, **; P<0.01, and ***; P<0.001.

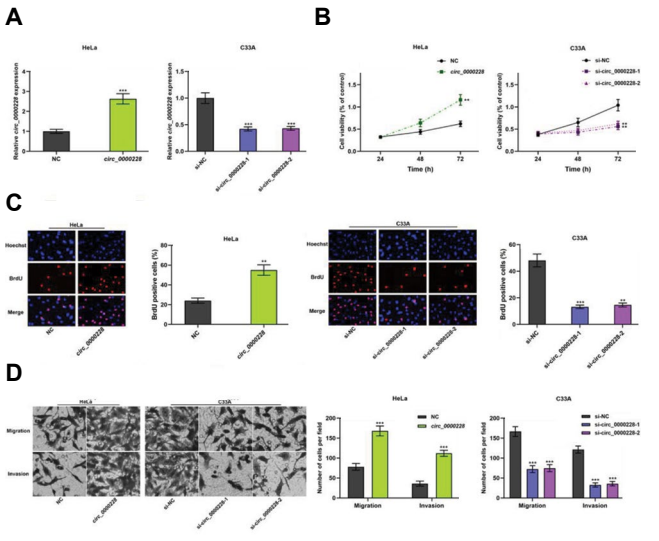

Fig.2: Regulatory role of *circ_0000228* in the CC cells phenotype. **A.** HeLa and C33A cells were transfected with *circ_0000228* overexpression plasmid and *circ_0000228* siRNAs, respectively, and also, the transfection efficiency was examined by qRT-PCR. **B, C.** The effects of *circ_0000228* overexpression or knockdown on the proliferation of HeLa and C33A cells were detected using CCK-8 colorimetric assay and BrdU experiment. **D.** Transwell experiments were used to examine the effects of *circ_0000228* overexpression and knockdown on the migration and invasion of HeLa and C33A cells. CC; Cervical cancer, qRT-PCR; Quantitative real-time polymerase chain reaction, **; P<0.01, and ***; P<0.001.

Circ_0000228 directly targeted *miR-337-3p*

To probe the downstream targets of *circ_0000228*, the CircInteractome database (https://circinteractome.nia.nih.gov/) was searched. *miR-337-3p* was selected as a one of the predicted target miRNAs (Fig.3A, P<0.001). Subsequently, *miR-337-3p* expression in the CC cell lines was examined by qRT-PCR. *miR-337-3p* expression was demonstrated to be diminished in the CC cell lines (Fig.3B, P<0.05). Nucleocytoplasmic separation assay showed that *circ_0000228* was expressed in the CC cells cytoplasm (Fig.3C, P<0.001). Dual-luciferase reporter experiment showed that *miR-337-3p* overexpression repressed the luciferase activity of WT *circ_0000228*, while *miR-337-3p* inhibition enhanced the luciferase activity of WT *circ_0000228* (Fig.3D, P<0.001). However, neither miR-337-3p mimic nor miR-337-3p inhibitor affected the luciferase activity of MUT *circ_0000228* (Fig.3D). Next, the results of RIP experiments showed that *circ_0000228* and *miR-337-3p* were enriched in the Ago2-containing microribonucleoproteins relative to IgG group, suggesting a direct interaction between *circ_0000228* and *miR-337-3p* (Fig.3E, P<0.001). Moreover, *circ_0000228* overexpression suppressed *miR-337-3p* expression in the HeLa cells; while *circ_0000228* knock down *circ_0000228* increased *miR-337-3p* expression in the C33A cells (Fig.3F, P<0.001). Also, *miR-337-3p* was unveiled to be down-modulated in the CC tissues by qRT-PCR (Fig.3G, P<0.001). Pearson's correlation analysis indicated that *circ_0000228* was negatively correlated with *miR-337-3p* expression in the CC tissues (Fig.3H, P<0.001).

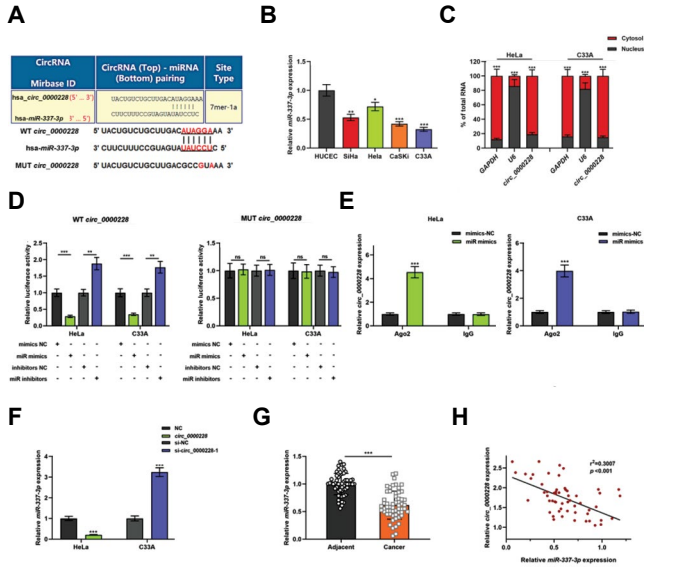

Fig.3: *Circ_0000228* directly targeted *miR-337-3p*. **A.** Bioinformatics analysis projected the binding site between *circ_0000228* and *miR-337-3p*. **B.** *MiR-337-3p* expression in the CC cell lines and HUCECs was examined by qRT-PCR. **C.** Nucleocytoplasmic separation experiment was conducted to verify the localization of *circ_0000228* in the CC cells. **D.** Dual-luciferase reporter gene experiment was implemented to validate the bioinformatics predicted binding site. **E.** RIP assays were utilized to prove the interaction between *circ_0000228* with *miR-337-3p*. **F.** The effect of *circ_0000228* overexpression and knockdown on the *miR-337-3p* expression in the CC cells was detected by qRT-PCR. **G.** *MiR-337-3p* expression in the 57 CC tissues and 57 paracancerous tissues was examined by qRT-PCR. **H.** Pearson's correlation analysis assessed the correlation between *miR-337-3p* expression and *circ_0000228* expression in the CC tissues. CC; Cervical cancer, qRT-PCR; Quantitative real-time polymerase chain reaction, RIP; RNA immunoprecipitation, *; P<0.05, **; P<0.01, and ***; P<0.001.

Circ_0000228 regulated the proliferation, migration and invasion of cervical cancer cells by adsorbing *miR-337-3p*

Subsequently, *circ_0000228* overexpression plasmid and *miR-337-3p* mimics were co-transfected into the HeLa cells. Also, si-circ_0000228-1 and *miR-337-3p* inhibitors were co-transfected into the C33A cells (Fig.4A). CCK-8 colorimetric assay, BrdU experiments and Transwell experiments showed that *circ_0000228* overexpression facilitated CC cell proliferation, migration and invasion (P<0.05), while transfection with *miR-337-3p* mimics attenuated these effects (P<0.05). On the other hand, knocking down *circ_0000228* repressed cell proliferation, migration, and invasion (P<0.05), while transfection of *miR-337-3p* inhibitors partially reversed these effects (Fig.4B-D, P<0.05).

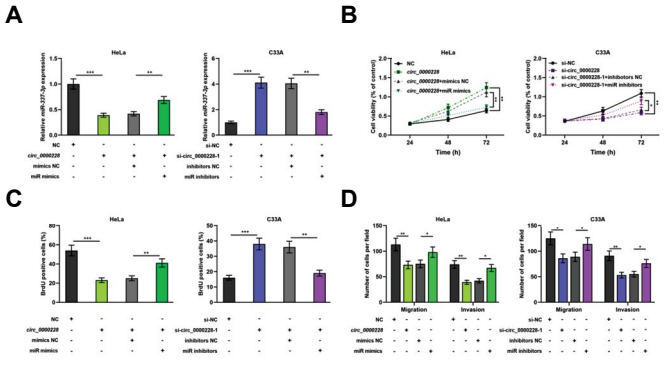

Fig.4: The effect of *circ_0000228/miR-337-3p* axis on the proliferation, migration and invasion of the CC cells. **A.** HeLa cells were co-transfected with *circ_0000228* overexpression plasmid and *miR-337-3p* mimics, and C33A cells were co-transfected with si-circ_0000228-1 and *miR-337-3p* inhibitors, and then the transfection efficiency was determined by qRT-PCR. **B, C.** CCK-8 colorimetric assay and BrdU experiments were used to examine the effects of *circ_0000228* and *miR-337-3p* on CC cell proliferation. **D.** Transwell test was applied to examine the effects of *circ_0000228* and *miR-337-3p* on the CC cell migration and invasion. CC; Cervical cancer, qRT-PCR; Quantitative real-time polymerase chain reaction, *; P<0.05, **; P<0.01, ***; P<0.001.

Circ_0000228 targeted *miR-337-3p* to up-modulate *TGFBR1* expression

The TargetScan database (http://www.targetscan.org/vert_72/) was used to predict the downstream targets of *miR-337-3p*, and *TGFBR1* was predicted as one of the potential downstream targets of *miR-337-3p* (Fig.5A). Dual-luciferase reporter experiment showed that miR-337-3p overexpression repressed the luciferase activity of WT TGFBR1, while miR-337-3p inhibition enhanced the luciferase activity of WT TGFBR1 (Fig.5B, P<0.001). However, neither miR-337-3p mimic nor miR-337-3p inhibitor affected the luciferase activity of MUT TGFBR1 (Fig.5B).

Western blot showed that *circ_0000228* overexpression enhanced *TGFBR1* expression in the HeLa cells (P<0.001), whereas transfection of *miR-337-3p* mimics attenuated this effect (Fig.5C, P<0.001). Knocking down *circ_0000228* impeded *TGFBR1* expression in C33A cells (P<0.001), whereas inhibition of *miR-337-3p* counteracted this effect (Fig.5C, P<0.001). By qRT-PCR, *TGFBR1* mRNA revealed overexpression in the CC tissues (Fig.5D, P<0.001). Notably, TGFBR1 mRNA expression in CC tissues was negatively correlated with miR-337-3p expression (P<0.001) and positively correlated with circ_0000228 expression (Fig.5E, F, P<0.001).

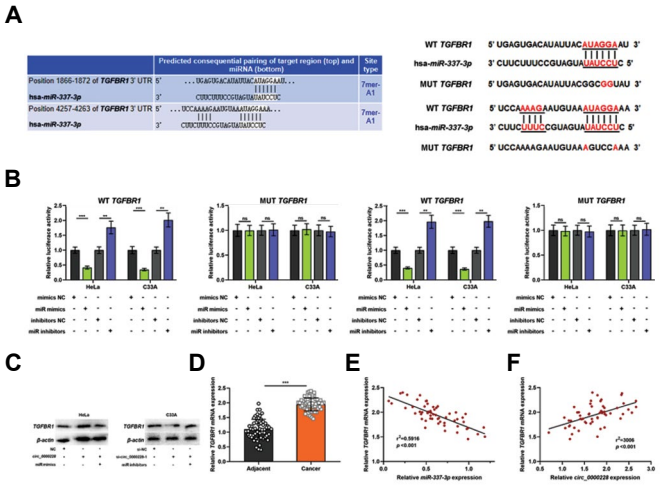

Fig.5: *Circ_0000228* up-regulated *TGFBR1* expression by sponging *miR-337-3p*. **A.** TargetScan projected the binding site between *miR-337-3p* and *TGFBR1*. **B.** Dual-luciferase reporter gene experiment was executed to prove the binding site between *miR-337-3p* and *TGFBR1* 3´UTR predicted by bioinformatics analysis. **C.** Western blot was utilized to examine the regulatory functions of circ_0000228 and miR-337-3p mimics on TGFBR1 expression. **D.** qRT-PCR was employed to examine *TGFBR1* mRNA expression in the CC tissues and paracancerous tissues. **E, F.** Pearson's correlation analysis analyzed the correlations between *TGFBR1* mRNA and *miR-337-3p/circ_0000228* expression in the CC tissues. CC; Cervical cancer, qRT-PCR; Quantitative real-time polymerase chain reaction, *; P<0.05, **; P<0.01, and ***; P<0.001.

Discussion

In this study, we observed that *circ_0000228* was up-regulated in the CC tissues and its overexpression was associated with to several adverse clinical parameters in the CC patients. Our experiments demonstrated that *circ_0000228* overexpression facilitates proliferation, migration and invasion of CC cells. We verified these findings with while knock down model of *circ_0000228*, and observed opposite effects. Several studies report that they are crucial regulators in cancer biology (20). For instance, *circ-ITCH* restrains the proliferation, migration and invasion of bladder cancer cells by sponging *miR-17/miR-224* to up-regulate PTEN expression (8). *Circ-SMARCA5* represses the development of multiple myeloma by decoying *miR-767-5p* (21). Knocking down *circ_0000285* suppresses the growth and migration of the CC cells (22). In the present work, our data indicated that *circ_0000228* is a new oncogenic factor in the CC tissues and cells.

As mentioned above, miRNAs are often negatively regulated by circRNAs via a competitive endogenous RNA mechanism (8). In this work, it was found

that *circ_0000228* directly targets *miR-337-3p* and *circ_0000228* enhances the CC cell proliferation, migration and invasion via adsorbing *miR-337-3p*. miRNAs are endogenous ncRNAs that are approximately 20 nucleotides in length that participate in the regulating diverse biological processes including epigenetic regulation, cell cycle, cell differentiation, proliferation, migration and so on (23, 24). miRNAs can function as either tumor-suppressive factors or oncogenic factors. For instance, *miR-324-3p* enhances the proliferation, migration, and invasion of colonic cancer cells, and impedes apoptosis (25). *MiR-338-3p* restrains CC progression by targeting *MACC1* to regulate the MAPK signaling pathway (26). *MiR-1284* represses the growth and metastasis of CC cells by targeting *HMGB1* and increases the sensitivity of CC cells to cisplatin (27). It is reported that *miR-337-3p* was a tumor suppressor in the CC cells and tissues (17, 18). Here, we reported that *miR-337-3p* counteracts with cancer-promoting effects of *circ_0000228* in CC cells and tissues, which also validated the anti-cancer effects of *miR-337-3p*. Moreover, we demonstrated that *miR-337-3p* can be adsorbed by circ_0000228, which is a reasonable explanation for the aberrant expression of *miR-337-3p* in the CC cells and tissues.

Usually, miRNAs exert their biological functions through binding to the 3′UTR of mRNAs target to induce translational repression or degradation of mRNAs (23). In this work, we found that *miR-337-3p* directly targets *TGFBR1* mRNA 3′UTR and negatively regulates *TGFBR1 mRNA* expression, and *circ_0000228* can promote *TGFBR1* expression in the CC cells. *TGFBR1* belongs to the TGF-β receptors family, which is involved in the TGF-β-mediated cell growth, differentiation and migration (28, 29). Accumulating studies have confirmed the regulatory role of *TGFBR1* in the different cancers (30-32). For instance, *TGFBR1* overexpression can enhance the proliferation, migration, invasion and the epithelial-mesenchymal transition process of gastric cancer cells (30).

In pancreatic cancer, *LINC00462* overexpression enhances the expression of *TGFBR1* and *TGFBR2*, thereby TGF-β/Smad pathway activating leads to facilitate proliferation, migration, and invasion of pancreatic cancer cells (31). In the non-small cell lung cancer (NSCLC), *miR-3607-3p* impedes tumor cell proliferation, invasion and migration by targeting *TGFBR1* (32). Also, in the CC, *TGFBR1* is reported to be a target of *let-7a*, and it mediates the activation of TGF-β/SMAD signaling in the CC cells (19). To our knowledge, this study is the first to identify *miR-337-3p* as an upstream miRNA of *TGFBR1* in the CC cells.

Conclusion

This research reveals that *circ_0000228* is highly expressed in the CC tissues and cells, and its highest expression is associated with adverse clinical parameters in the affected. Functionally and mechanistically, we confirm that *circ_0000228* enhances proliferation, migration and invasion of CC cells via modulating the *miR-337-3p*/*TGFBR1* axis. This work may provide novel ideas for the diagnosis, therapy, and prognosis of CC patients.

Acknowledgments

We thank the staff of the Department of Gynecology and Obstetrics and Department of Pathology of the Shengli Oilfield Central Hospital for their help and support in this study. We also thank Hubei Yican Health Industry Co., Ltd. for its linguistic assistance during the preparation of this manuscript. There is no financial support and conflict of interest in this study.

Authors´ Contributions

Y.X., X.D.; Contributed to conception and design. X.D., B.M., P.M.; Contributed to all experimental work, data, statistical analysis, and interpretation of data. Y.X., X.D.; Were responsible for overall supervision. Y.X., X.K., D.L.; Drafted the manuscript, which was revised by Y.X., X.D. All authors read and approved the final manuscript.

Reference

1. Bray F, Ferlay J, Soerjomataram I, Siegel RL, Torre LA, Jemal A. Global cancer statistics 2018: GLOBOCAN estimates of incidence and mortality worldwide for 36 cancers in 185 countries. CA Cancer J Clin. 2018; 68(6): 394-424.
2. Small W Jr, Bacon MA, Bajaj A, Chuang LT, Fisher BJ, Harkenrider MM, et al. Cervical cancer: a global health crisis. Cancer. 2017; 123(13): 2404-2412.
3. Ning MS, Ahobila V, Jhingran A, Stecklein SR, Frumovitz M, Schmeler KM, et al. Outcomes and patterns of relapse after definitive radiation therapy for oligometastatic cervical cancer. Gynecol Oncol. 2018; 148(1): 132-138.
4. Qu S, Yang X, Li X, Wang J, Gao Y, Shang R, et al. Circular RNA: a new star of noncoding RNAs. Cancer Lett. 2015; 365(2): 141-148.
5. Memczak S, Jens M, Elefsinioti A, Torti F, Krueger J, Rybak A, et al. Circular RNAs are a large class of animal RNAs with regulatory potency. Nature. 2013; 495(7441): 333-338.
6. Qu S, Zhong Y, Shang R, Zhang X, Song W, Kjems J, et al. The emerging landscape of circular RNA in life processes. RNA Biol. 2017; 14(8): 992-999.
7. Hansen TB, Jensen TI, Clausen BH, Bramsen JB, Finsen B, Damgaard CK, et al. Natural RNA circles function as efficient microRNA sponges. Nature. 2013; 495(7441): 384-388.
8. Yang C, Yuan W, Yang X, Li P, Wang J, Han J, et al. Circular RNA circ-ITCH inhibits bladder cancer progression by sponging miR-17/miR-224 and regulating p21, PTEN expression. Mol Cancer. 2018; 17(1): 19.
9. Du WW, Yang W, Li X, Awan FM, Yang Z, Fang L, et al. A circular RNA circ-DNMT1 enhances breast cancer progression by activating autophagy. Oncogene. 2018; 37(44): 5829-5842.
10. Guo J, Wang Z, Miao Y, Shen Y, Li M, Gong L, et al. A two-circRNA signature predicts tumour recurrence in clinical non-functioning pituitary adenoma. Oncol Rep. 2019; 41(1): 113-124.
11. Zhu X, Wang X, Wei S, Chen Y, Chen Y, Fan X, et al. hsa_circ_0013958: a circular RNA and potential novel biomarker for lung adenocarcinoma. FEBS J. 2017; 284(14): 2170-2182.
12. Zhao ZJ, Shen J. Circular RNA participates in the carcinogenesis and the malignant behavior of cancer. RNA Biol. 2017; 14(5): 514-521.
13. Ding L, Zhao Y, Dang S, Wang Y, Li X, Yu X, et al. Circular RNA circ-DONSON facilitates gastric cancer growth and invasion via NURF complex dependent activation of transcription factor SOX4. Mol Cancer. 2019; 18(1): 45.
14. Tang Q, Chen Z, Zhao L, Xu H. Circular RNA hsa_circ_0000515 acts as a miR-326 sponge to promote cervical cancer progression through up-regulation of ELK1. Aging (Albany NY). 2019; 11(22): 9982-9999.

15. Rong X, Gao W, Yang X, Guo J. Downregulation of hsa_circ_0007534 restricts the proliferation and invasion of cervical cancer through regulating miR-498/BMI-1 signaling. Life Sci. 2019; 235: 116785.
16. Chen XJ, Deng YR, Wang ZC, Wei WF, Zhou CF, Zhang YM, et al. Hypoxia-induced ZEB1 promotes cervical cancer progression via CCL8-dependent tumour-associated macrophage recruitment. Cell Death Dis. 2019; 10(7): 508.
17. Cao XM. Role of miR-337-3p and its target Rap1A in modulating proliferation, invasion, migration and apoptosis of cervical cancer cells. Cancer Biomark. 2019; 24(3): 257-67.
18. Meng QH, Li Y, Kong C, Gao XM, Jiang XJ. Circ_0000388 exerts oncogenic function in cervical cancer cells by regulating miR-337-3p/TCF12 axis. Cancer Biother Radiopharm. 20201; 36(1): 58-69.
19. Wu T, Chen X, Peng R, Liu H, Yin P, Peng H, et al. Let-7a suppresses cell proliferation via the TGF-β/SMAD signaling pathway in cervical cancer. Oncol Rep. 2016; 36(6): 3275-3282.
20. Zhang HD, Jiang LH, Sun DW, Hou JC, Ji ZL. CircRNA: a novel type of biomarker for cancer. Breast Cancer. 2018; 25(1): 1-7.
21. Liu H, Wu Y, Wang S, Jiang J, Zhang C, Jiang Y, et al. Circ-SMARCA5 suppresses progression of multiple myeloma by targeting miR-767-5p. BMC Cancer. 2019; 19(1): 937.
22. Chen RX, Liu HL, Yang LL, Kang FH, Xin LP, Huang LR, et al. Circular RNA circRNA_0000285 promotes cervical cancer development by regulating FUS. Eur Rev Med Pharmacol Sci. 2019; 23(20): 8771-8778.
23. Zhang Y, Wang Z, Gemeinhart RA. Progress in microRNA delivery. J Control Release. 2013; 172(3): 962-974.
24. Ha M, Kim VN. Regulation of microRNA biogenesis. Nat Rev Mol Cell Biol. 2014; 15(8): 509-524.
25. Yan D, Liu W, Liu Y, Luo M. LINC00261 suppresses human colon cancer progression via sponging miR-324-3p and inactivating the Wnt/β-catenin pathway. J Cell Physiol. 2019; 234(12): 22648-22656.
26. Hua FF, Liu SS, Zhu LH, Wang YH, Liang X, Ma N, et al. MiRNA-338-3p regulates cervical cancer cells proliferation by targeting MACC1 through MAPK signaling pathway. Eur Rev Med Pharmacol Sci. 2017; 21(23): 5342-5352.
27. Chen J, Li G. MiR-1284 enhances sensitivity of cervical cancer cells to cisplatin via downregulating HMGB1. Biomed Pharmacother. 2018; 107: 997-1003.
28. Morikawa M, Derynck R, Miyazono K. TGF-β and the TGF-β family: context-dependent roles in cell and tissue physiology. Cold Spring Harb Perspect Biol. 2016; 8(5): a021873.
29. Colasante A, Aiello FB, Brunetti M, di Giovine FS. Gene expression of transforming growth factor beta receptors I and II in non-small-cell lung tumors. Cytokine. 2003; 24(5): 182-189.
30. Ishimoto T, Miyake K, Nandi T, Yashiro M, Onishi N, Huang KK, et al. Activation of transforming growth factor beta 1 signaling in gastric cancer-associated fibroblasts increases their motility, via expression of rhomboid 5 homolog 2, and ability to induce invasiveness of gastric cancer cells. Gastroenterology. 2017; 153(1): 191-204. e16.
31. Zhou B, Guo W, Sun C, Zhang B, Zheng F. Linc00462 promotes pancreatic cancer invasiveness through the miR-665/TGFBR1-TGFBR2/SMAD2/3 pathway. Cell Death Dis. 2018; 9(6): 706.
32. Gao P, Wang H, Yu J, Zhang J, Yang Z, Liu M, et al. miR-3607-3p suppresses non-small cell lung cancer (NSCLC) by targeting TGFBR1 and CCNE2. PLoS Genet. 2018; 14(12): e1007790.

Original Article

Epigenetic Dysregulation of *BRDT* Gene in Testis Tissues of Infertile Men: Case-Control Study

Fereshteh Kohandani, M.Sc.[1, 2#], Parham Jazireian, M.Sc.[1#], Raha Favaedi, M.Sc.[1], Mohammad Ali Sadighi Gilani, M.D.[3, 4], Seyed Mohammad Moshtaghioun, Ph.D.[2*], Maryam Shahhoseini, Ph.D.[1, 5, 6*]

1. Department of Genetics, Reproductive Biomedicine Research Center, Royan Institute for Reproductive Biomedicine, ACECR, Tehran, Iran
2. Biology Department, Faculty of Science, Yazd University, Yazd, Iran
3. Department of Andrology, Reproductive Biomedicine Research Center, Royan Institute for Reproductive Biomedicine, ACECR, Tehran, Iran
4. Department of Urology, Shariati Hospital, Tehran University of Medical Sciences, Tehran, Iran
5. Reproductive Epidemiology Research Center, Royan Institute for Reproductive Biomedicine, ACECR, Tehran, Iran
6. Department of Cell and Molecular Biology, School of Biology, College of Science, University of Tehran, Tehran, Iran

 # These authors contributed equally to this work.

**Corresponding Addresses: P.O.Box: 81195-741, Biology Department, Faculty of Science, Yazd University, Yazd, Iran*
P.O.Box:16635-144, Royan Institute for Reproductive Biomedicine, ACECR, Tehran, Iran
Emails: moshtaghiun@yazd.ac.ir, m.shahhoseini@royan-rc.ac.ir, shahhoseini244@gmail.com

Received: 18/July/2020, Accepted: 28/November/2020

Abstract

Objective: Bromodomain testis associated (BRDT), a testis-specific member of the Bromo- and Extra-Terrminal domain (BET) protein family, is involved in spermatogenesis and, more specifically, chromatin remodeling. In the post-meiotic spermatogenic cells, BRDT protein binds to the hyperacetylated histones and facilitates their replacement with transition proteins (TPs), particularly protamines, which are essential for chromatin condensation. The current research was conducted to assess the expression and epigenetic profile of *BRDT* in the testis tissues of infertile men.

Materials and Methods: In this case-control study, three groups were included: positive control group: obstructive azoospermia (OA, n=10), round spermatid maturation arrest group (SMA, n=10) and negative control group: sertoli cell-only syndrome (SCOS, n=10). Using quantitative real-time polymerase chain reaction (PCR), the expression profile of *BRDT* was generated. Also, ChIP-real time PCR was used to measure the following histone marks: H3K9ac, H3K9me3, H3K4me3, H3K27me3 on the promoter region of *BRDT*.

Results: Our data indicated that *BRDT* expression decreased in the SMA group in comparison with the positive control group and this finding is in line with the ChIP results obtained in this group.

Conclusion: Based on these data, we postulate that *BRDT* gene has a vital role in the spermatogenesis and its decreased expression due to an aberrant epigenetic signaling might be associated with male infertility.

Keywords: *BRDT*, Epigenetics, Histone Modification, Spermatogenesis Failure

Cell Journal(Yakhteh), Vol 24, No 2, February 2022, Pages: 99-102

Citation: Kohandani F, Jazireian P, Favaedi R, Sadighi Gilani MA, Moshtaghioun SM, Shahhoseini M. Epigenetic dysregulation of BRDT gene in testis tissues of infertile men: case-control study. Cell J. 2022; 24(2): 99-102. doi: 10.22074/cellj.2022.7724.

Introduction

Spermatogenesis is a dynamic process in which undifferentiated diploid cells pass a series of mitotic and meiotic divisions to produce spermatozoa cells. During the last stages of this process, spermatogenic cells' core histones are hyperacetylated and then replaced by transition proteins (TPs) and protamines (PRMs) (1, 2). Bromodomain testis associated (BRDT) binding to the acetylated histone H4, emerges a hyperacetylation signal via a BRDT-dependent replacement of histones by TPs and PRMs (3, 4).

BRDT protein, a member of bromodomain and extra-terminal (BET) protein family, is expressed in the spermatocytes as well as in the round and elongating spermatids (5). BRDT plays two types of essential roles during spermatogenesis: first, BRDT attaches to acetylated histones at promoters of meiotic and post-meiotic genes through its bromodomains to facilitate the activity of these genes in an appropriate time frame. Second, BRDT attach to hyperacetylated histones during post-meiotic phase of spermatogenesis and help their removal and substitution (6). It should be mentioned that histone hyperacetylation is an important process during histone removal and substitution in the elongating spermatids (7).

Epigenetic modifications such as histone acetylation and methylation are essential regulators in the spermatogenesis and testis genes expression. For instance, acetylation lysine 9 of histone H3 (H3K9ac) mediates gene transcriptional activity, while methylation of lysine

9 of histone H3 (H3K9me3) mediates gene transcriptional repression (8).

Furthermore, there are two other histone marks, trimethylated lysine 4 on histone H3 (H3K4me3) and trimethylated lysine 27 on histone H3 (H3K27me3), which are associated with promoters of the developmental regulator genes. H3K27me3 mediates gene silencing, while H3K4me3 is associated with the gene transcriptional activity. Contemporary presence of H3K27me3 and H3K4me3 on the genes in the stem cells, identifies a category of bivalent silent developmentally regulated genes (9).

Using testicular biopsies of infertile men, this study highlights the occurrence of an aberrant epigenetic signaling associated with a decreased expression of *BRDT*. For the first time, we made more attention to the importance of *BRDT* expression that may lead to spermatogenesis failure and men infertility.

Materials and Methods

Subjects

In this case-control study, testicular biopsy specimens were obtained from 30 infertile patients who referred to Royan Institute, Tehran, Iran. All samples were collected from testicular sperm extraction (TESE) operation in order to obtain sperm for intracytoplasmic sperm injection (ICSI). Reproductive Biomedicine Research Center and the Ethics Committee of Royan Institute, Tehran, Iran approved this study (IR.ACECR.ROYAN.REC.1394.135). Following obtain written consents from all volunteer patients, residuals of their therapeutic/diagnostic samples were used in the present study.

The samples of 3 patient groups provided our 3 study groups, including: obstructive azoospermia (OA): positive control group, round spermatid maturation arrest (SMA): SMA group and sertoli cell only syndrome (SCOS): negative control group.

RNA isolation and cDNA synthesis

In order to evaluate *BRDT* gene expression, RNA was extracted from tissue samples by using TRIzol reagent (Cat No.15596018, Ambion, USA). To eliminate genomic contaminations, the extracted RNAs were treated using Recombinant DNase I kit (RNase-free), (Cat No. 2270A, Takara, Japan). Then, cDNA was synthesized using RevertAid H Minus First Strand cDNA Synthesis Kit (Cat No.k1632, Thermofisher, USA) according manufacturers' instruction. Also, this synthesized cDNA was used for polymerase chain reaction (PCR) amplification, and the results were normalized by PCR reaction by using specific primers for *GAPDH* gene. All gene expression and epigenetic tests performed individually.

Gene expression analysis of *BRDT* gene by reverse transcription real-time quantitative polymerase chain reaction

The cDNA samples were quantified with RT-qPCR in the groups by using SYBR Green PCR master mix (Applied Biosystems, USA) on a Step One Plus Real-Time PCR System (Applied Biosystem, USA). Preventing DNA contaminations, primer pairs were designed using Perl Primer (v1.1.19) software from an exon-exon junction area of the genes (Table 1).

Therefore, cDNA amplification was carried out with the following profile: initial denaturation at 95°C for 4 minutes, followed by 35 cycles of denaturation at 95°C for 10 seconds, annealing at 60°C for 1 minute. Each 25 µl reaction contained 2 µl of template cDNA (12.5 ng/µl), 1 µl of each 5 pmol/µl primer (Sinaclone, Iran), 12 µl of SYBR Green PCR master mix and 9 µl dH_2O.

Two replicates were carried out for each sample and relative gene expression level was quantified by using the $2^{-\Delta\Delta Ct}$ quantitative method (10) and the results were normalized with *GAPDH* gene.

Chromatin immunoprecipitation-quantitative polymerase chain reaction

Presence of acetylated histone H3K9, trimethyl H3K9, trimethyl H3K27 and trimethyl H3K4 on the promoter region of *BRDT* was evaluated by Chromatin immunoprecipitation using the Histone ChIP kit (Cat No. kch-orgHIS-012, Diagenode, Belgium) followed by real time PCR in the three studied groups, including OA (n=5), SMA (n=5) and SCOS (n=5). Anti-H3K9ac, anti-H3K9me3, anti- H3K27me, and anti- H3K4me3antibodies (Cat No. ab4441, ab8898, ab6002, ab1012 respectively, Abcam, UK) were exploited in this method. qPCR method was used in order to amplify immunoprecipitated DNA and input control DNA on a real time PCR system (Step One Plus Real time PCR system, AB Applied Biosystems, USA) by using SYBR Green master mix (Cat No. 4367659, Power SYBR Green PCR Master, Applied Biosystems, USA) and primer pairs designed using Perl primer software to cover the transcriptional start site (TSS) (-96 to +14) of the *BRDT* gene (Table 1). Also, qPCR reaction was carried out with the following profile: initial denaturation at 95°C for 4 minutes, followed by 35 cycles of denaturation at 95°C for 10 seconds, annealing at 60°C for 1 minutes. The obtained results were normalized to input DNA and presented as a percentage of input DNA.

Statistical analysis

Statistical analyses, among the three groups were performed using Kruskal-Wallis test. version 8.0.2 for Windows, GraphPad Software, La Jolla California USA). Differences between groups were considered to be statistically significant at $P \leq 0.05$.

Table 1: Primer pairs used in this study

Gene	Primer sequence (5′-3′)	Annealing temperature (ºC)	Product size (bp)
RT-PCR primers			
GAPDH	F: CTCATTTCCTGGTATGACAACGA	60	122
	R: CTTCCTCTTGTGCTCTTGCT		
BRDT	F: AGAACAGGCGTCACACAGAT	58.4	109
	R: GGTGGTGATTTGGTGGCATT		
ChIP-qPCR primers			
BRDT	F: GGCTCAGACTCCTACACCTTTT	62.1	110
	R: CAGGCGCTTTTATAGAAGACCC		

RT-PCR; Reverse transcription polymerase chain reaction and ChIP-qPCR; Chromatin Immunoprecipitation quantitative real-time PCR.

Results

Expression pattern of the *BRDT* gene

The mRNA expression level of the *BRDT* gene was evaluated by using real time-RT-qPCR. Amongst the three groups, there was a decrease in the *BRDT* gene expression in the SMA group in comparison with the OA control group while, SCOS group showed less expression level (Fig.1).

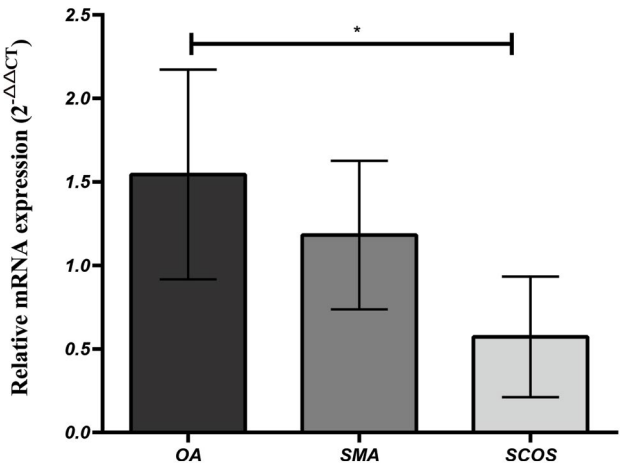

Fig.1: Relative mRNA expression of *BRDT* gene normalized to *GAPDH* in testicular samples with OA (n=10), SMA (n=10) and SCOS (n=10). Values are mean ± SEM. *; P≤0.05, OA; Obstructive azoospermia, SMA; Round spermatid maturation arrest, and SCOS; Sertoli cell-only syndrome.

Incorporation of histone marks: H3K9ac, H3K9me3, H3K4me3 and H3K27me3 on the *BRDT* gene promoter

Incorporation of H3K9ac, H3K9me3, H3K4me3, H3K27me3 on the promoter region of *BRDT* gene was evaluated by ChIP-qPCR assay. Compared to the OA control group, in the SMA group, the active histone marks of H3K9ac and H3K4me3 decreased on the *BRDT* gene promoter, while the repressive marks of H3K9me3 and H3K27me3 showed some increase in this group. All results are presented in Figure 2.

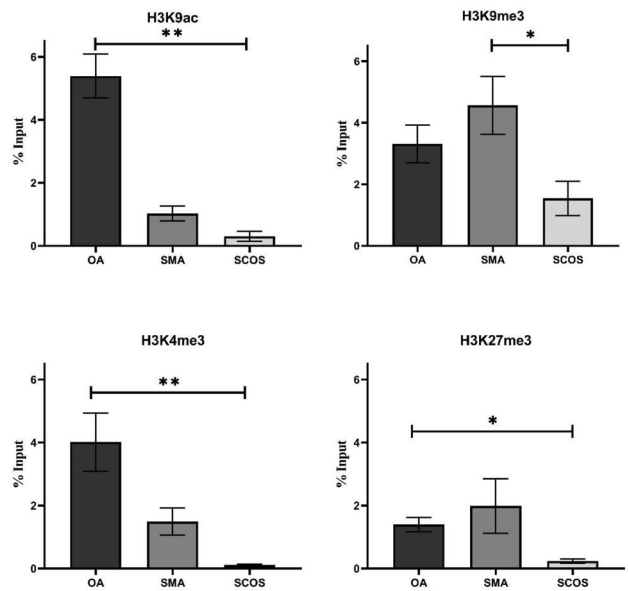

Fig.2: Incorporation of H3K9ac, H3K9me3, H3K4me3, H3K27me3 on the regulatory region of *BRDT* gene in patients of different groups: OA (n=5), SMA (n=5) and SCOS (n=5). Values are mean ± SEM. **; P≤0.01, *; P≤0.05, OA; Obstructive azoospermia, SMA; Round spermatid maturation arrest, and SCOS; Sertoli cell-only syndrome.

Discussion

Spermiogenesis is one of the most important stages of spermatogenesis. During spermiogenesis, the haploid spermatids completely transform and differentiate to mature spermatozoa which contain a highly condensed genome (11).

BRDT plays an important role in the acetylation-dependent histone substitution during spermiogenesis

(3, 4, 6) and its reduced expression level might cause spermatogenesis failure (12). Omitting first bromodomain of Brdt, Shang et al. observed defects during spermiogenesis in a mouse model (7). In parallel with these findings, Gaucher et al. (6) concluded by *Brdt* knock-out mice that Brdt is required at both meiotic and post-meiotic stages.

Our findings showed that in the infertile men with post-meiotic defects, the *BRDT* expression level is decreased in comparison with the positive control group. Also, our ChIP results indicated that the reduced expression of *BRDT* in these patients could be due to a wrong epigenetic signaling.

Indeed, association H3K9ac at the regulatory regions of *BRDT* with its active expression, a decrease in may lead to a lower the *BRDT* expression level in the SMA group. In addition, the occurrence H3K9me3 on the *BRDT* regulatory regions could prompt gene silencing in the SMA group.

Furthermore, histone methylations of H3K4me3 and H3K27me3 on the *BRDT* promoter can modulate gene expression and gene silencing, respectively. Our ChIP results showed that H3K4me3 was decreased in the SMA group, while H3K27me3 was slightly higher in the same group in compared with the positive control group. These results are completely in line with our conclusions on the epigenetic perturbation of *BRDT* genes in the SMA group. It is worthwhile to mention that in order to assess this matter more accurately, further investigations with a larger number of patients including more epigenetic marks are required.

Conclusion

It can be assumed that epigenetic regulation of *BRDT* gene and its deregulated expression is associated with male infertility in patients with round spermatid maturation arrest.

Acknowledgments

This research paper is dedicated to the memory of Dr. Saeid Kazemi Ashtiani, the late founder of Royan Institute and we would like to thank all patients for their contribution to this study. This study was financially supported by the Royan Institute, Tehran, Iran. The authors declare that there are no conflicts of interest in this study.

The authors certify that all procedures contributing to this work comply with the ethical standards of the relevant national guidelines on human experimentation (testicular sperm extraction operation) and the Helsinki Declaration of 1975, 2008 revised version.

Authors' Contributions

F.K.; Study performance and manuscript drafting. P.J.; Statistical analysis, manuscript drafting and revision. R.F.; Technical performance supporter and data analysis. M.A.S.G.; Urologist and the administrative supporter for collecting samples. S.M.M.; Research supervisor. M.S.; Study designer and supervisor and manuscript revision collaborator. All authors read and approved the final manuscript.

References

1. Carrell DT, Hammoud SS. The human sperm epigenome and its potential role in embryonic development. Mol Hum Reprod. 2009; 16(1): 37-47.
2. Barral S, Morozumi Y, Tanaka H, Montellier E, Govin J, de Dieuleveult M, et al. Histone variant H2A.L.2 guides transition protein-dependent protamine assembly in male germ cells. Mol Cell. 2017; 66(1): 89-101.
3. Shiota H, Barral S, Buchou T, Tan M, Couté Y, Charbonnier G, et al. Nut directs p300-dependent, genome-wide h4 hyperacetylation in male germ cells. Cell Rep. 2018; 24(13): 3477-3487.
4. Goudarzi A, Shiota H, Rousseaux S, Khochbin S. Genome-scale acetylation-dependent histone eviction during spermatogenesis. J Mol Biol. 2014; 426(20): 3342-3349.
5. Berkovits BD, Wolgemuth DJ. The first bromodomain of the testis-specific double bromodomain protein Brdt is required for chromocenter organization that is modulated by genetic background. Dev Biol. 2011; 360(2): 358-368.
6. Gaucher J, Boussouar F, Montellier E, Curtet S, Buchou T, Bertrand S, et al. Bromodomain-dependent stage-specific male genome programming by Brdt. EMBO J. 2012; 31(19): 3809-3820.
7. Shang E, Nickerson HD, Wen D, Wang X, Wolgemuth DJ. The first bromodomain of Brdt, a testis-specific member of the BET subfamily of double-bromodomain-containing proteins, is essential for male germ cell differentiation. Development. 2007; 134(19): 3507-3515.
8. McSwiggin HM, O'Doherty AM. Epigenetic reprogramming during spermatogenesis and male factor infertility. Reproduction. 2018; 156(2): R9-21.
9. Meshorer E, Misteli T. Chromatin in pluripotent embryonic stem cells and differentiation. Nat Rev Mol Cell Biol. 2006; 7(7): 540-546.
10. Livak KJ, Schmittgen TD. Analysis of relative gene expression data using real-time quantitative PCR and the 2(-delta delta c(t)) method. Methods. 2001; 25(4): 402-408.
11. Nishimura H, L'Hernault SW. Spermatogenesis. Curr Biol. 2017; 27(18): R988-R994.
12. Steilmann C, Cavalcanti MC, Bartkuhn M, Pons-Kühnemann J, Schuppe HC, Weidner W, et al. The interaction of modified histones with the bromodomain testis-specific (BRDT) gene and its mRNA level in sperm of fertile donors and subfertile men. Reproduction. 2010; 140(3): 435-443.

Commentary

Ribosome Profiling: A Useful Approach to Discover Hidden Corners of SARS-CoV-2

Milad Zandi, Ph.D.[1]*, Emad Behboudi, Ph.D.[2], Parisa Zeinali, M.Sc.[3], Saber Soltani, Ph.D.[1], Mohammad Reza Shojaei, Ph.D.[2]

1. Department of Virology, School of Public Health, Tehran University of Medical Sciences, Tehran, Iran
2. Department of Microbiology, School of Medicine, Golestan University of Medical Sciences, Gorgan, Iran
3. Department of Biochemistry and Biophysics, School of Medicine, Metabolic Disorders Research Center, Golestan University of Medical Sciences, Gorgan, Iran

**Corresponding Address: P.O.Box: 1417613151, Department of Virology, School of Public Health, Tehran University of Medical Sciences, Tehran, Iran*
Email: miladzandi416@gmail.com

Received: 22/December/2021, Accepted: 23/January/2022

Abstract

Following SARS-CoV-2 China epidemic in the December 2019, researches have attended to the genome of novel coronavirus. Hidden corners of SARS-CoV-2, maybe a shiny way to discover its pathogenicity and virulence. To design therapeutic agents, it is critical to map the complete repertoire of viral-translated proteins. Ribosome profiling is considered as a snapshot of all active ribosomes in a cell at a specific time point.

Keywords: Genome, Open Reading Frames, Ribo-seq, SARS-CoV-2

Cell Journal(Yakhteh), Vol 24, No 2, February 2022, Pages: 103-104

Citation: Zandi M, Behboudi E, Zeinali P, Soltani S, Shojaei MR. Ribosome profiling: a useful approach to discover hidden corners of SARS-CoV-2. Cell J. 2022; 24(2): 103-104. doi: 10.22074/cellj.2022.8387.

Coronaviruses (CoVs) are recognized as a single-stranded RNA virus with a genome length from 26 to 32 kilobases, that belongs to the *Coronaviridae* family. Severe acute respiratory syndrome coronavirus 2 (SARS-CoV-2), a novel member of this family, is known as the first global concern since 2019 and still, kills so many people every day (1-4). Since the first days, so many studies focused on its full genome. The SARS-CoV-2 genome displays a body similar to other CoVs. This positive-sense single-stranded RNA (+ssRNA) virus contains a 5′-cap and a 3′-poly-A tail (5, 6). Like the other CoVs, a frameshift mechanism at the 5′-end of SARS-CoV-2 between viral open reading frames (ORFs), including ORF1a and ORF1b, facilitates the synthesis of two polypeptides One of these viral proteases, that named 16 non-structural proteins (Nsp1-16), are necessary for different stages of the virus life cycle (7). These nonstructural proteins are included viral proteases, nuclease, helicase, methyltransferase, RNA-dependent RNA polymerases (1, 8, 9).

Hidden corners pathogenicity and virulence of SARS-CoV-2 are critical points to design effective therapeutic agents. Mapping the complete repertoire of viral-translated proteins is one of these points. The present map of viral translation capacity is according to bioinformatical analysis, and its homology with other CoVs (10). Since the protein profile is various among CoVs, particularly about the accessory proteins, it is essential to describe the exact variety of viral proteins in an open-ended way. Hence, in a recent study, ribosome-profiling methods were used as a high-resolution approach for mapping of coding regions in this RNA virus to precisely account for the canonical viral ORFs in the proteome level to identify viral ORFs (11). Ribosome profiling is also known as ribo-seq is a useful approach that offers *in vivo* genome-wide data on protein synthesis (GWIPS). This technique is established based on deeply sequencing of ribosome protected sequences of mRNA that provides the analysis of ribosome density associate with total RNAs existing in cells. Also, its capacity in high resolution analysis provides a good chance to detailed analysis for individual RNAs (12).

In this technique, mRNA fragments and recovered footprints are transformed into an appropriate feature for massive sequencing. Performing analysis on its outcomes will give us the measured translation capacity of ribosomes at the scale of whole-genome. So ribosome profiling is capable to be utilized for assessing the quantity of viral protein translation. While a large quantity of transcripts in a fraction of polysome is evaluated by microarray techniques or RNA-seq, Ribo-seq method has been identified as a common approach to discovering genes involved in the translation process. Although, ribo-seq previously was applied for polysome analysis in which isolation of protein-coding mRNAs occurs by a gradient of sucrose (13). The actual potential of ribosome profiling is its capability to acquire data on the distinct position by considering ribosome positions on mRNAs, what makes its priority to similar methods. This point is critical for some details. Detection of an mRNA fragment in association ribosomes necessarily does not tell us that our fragment of the mRNA is completely translated. In

other words, ribosomes can associate with an mRNA fragment that do not generate a protein, since translation can't happen at non-coding mRNA (14).

The genome of SARS-CoV-2 encodes at least 13 known open reading frames, organized largely linearly from the 5′ end to the 3′ end (15, 16). However, Salehi et al. (17) reported that the full genome sequence of SARS-CoV-2 has 10 ORFs.

Ribosome profiling as a novel and useful technique can be used to discover hidden corners of pathogens. It is important to map the complete repertoire of viral-translated proteins to design and develop effective therapeutic agents.

Acknowledgements

There is no financial support and conflict of interest in this study.

Authors' Contributions

M.Z.; Performed to conception and design and supervised the study. E.B., P.Z.; Contributed to write and draft the manuscript. S.S., M.R.S.; Performed editing. All the authors approving the final version of this paper for submission, also participated in the finalization of the manuscript and approved the final draft.

References

1. Behboudi E, Hamidi-Sofiani V, Zeynali P. Review of therapeutic candidates for the new corona virus (COVID-19). RJMS. 2020; 27(8): 65-77.
2. Wang H, Li X, Li T, Zhang S, Wang L, Wu X, et al. The genetic sequence, origin, and diagnosis of SARS-CoV-2. Eur J Clin Microbiol Infect Dis. 2020; 39(9): 1629-1635.
3. Hosseini P, Dehghan A, Navand AH, Moghadami M, Soltani S, Zandi M. Coronavirus disease 2019 (COVID-19): immune responses, transmission and clinical features: an update. JCMA. 2020; 5(4): 266-268.
4. Zandi M, Rashid S, Nasimzadeh S, Pourhossein B, Fazeli M. A snapshot of different types of under research vaccines against COVID-19: a review. Arch Med Lab Sci. 2020; 6: 1-7.
5. Behboudi E, Hamidi-Sofiani V. New mutations causing the 2019 novel Coronavirus (2019-nCoV) epidemic: letter to the editor. TUMS. 2020; 78(3): 188.
6. Zandi M. ORF8/ORF8a: a difference between SARS-CoV-2 and SARS-CoV. Eur Respir J. 2021: 2102818.
7. Suryawanshi RK, Koganti R, Agelidis A, Patil CD, Shukla D. Dysregulation of cell signaling by SARS-CoV-2. Trends Microbiol. 2021; 29(3): 224-237.
8. Wu A, Peng Y, Huang B, Ding X, Wang X, Niu P, et al. Genome composition and divergence of the novel coronavirus (2019-nCoV) originating in china. Cell Host Microbe. 2020; 27(3): 325-328.
9. Zandi M. Severe acute respiratory syndrome-2 encodes hemagglutinin esterase? Rev Med Virol. 2021: e2294.
10. Michel CJ, Mayer C, Poch O, Thompson JD. Characterization of accessory genes in coronavirus genomes. Virol J. 2020; 17(1): 131.
11. Finkel Y, Mizrahi O, Nachshon A, Weingarten-Gabbay S, Morgenstern D, Yahalom-Ronen Y, et al. The coding capacity of SARS-CoV-2. Nature. 2021; 589(7840): 125-130.
12. Michel AM, Baranov PV. Ribosome profiling: a Hi-Def monitor for protein synthesis at the genome-wide scale. Wiley Interdiscip Rev RNA. 2013; 4(5): 473-490.
13. Larsson O, Sonenberg N, Nadon R. Identification of differential translation in genome wide studies. Proc Natl Acad Sci USA. 2010; 107(50): 21487-21492.
14. Erhard F, Halenius A, Zimmermann C, L'Hernault A, Kowalewski DJ, Weekes MP, et al. Improved Ribo-seq enables identification of cryptic translation events. Nat Methods. 2018; 15(5): 363-366.
15. Malone B, Urakova N, Snijder EJ, Campbell EA. Structures and functions of coronavirus replication-transcription complexes and their relevance for SARS-CoV-2 drug design. Nat Rev Mol Cell Biol. 2022; 23(1): 21-39.
16. Kesheh MM, Hosseini P, Soltani S, Zandi M. An overview on the seven pathogenic human coronaviruses. Rev Med Virol. 2021: e2282.
17. Salehi N, Amiri-Yekta A, Totonchi M. Profiling of Initial available SARS-CoV-2 sequences from Iranian related COVID-19 patients. Cell J. 2020; 22 Suppl 1: 148-150.